2005

Use of acoustic emission signals through steel reinforcement to detect the onset of corrosion

Weiben Chen
University of Windsor

USE OF ACOUSTIC EMISSION SIGNALS THROUGH STEEL REINFORCEMENT TO DETECT THE ONSET OF CORROSION

By

Weiben Chen

A Thesis
Submitted to the Faculty of Graduate Studies and Research
through Civil and Environmental Engineering
in Partial Fulfillment of the Requirements for
the Degree of Master of Applied Science at the
University of Windsor

Windsor, Ontario, Canada

2005

Your file Votre référence
ISBN: 0-494-09781-7
Our file Notre référence
ISBN: 0-494-09781-7

ABSTRACT

Corrosion processes produce elastic energy waves in the form of acoustic emission (AE). For corrosion in reinforced concrete structures, AE waves are emitted beginning with the depassivation of oxide layers of reinforcing steel, the initial stage of corrosion processes. This study examines the feasibility of using AE technique to detect corrosion through steel reinforcement, which has relatively lower attenuation than concrete. Comparison of coupling AE sensors on steel and on concrete was made. Accelerated corrosion regime and two-channel multifunctional AE equipment with piezoelectric sensors were employed for laboratory experiments. The detectable distance from corrosion source to sensor was estimated via the calculation of attenuation coefficient and particle surface displacement. The analysis of source location demonstrates that surface wave is the predominant AE wave propagating in rebars with one-inch diameter. Furthermore, an important experiment was performed to compare AE measurement with half-cell potential measurement. As a result, AE was proved to be a promising tool for corrosion detection in reinforced concrete structures.

ACKNOWLEDGEMENTS

I would like to thank Professor N. Hearn for giving me the opportunity to work on such an interesting project. I sincerely appreciate her for her guidance and help that make my graduate study and my life in Canada different. I would like to express special thanks to Professor Maev and Professor Ghrib for their guidance and suggestions.

It was a successful experience to work with Anna Ovanesova and Matt Zajmalowski. I am grateful for their helps. I would like to thank Ozgun Dervisoglu for his introduction of DW system. I would like to thank also the technical staff of University of Windsor Lucian Pop and Patrick Seguin for their help to set up the experiments. My gratitude extends to Sepanka Elias, Cathy Lee and Ozgun again for their research contributions in the field of ultrasonic / AE and corrosion. Finally, I would like to thank my wife Xiaoying Chen for her support.

TABLE OF CONTENTS

LIST OF TABLES

LIST OF FIGURES

CHAPTER 1. INTRODUCTION

1.1 Background

Many reinforced concrete (RC) structures deteriorate due to the corrosion of the reinforcement. Structures exposed to chlorides, such as highway bridges and parking structures in cold regions with the use of de-icing salts, and marine structures are particularly vulnerable to corrosion attack.

In most cases, corrosion is detected once extensive deterioration has occurred, such as cracking, delaminations and reduction in the steel's cross-section. "The corrosion of metals, especially steel, in concrete has received increasing attention in recent years because of its widespread occurrence in certain types of structures and the high cost of repairs" [ACI Committee 222, 1985].

The use of non-destructive monitoring in reinforced concrete structures is still very limited. Fortunately, the need and awareness of monitoring and assessment is being recognized by many organizations such as Departments of Transportation funding projects in USA, and in Canada the formation of a Canadian Centre of Excellence on Intelligent Sensing in Innovative Structures (ISIS).

In addition to the commonly used non-destructive methods, Acoustic Emission (AE) and ultrasonic measurements, such as Ultrasonic Pulse Velocity (UPV), Pulse-echo and

Impact-echo, have been employed to correlate material properties and detect the deterioration in reinforced concrete structures, e.g. the integrity testing of bridges in the Federal Lands Highway Program conducted by US Department of Transportation and Federal Highway Administration [Rosh, 2003].

1.2 Problem Statement

Non-destructive testing of the state of corrosion of a concrete structure is limited to several tests: visual inspection, chain drag sounding, half-cell potential mapping, sonic and radiographic methods.

- Visual inspection

Visual inspection uses direct or remote observation to obvious signs of corrosion, such as spalling, cracking and staining. This method provides detection only after significant corrosion has occurred, when large-scale repair or rehab is usually inevitable. The further test, core sampling, is destructive and requires repair of concrete.

- Chain drag sounding

In this method, the hollow sound indicates the occurrence of delamination between steel reinforcement and concrete. Like visual inspection, this method can only reflect the latter effect of corrosion causing deterioration.

- Half-cell potential mapping

Half-cell potential mapping, the most common electrochemical method, can be used to determine the probability of corrosion at the time of the reading (ASTM C876). However, the measurement depends on the condition of concrete. Moisture level and the amount of

carbonation and salt concentration can affect the reading or give erroneous readings. Furthermore, half-cell potential measurement does not provide information on the rate of corrosion [Zdunek et al, 1995].

Ultrasonic methods in concrete have been limited to the following uses:

- Assess the uniformity and relative quality of concrete
- Indicate the presence of voids and cracks
- Estimate the severity of deterioration
- Measure the thickness or length of objects

Radiographic methods use X-ray or gamma rays and require extensive safety precautions. They are impractical to perform inspections for many in-service structures [Malhotra, 1991]. The above methods are not capable of monitoring structures continuously and providing the early detection of corrosion. Acoustic emission may be the solution for these problems.

Acoustic Emission (AE) refers to generation of transient elastic waves during rapid release of energy from localized sources within a material. The source of these emissions, similar with a small seismic, is closely associated with the dislocation movement, plastic deformation, cracking, or matrix debonding [Carlos, 2003].

Research has been conducted and implemented in using AE to monitor the corrosion of the post-tensioned cables. A recent project in Virginia US to inspect all of the post-tensioned ducts in Virginia bridges was sponsored by Virginia Transportation Research Council

[Duke, 2002]. The SoundPrint acoustic monitoring system, invented and developed in Canada, has used to detect and locate the breaks of post-tensioned cables in North America, UK, Germany and France since 1994. e.g. the monitoring of railway viaducts in Huntington, UK. The system detects acoustic waves with lower frequencies than that in common AE monitoring [Cullington, 1998].

Corrosion, especially pitting and exfoliation produce large amount of AE events [Geng, 2001]. AE from a corrosion source in reinforced concrete is mostly caused by breakdown of passive oxide layer (the initiative), exfoliation of steel layers, debonding at the concrete-steel interface, cracking of concrete (Section 2.1.4). Debonding and cracking of concrete, caused by the built-up of corrosion products, are latter phenomena of corrosion processes. The elastic AE wave can travel through concrete or along the reinforcing steel, which acts as a waveguide [Idrissi, 2003].

Although the attenuation of AE in concrete has been a concern in the past, unique placement of AE sensors on the steel reinforcement and using the steel as the AE wave propagation medium should allow the onset of steel corrosion to be detected [Zdunek et al, 1995].

1.3 Research Significance and Objectives

Corrosion of steel reinforcement is one of the most important causes of deterioration of reinforced concrete structures. The conventional NDT / NDE techniques both electrochemical and non-electrochemical methods are not capable of providing continuous

early detection of corrosion. AE technique offers a distinct advantage of AE that it allows for real-time monitoring in-service structures because AE results directly from the process of flaw growth [Shi et al, 2002]. It is possible that AE can be a promising technique for corrosion detection and intelligent sensing reinforced concrete structures, which can dramatically reduce the structural rehabilitation cost. At the initial research stage, the feasibility of this approaching is of critical importance.

The objectives of this study are to find answers of the following key issues regarding the feasibility of using AE technique to detect the initial stages of reinforcement corrosion.

- Can steel corrosion be "heard" by the AE sensors?
- Are the AE signals in reinforced concrete due to corrosion or other processes?
- Is it better to put the sensors on the steel or concrete?
- How far can we measure away from the corrosion source?

CHAPTER 2. LITERATURE REVIEW

Deterioration of reinforced concrete, caused by corrosion of the rebar, has become a widespread problem and is the major cause of failure of aging RC structures [Schiessel, 1988]. Due to the increasing repair and rehabilitation cost of aging infrastructure, monitoring and detecting techniques of corrosion and structural integrity have become more and more important. To protect structures from deterioration, early damage detection is needed. The conventional measurements both electrochemical and non-electrochemical methods have their disadvantages and limitations.

Successful detecting and monitoring of the corrosion require an understanding of the cause and mechanism of the corrosion process. In Section 2.1, the mechanism of steel corrosion in concrete, the pitting corrosion, corrosion periods, corrosion processes that generate AE, and laboratory accelerated corrosion are reviewed. The measurements of corrosion in reinforced concrete, both electrochemical and non-electrochemical method, are briefly covered in Section 2.2 including their descriptions, advantages and limitations. In Section 2.3, ultrasonic NDT techniques and acoustic emission are reviewed. In order to understand how to detect the corrosion in reinforced concrete structures, wave propagation and instrumentation are reviewed in Section 2.4 and 2.5. Finally, Section 2.6 concludes the importance of developing acoustic emission technique for corrosion detection in reinforced concrete structures.

2.1 Corrosion of Steel in Concrete

2.1.1 Mechanism of corrosion of steel in reinforced concrete

Normal steel reinforcement is protected by passive dense oxide layer due to the high alkalinity of the surrounding concrete. When carbonation of cover and contamination with chlorides occurred, concrete is unable to maintain passivity and the corrosion process starts.

The basic anodic reaction is the dissolution of metal into metal ions, as follows:

$Fe \rightarrow Fe^{2+} + 2e^-$

The basic cathodic reaction is:

$^1/_2 O_2 + H_2O + 2e^- \rightarrow 2OH^-$

The reaction products are various oxides and hydroxides of iron depending on the surrounding environment.

$Fe^{2+} + 2OH^- \rightarrow Fe(OH)_2$

$4Fe(OH)_2 + 2H_2O + O_2 \rightarrow 4Fe(OH)_3$ (ferric hydroxide, usually referred to rust)

$2Fe(OH)_2 \xrightarrow{H_2O} Fe_2O \cdot n H_2O$

The corrosion product has a greater volume than the original steel (Fig. 2.1) and this creates the pressure that causes debonding, cracking and subsequent spalling of the surrounding concrete.

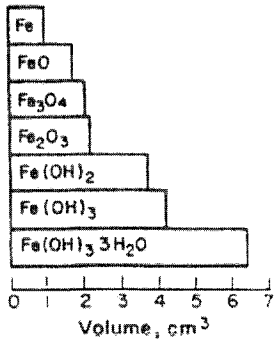

Fig. 2.1 Volumetric expansion of corrosion products [Brasunas, 1984]

The major corrosion types in reinforced concrete are macro-cell corrosion (general corrosion), micro-cell corrosion, pitting corrosion and low-potential active corrosion

Micro-cell corrosion takes place when O_2 is available at cathode and concrete is conductive to allow ionic movement between cathode-anode couples (Fig. 2.2). A micro-cell is often associated with pitting corrosion.

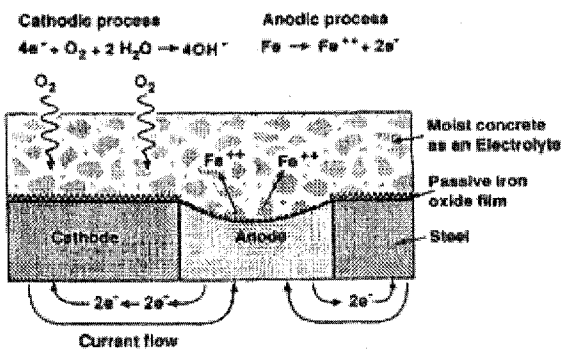

Fig. 2.2 Micro-cell corrosion [Schiessl, 1988]

A macro-cell is referred to as general corrosion. Large area of steel are involved in this type of corrosion, and the corrosion rate is more uniform than micro-cell corrosion.

When the supply of oxygen is insufficient to maintain passive layer in submerged or buried concrete, low-potential active corrosion occurs accompanied by evolution of H_2 causes hydrogen embrittlement of metal. Most corrosions of aluminum alloy are associated with this type of corrosion [Baboian, 1995].

For steel, the cathodic reaction is:

$2\ H_2O + 2e^- \rightarrow H_2 + 2OH^-$

The anodic reaction is:

$Fe \rightarrow Fe^{2+} + 2e^-$

The corrosion types and rates or the states of passivisity and immunity depend on steel potential, oxygen availability, PH and chloride concentrations. Fig. 2.3 shows their relationships.

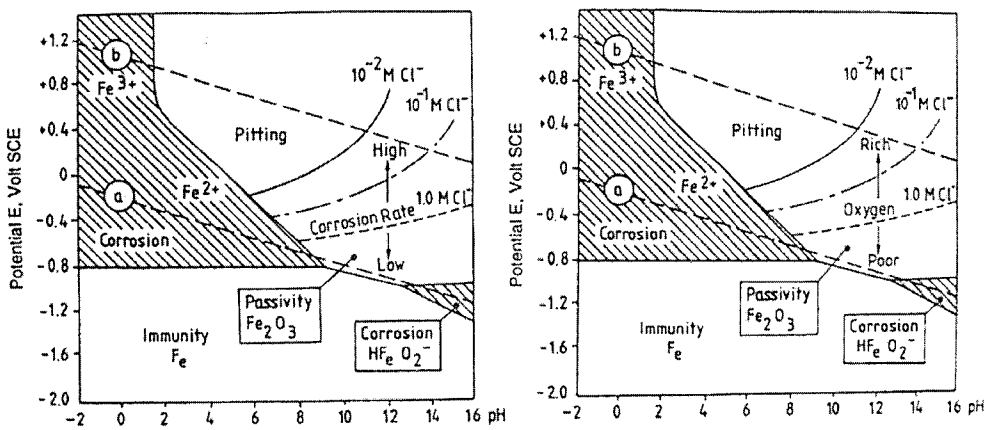

Fig. 2.3 Ordinary steel in concrete regarding corrosion rate, steel potential, oxygen availability and chloride concentrations [Sandberg, 1995]

The Potential-PH diagrams sometimes referred to Pourbaix Diagrams that indicate whether

corrosion or passivation is thermodynamically possible. The steel potential in a given environment represents a balance of cathodic reactions, anodic reactions and any external current from metals connected to the steel [Sandberg, 1995].

2.1.2 Pitting corrosion and the effect of chloride

Most corrosion encountered in engineering practice is of a more localized type, rather than diffused general attack. The most common type of localized corrosion is pitting, in which small volumes of metal are removed by corrosion from certain areas on the surface to produce pits or craters. Pitting corrosion is driven by galvanic action between relatively large areas of passive steel acting as a cathode and a small anodic pit [Tonini, 1980]. The visual differences between general attack and localized attack (pitting) are illustrated in Fig. 2.4.

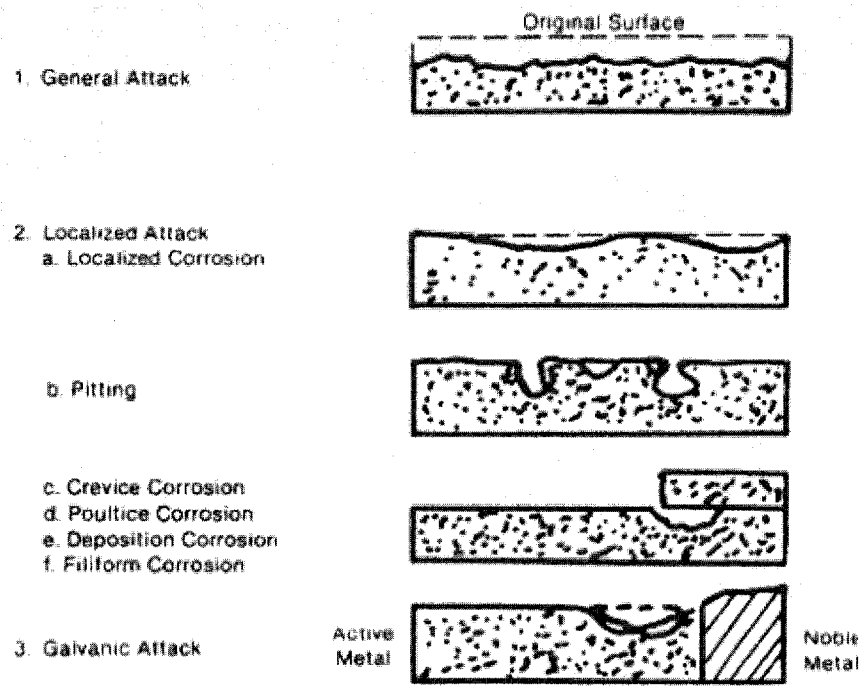

Fig. 2.4 Corrosion schematics [Brasunas, 1984]

Pitting corrosion can be particularly severe in chloride environment, since chloride ions help dissolve irons, and then get recycled back into solution to maintain high chloride concentration.

The following equations demonstrate the recycling of chloride ions:

Dissolution of iron by chlorides: $Fe + 2Cl^- \longrightarrow FeCl_2 + 2e^-$

Dissolution of iron chloride by water: $FeCl_2 + 2H_2O \longrightarrow Fe(OH)_2 + 2Cl^- + 2H^-$

Deposition of rust-ferric oxide and release of ions and back into solution:

$6FeCl_2 + O_2 + 6H_2O \longrightarrow Fe_3O_4 + 12Cl^- + 12H^-$

Chloride ions penetrate the oxide layer at certain position and establish a pit, where the PH is lower and the corrosion attack is severer. The low PH will keep the corrosion products in solution. The corrosion products, ferrous hydroxide and other solid corrosion products, will form in the regions that are rich in hydroxides and oxygen. Pitting corrosion is therefore very dangerous in practice, since the corrosion attack is concentrated to very small areas and since it may take place unnoticed from the outside. Since the corrosion products are soluble in the local acid pit, they can be accommodated without any spalling of the concrete cover [Sandberg, 1995].

2.1.3 Stages of corrosion

The state of corrosion of steel in concrete is function of time. It is divided to the initiation period and corrosion period, which consists of depassivation, propagation of corrosion, and final state. In the initiation period, environmental changes in concrete, such as penetrations of carbonation and chloride, gradually decrease and eventually

terminate the passivity of steel. The corrosion period begins at the depassivation and propagates at a significant rate until the final state is reached [Schiessl, 1988].

Depassivation is a critical period of corrosion stages. It occurs when the passivation provided to the steel by the alkaline hydrated cement matrix is destroyed either locally or generally. Reduction of alkalinity and the presence of aggressive ions in sufficient concentration lead to the destruction of passivity [Schiessl, 1988]. In the high chloride concentration environment, chloride ions will penetrate the passive oxide layers and initiate active corrosion.

The oxide layers of steel reinforcement embedded in concrete are scale, passive film and iron oxide layer (Fig. 2.5). The scale formed by the hot-rolling process is approximately 50 microns thick. The composition of scale is not very different from the oxide layer formed in alkaline solution. The oxide film on ordinary steel in alkaline environment is very thin, about 1-5E-3 microns thick. The composition of the oxide film mostly is Fe_3O_4 and Fe_2O_3, but it depends on the chemical environment such as pH and oxygen. The iron oxide layer formed in old concrete is usually regarded "semi-passive" due to its inhomogeneity and ion permeability. The thickness of the oxide layer can be up to hundreds of microns and grows with time. Such a thick oxide layer is normally considered to have a less efficient passivation than ideal thin layers [Sandberg, 1995].

The depassivation period extends to propagation period when the corrosion products want to develop outward, accompanying with the breakdown of oxide layers. The propagation

period extends from the form of corrosion products to the cracking and spalling of concrete cover or the local attack on the reinforcement becomes sufficiently severe to impair its load-carrying capacity. The final state is reached when damage due to cracking or spalling, the structural integrity, serviceability or appearance becomes unacceptable [Schiessl, 1988]

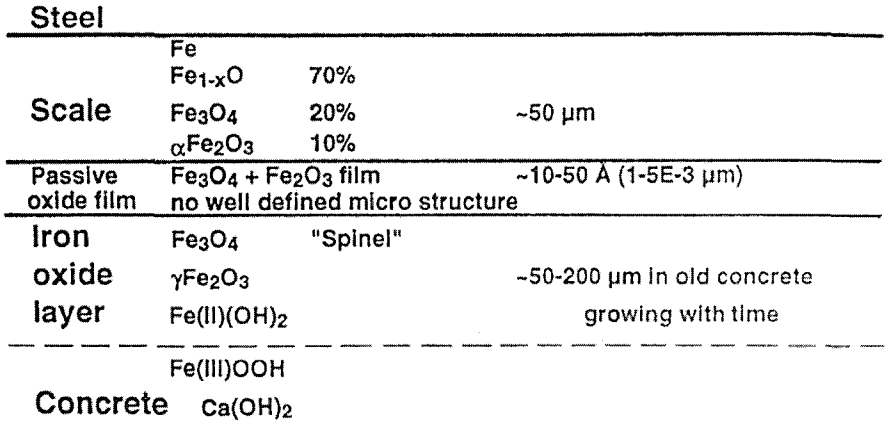

Fig. 2.5 Initially separated iron oxide phases on ordinary steel in concrete [Sandberg, 1995]

2.1.4 Corrosion processes that create acoustic emission

Corrosion processes produce elastic energy wave in the form of acoustic emission. AE waves are theoretically emitted from the following corrosion processes (Fig. 2.6):

- Depassivation of oxide layers, described in previous section, is the initiator of AE
- Exfoliation of steel layers generates large amount of AE waves.
- Dissolution of metal can create AE waves, but it is debatable to sense these waves based on current technology [Geng, 2002].

- Cracking and plastic deformation due to stress are also the sources of AE waves.
- Debonding at the interface between rebar and concrete when the expanding stress built–up by corrosion products.
- Microcracking of concrete may occurs with debonding when corrosion products formed on a corroding rebar push out the surrounding concrete.

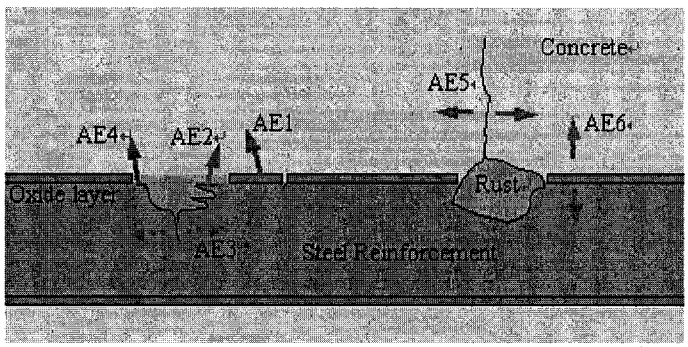

AE1:Depassivation and breakdown of oxide layer
AE2:Exfoliation of steel layers
AE3:Cracking / plastic deformation of steel under stress
AE4:Dissolution of metal
AE5:Cracking of concrete
AE6:Debonding at the concrete-steel interface

Fig. 2.6 Schematic illustration of AE created by corrosion in RC structures

2.1.5 Accelerated corrosion

Corrosion of steel in reinforced concrete is usually a very slow process. It may take years before the damage can be seen. For research purposes, corrosion in the laboratory is often accelerated in order to have manageable time frame for testing. According to the mechanism of corrosion, the following method is proved to be most effective.

Current is imposed to the sample and cathode to accelerate sample (anode) releasing electrons and cathode gaining electrons (Fig. 2.7).

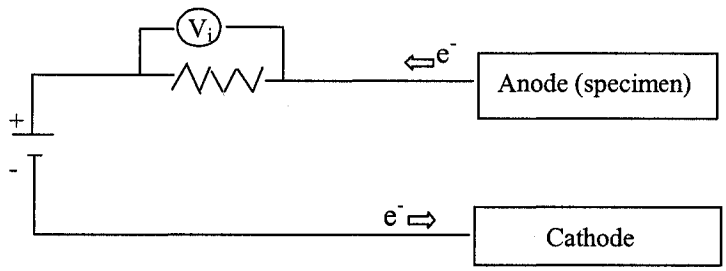

Fig. 2.7 Schematic sketch of accelerated corrosion cell

The accelerated corrosion requirements are

- Applying DC voltage usually is from 6 V to 12 V, the current in reinforced concrete usually is from 60mA to 120mA and the current in rebar alone usually is from 0.6 A to 1.1 A.
- Providing much larger surface area of cathode than that of anode, more than ten times
- Exposing specimens to high humidity environment i.e. wet-dry cycling, ponding.
- Supplying of sufficient chlorides by adding salt directly into the mixing water, or by ponding specimens in a chloride solution.
- Supplying of sufficient oxygen via wet-dry cycling

The research of accelerated corrosion conducted by University of Toronto for ISIS projects is taken as a reference [Lee, 1998].

2.2 Testing / Measuring of Corrosion in RC Structures

2.2.1 Electrochemical methods

The electrochemical methods commonly used in corrosion detection are Half-cell Potential Mapping, Polarization Curve, Polarization Resistance, A.C. Impedance, Electrical Resistance Probe and Electrochemical Noise. Their descriptions, advantages and disadvantages are as follows: [References for the following are taken from Scchiessl, 1998; Coitis, 2002; Tonini, 1980].

- Half-cell potential mapping

Half-Cell Potential Mapping, first developed in 1950's, is most common and convenient in use. It compares the electrode potential of the steel in concrete with that of a reference electrode, which usually is silver/silver chloride, copper / copper sulphate (CSE) or saturated calomel (SCE). The mechanism of half-cell potential is described in Section 4.8. The advantages are inexpensive, simple to perform, whole structure quickly surveyed and straightforward data analysis. The limitations are: (i) limited information for potentials between –200 and –350mV CSE; (ii) no information on corrosion rate; and (iii) depends on the condition of concrete e.g. difficult to perform when contaminants present on or in concrete.

- Polarization curve (Tafel plot)

In this technique, there are three electrodes, a working electrode (steel under test), a counter electrode and a reference electrode. The potential applied to the embedded steel

and the counter reference is at a level of several hundred millivolts. By finding corrosion current, the mass loss of steel can be determined and then the corrosion rate can also be determined assuming anodic area is known. The major advantage of polarization curves is that this technique gives information about the steel's behavior at potentials rather than the immediate corrosion potential [Hansson, 1986]. The major disadvantages of the polarization curve technique are: (i) it takes a long time to perform; and (ii) the polarization will change the environment at the steel-concrete interface, such a measurement will not accurately reflect the behavior of the steel in its natural surroundings and that the test cannot be regarded as non-destructive.

- Polarization resistance (Linear polarization)

This technique is similar to polarization curve, but with much small scan potential. The current vs. potential is linear. The advantages of this technique are rapid test, relatively inexpensive, simple to perform and corrosion rate determined. The limitations of the polarization resistance technique in general are: (i) area of steel under test must be known; (ii) IR drop; and (iii) the Tafel slopes are unknown or vary from time.

- A.C. impedance

In A.C. impedance measurement, an AC signal (typically, 10 to 20 mV) is applied to the steel-concrete system and the modulus of impedance and phase shift is considered over a range of frequencies (typically 100 kHz to 1 MHz). The advantages are that information relating to corrosion mechanism can be established and corrosion rate can be determined. The limitations of this technique are long test duration, difficult to measure corrosion rates,

high equipment costs and complex data processing.

- Electrical Resistance Probe

This technique is based on electrical resistance measurements on thin steel sections embedded in the concrete. As the resistance of steel is inversely proportional to its diameter, when corrosion proceeds, the steel becomes thinner and its resistance shows a corresponding increase. The advantages of this technique are inexpensive, simple to perform, straightforward data analysis and corrosion rate determined. The limitations are that it is unsuitable for pitting, only provides information locally at probe position, and probe installation is preferable during construction.

- Electrochemical Noise

Small fluctuations in corrosion potential are related to the presence and nature of corrosion on the reinforcing steel surface. The major advantage of this technique is non-perturbative because no potential or current is applied to the steel. The disadvantages are long test duration, no quantitative results and high equipment cost etc. [Hansson, 1986].

2.2.2 Non-electrochemical methods

- Visual Inspection and Microscopic Observation.

The visual or microscopic observation of concrete surface may provide approximate information about the severity of corrosion attack. But this information is not sufficient because it may lead to erroneous and subjective conclusions and usually must be completed with other tests e.g. core sampling. Furthermore, this method provides corrosion detection only after significant corrosion has occurred [Zdunek et al, 1995; Schiessl, 1988]

- Weight Loss

Weight loss can accurately quantify a corrosion attack. But it is only applicable to the laboratory.

- Infrared thermography

Infrared thermography has been used to measure the surface temperature of the concrete. As the concrete heats and cools during daily cycle, the delaminated areas interrupt the heat transformation and result a difference in surface temperature of concrete [Schiessl, 1988]. This method has less success and very low level of application.

- Radar

Ground Penetrating Radar (GPR), also called Short-pulse Radar, uses electromagnetic wave to access integrity and thickness of concrete and other structures. It is the

electromagnetic analog of sonic methods. The GPR instrument consists of a recorder and a transmitting and receiving antenna. GPR is most commonly used for evaluating concrete or asphalt roadbed surface. For concrete structure, GPR can be used to map the rebar and tendons as well as locate voids underneath slabs. However, it is seldom used for corrosion detection [Malhotra, 1991].

- Radiography

This method involves producing high-energy X-ray or Gamma-ray beams to produce a high- resolution picture of the object. Radiography produces the high quality NDT imagine of the interior structure of concrete. It can locate rebar, post-tensioned cable and conduit. But this method requires extensive safety precautions and, therefore, is impractical for many in-service structures. The high initial cost and the immobility of the testing equipment have also been the main limitations [ACI Committee 224, 1993].

2.2.3 Summary

The foregoing methods are valuable for corrosion detection, but most of them have low level of real application in-situ due to their respective limitations. Table 2.1 shows that only half-cell potential and visual inspection got high level of application in real world.

Table 2.1 Summary of the techniques used to study the corrosion of steel in concrete [Schiessl, 1988]

Techniques		Actual Level of Application		Indication on the Level of Corrosion
		In Lab.	On-site	
Electro-chemical	Half-cell Potential	High	High	Qualitative
	Concrete Resistivity	Medium	Low	Semi-qualitative
	Reinforcement Resistivity	Low	Low	Semi-qualitative
	Polarization Resistance	Medium	Very low	Qualitative
	Impedance	Low	Very low	Qualitative
	Elect. Noise	Very low	Very low	Semi-qualitative
Non-Electro-chemical	Visual inspection	High	High	Qualitative
	Weight Loss	Low	---	Qualitative
	Infrared Thermograghy	Very low	Very low	Qualitative
	Radar	Very low	Very low	Qualitative
	Radiography	Very low	Low	Qualitative

Several electrochemical methods are applicable to metal in solution, but the validity to determine the corrosion of steel embedded in concrete is uncertain [Mannning, 1986].

Limitations over both electrochemical and non-electrochemical methods are time-consuming, localized detection and unable to provide continuous detection. Methods using sonic technique are introduced in Section 2.3.

2.3 NDT Methods in RC Using Sonic Technique

The oldest sonic methods for corrosion detection in RC can be traced to the use of hammer sounding and chain drag sounding. These two methods depend on experiences and only detect large size flaws. Ultrasonic techniques and acoustic emission technique use or detect sonic waves in the ultrasonic ranges.

2.3.1 Ultrasonic techniques

- Ultrasonic Pulse Velocity (UPV)

This technique involves measuring the travel time of ultrasonic pulses through material with a know thickness. It uses the relationship between the quality of concrete and the velocity of an ultrasonic pulse to predict the strength of early stage concrete. UPV is good for investigating the uniformity of concrete [Malhotra, 1991]. Voids honeycomb, cracks, and other damage to concrete can also be located.

This method has provided in-situ measurements of the severity and area of deterioration, and assessment of the condition of concrete structure. The equipment can produce ultrasonic waves that penetrate over 90 m of continuous concrete with the aid of amplifiers or up to 7.5 m without amplifiers [Rosh, 2003]. The major limitations of the method are the requirement of two-sided access of the tested object and the influence of steel reinforcement.

- Impact-Echo (IE)

The IE tests are based on the reflection of compressional waves from the bottom of the structure member or from flaws. A stress pulse is introduced into the structure from a hammer or other impact instrument. An ultrasonic transducer on the surface of the structure receives the resulting stress waves. These stress waves travel several times between the surface and the voids or delaminations that may exist in the structure. The distance from the surface of the structure to the void or delamination can be determined by the pulse velocity in the material, and the observed resonant frequency, particularly in plate-like structures (e.g. pavements) where the void tends to be parallel to the structure surface. However, smaller cracks and discontinuities are more difficult to detect with this technique due to the relatively low frequencies involved [Landis et al, 1994].

- Spectral Analysis of Surface Waves (SASW)

This method is based on the propagation of mechanically induced surface waves; it utilizes a property of surface waves that the dispersion of the surface wave is a function of the material properties at different depths. The technique has been successfully applied to evaluation of airport runway pavements. Attempts have been made to adapt the technique to concrete structures [Landis et al, 1994]. In SASW analysis, a surface wave is generated on the structure using an impact source similar to that used in the impact-echo technique. Two in-line transducers a certain distance away from the source then measure the surface wave. The waveforms measured at each transducer can then be analyzed to

determine the frequency-dependent dispersion of the surface wave. From the dispersion curve, the elastic profile for the structure can be estimated.

This method measures the layer thickness as well as stiffness, and requires only one-side access. However, it is only suitable for thin structures such as pavements and slabs. SASW does not isolate fundamental mode Rayleigh waves in determining the velocity dispersion curves. For investigations of reinforced concrete structures, the presence of rebar will probably influence the data [Rosh, 2003].

The above ultrasonic techniques are used for either assessing the uniformity, thickness and quality of concrete or indicating the presence of voids and cracks. But they are unable to measure reinforcement corrosion itself.

2.3.2 Acoustic emission

Acoustic Emission is unique over other sonic techniques because the stress waves are generated by the tested structure itself rather than an external source.

The AE technique is based on the detection of high frequency elastic waves emanating from the source by converting them into electrical signals. This is accomplished by directly coupling transducers (usually of piezoelectric type) on the surface of the structure under test to 'listen' to a wide range of events that may take place inside. The output of the sensors is amplified through a low-noise preamplifier, filtered to remove any extraneous noise and further processed by suitable electronics [Kishi et al, 2000].

AE technique has been widely used in many industrial areas in recent decades. AE has been commercially available for forty years. The applications include detection or monitoring of structural integrity and micro-crack of concrete, crack of mine and rock, faults or leakage in pipeline and tanks, corrosion and stress corrosion, pressure vessels, aircraft, welding defect and fatigue damage [Ian, 1991; Williams, 1980].

The up-to-date research in AE technique of reinforced concrete is mostly limited to crack growth and location [Kishi et al, 2000; Malhotra, 1991], however, research of using AE for corrosion detection in concrete has been conducted by Northwestern University in 1995 [Zdundek et al, 1995]. Idrissi H. et al did another research in 2003.

- AE monitoring corrosion in RC structures

The study of AE monitoring corrosion in concrete can be divided to three stages: AE source, wave propagation and AE instrumentation (Fig. 2.8). The AE source has been described in Section 2.1.4. Depassivation is supposed to be the first process that creates AE events. The wave propagation and AE instrumentation are presented in Section 2.4 and Section 2.5.

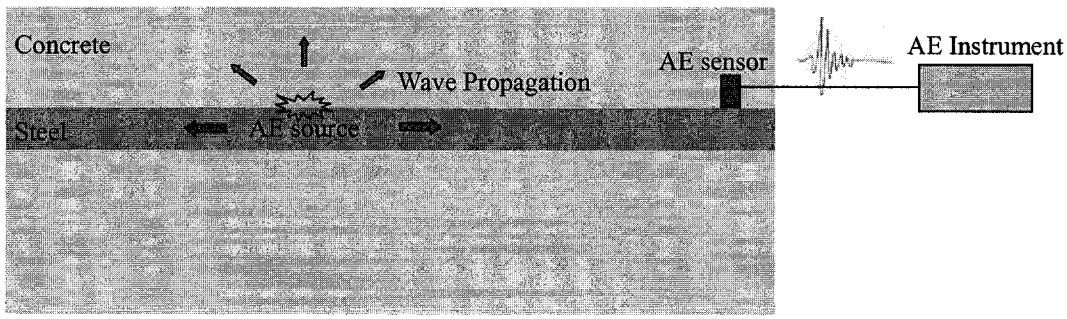

Fig. 2.8 Schematic illustration of AE monitoring corrosion in RC structures

The spectrum of AE for engineering practices is typically from 20 KHz to 1 MHz, sometimes up to 2MHz. Higher frequencies are limited by attenuation and low frequencies may be contaminated by noise. Fig. 2.9 shows how the frequencies met in AE signals compare with those used in ultrasonic NDT and other applications.

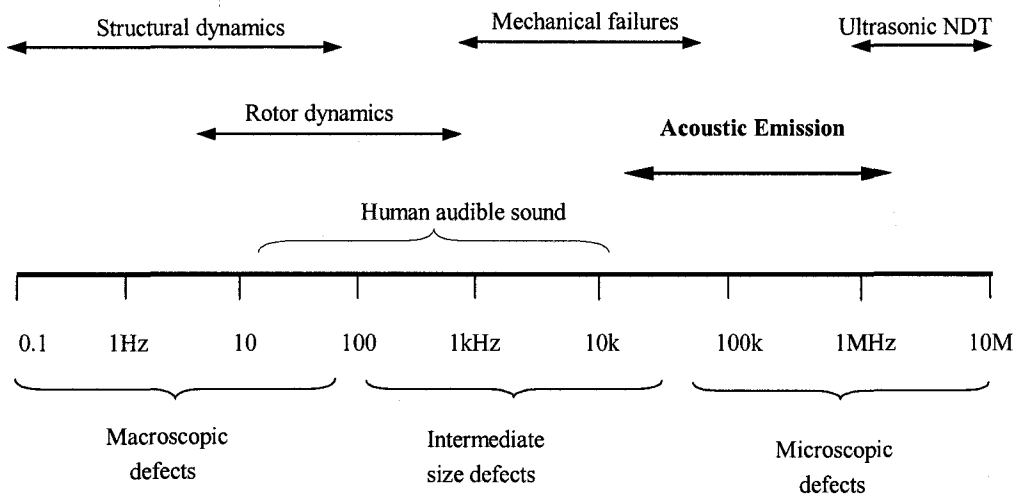

Fig. 2.9 Spectra of AE and others [Williams, 1980]

- Advantages of AE technique

"One of the key advantage of AE over other nondestructive test methods is the fact that it detects signals in real-time that are emanating from the materials themselves" [Carlos, 2003]. It is supposed that the major advantages of AE technique use for corrosion detection in reinforced concrete are: real-time monitoring structures; triggered by internal activity; detecting corrosion from its early stage; long-term and long-distance monitoring in-service structures under any weather condition; and detecting the position where the traditional techniques are unable or difficult to reach.

2.4 Wave Transmission

To understand how acoustic waves travel in steel and concrete and what is the difference of waves traveling in these two media, the theory of wave transmission has to be reviewed.

2.4.1 Wave theory

Acoustic emission fundamentals and wave equations

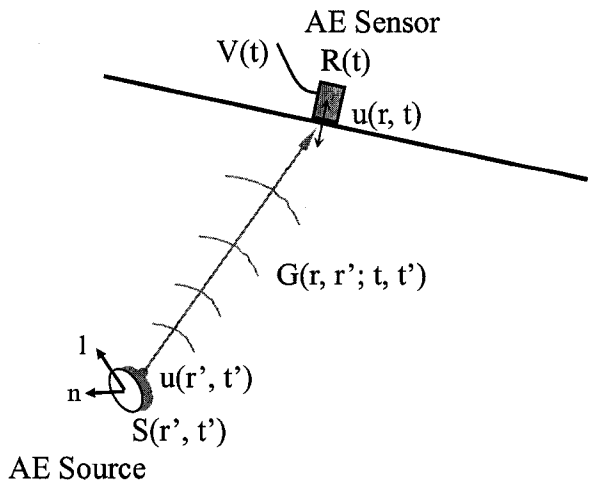

Fig. 2.10 Schematic of AE source and Green's function

A micro-crack (l-n) creates moment tensor at an AE source (r', t') with source function S(r', t'). The Green's function is the appropriate transfer function for the medium to convolute the source tensor to obtain the displacement u(r, t) of point r at time t due to an impulse force applied at x' at time t' [Scott, 1991; Vahaviolos, 1999].

The sensor output V(t) is function of u(r, t) by sensor's response function R(t). Therefore,

in a simplified way, the sensor output can be written as V(t) = S(t) * G(t) * R(t), and the displacement can be written as u(r, t) = S(t) * G(t), where S is the source function, G is the Green's function, and R is sensor's response function [Ian, 1991; Landis, 1995]. The Green's function is related to the material properties of a wave propagation medium. The following 3-D wave equations present the mathematical expressions for the displacement convoluted by this function.

The one-dimensional wave equation (with no source term) is [Pain, 1999]:

$$\frac{\partial^2 u}{\partial x^2} = \frac{1}{c^2}\frac{\partial^2 u}{\partial t^2} \qquad \text{(Longitudinal wave)}$$

The general solution, known as D'Alembert's solution, is

$$u(x,t) = F(x - ct) + E(x + ct)$$

For transverse wave, u(x, t) should be y(x, t). F(x-ct) represents forward solution and E(x+ct) backward.

The 3-D wave equation (with source term) is [Fitzpatrick, 2002]:

$$(\nabla^2 - \frac{1}{c^2}\frac{\partial^2}{\partial t^2})u = S(r',t')$$

Where ∇^2 is the Laplacian operator; c is the group velocity; Waves travel outwards from point where S(r', t') is non-zero towards infinity.

Applying the Green's function G(r, r'; t, t'), the transfer function for the medium to obtain the displacement u(r, t) that generated by a point impulse located at position r' and applied at time t', the wave equation can be written as:

$$(\nabla^2 - \frac{1}{c^2}\frac{\partial^2}{\partial t^2})G(r,r';t,t') = \delta(r-r')\delta(t-t')$$

The solution of displacement at point r at time t is [Fitzpatrick, 2002]:

$$u(r,t) = \iint G(r,r';t,t')S(r',t')d^3r'dt'$$

The Green's function is based on linear system assumption i.e. the elastic behavior of the medium. In other words, the Green's function depends on the elastic properties of the material and the geometric relationship between the source and the sensor. Once the elastodynamic Green's function is determined it can be used to evaluate the ultrasonic properties of the material [Landis, 1995]. Landis presented that the velocities of the P- and S-wave components can be directly estimated from a plot of Green's function using the arrival times at the sensor. Theoretically, the attenuation can be evaluated by comparing the Green's function of the actual material to that of a reference non-attenuative ideal material.

Wave modes

In solids, acoustic waves can propagate in four principal modes that are based on the way the particles oscillate. They can propagate as longitudinal waves, shear waves, surface waves, and in thin materials as plate waves [Pain, 1999; Dual, 2003].

In longitudinal waves (P-Wave), the oscillations occur in the longitudinal direction or the direction of wave propagation. Since compressional and dilatational forces are active in these waves, they are also called pressure or compressional waves. Group velocity for

longitudinal wave in homogenous, isotropic and linearly elastic bulk solid is [Frederick, 1965]:

$$c_p = \sqrt{\frac{E(1-\nu)}{\rho(1+\nu)(1-2\nu)}}$$

Group velocity for long thin rod with diameter $< 0.1\lambda$:

$$c_p = \sqrt{\frac{E}{\rho}}$$

In transverse or shear wave (S-Wave), the particles oscillate transverse to the direction of propagation. Shear waves require solid materials for effective propagation and, therefore, are not effectively propagated in liquids or gases. Shear waves have lower speed than longitudinal waves [Frederick, 1965].

$$c_S = \sqrt{\frac{G}{\rho}} = \sqrt{\frac{E}{\rho}\frac{(1-2\nu)}{2(1-\nu)}}$$

By comparison, transverse (S-) wave and longitudinal (P-) waves also have the following two major differences: (i) the Poisson's ratio being always between 0 and 0.5 causes S-wave to travel at speed between 0-0.7 of the P-wave; and (ii) S-wave has a shorter wavelength than P-wave [Bedford, 1994].

Surface - Rayleigh waves travel the surface of a relative thick solid material within a depth of one wavelength. The particle movement has an elliptical orbit.

$$c_r = \frac{0.87+1.12\nu}{1+\nu} \cdot c_S = \frac{0.87+1.12\nu}{1+\nu}\sqrt{\frac{G}{\rho}} = \frac{0.87+1.12\nu}{1+\nu}\sqrt{\frac{E}{\rho}\frac{(1-2\nu)}{2(1-\nu)}}$$

$$c_r = 0.9 \cdot c_S = 0.9\sqrt{\frac{G}{\rho}}$$

The velocity of surface wave is similar with the velocity of transverse wave. It can be calculated from the above equations [Malhotra et al, 1991]. Surface wave –Love wave is possible in a thin layer of material lying on a substrate. The direction of vibration of the particles of the layer is parallel to the surface, but transverse to the direction of wave propagation.

- Lamb wave

Lamb waves (Plate waves) can propagate only in very thin metals. Lamb waves are the most commonly used plate waves in NDT. Lamb waves are a complex vibrational wave that travels through the entire thickness of a material. Lamb waves are essentially combined by longitudinal wave and transverse wave. Propagation of Lamb waves depends on density, elastic, and other material properties, and they are greatly influenced by the frequency and material thickness. With Lamb waves, a number of modes of particle vibration are possible, but the two most common are symmetrical and asymmetrical. The complex motion of the particles is similar to the elliptical orbits for surface waves [Kinsler, 1982]. The group velocity of Lamb wave depends on type and mode as shown in the following figure. S_0, S_1, S_2 ... are symmetrical modes; A_0, A_1, A_2 ... are asymmetrical modes.

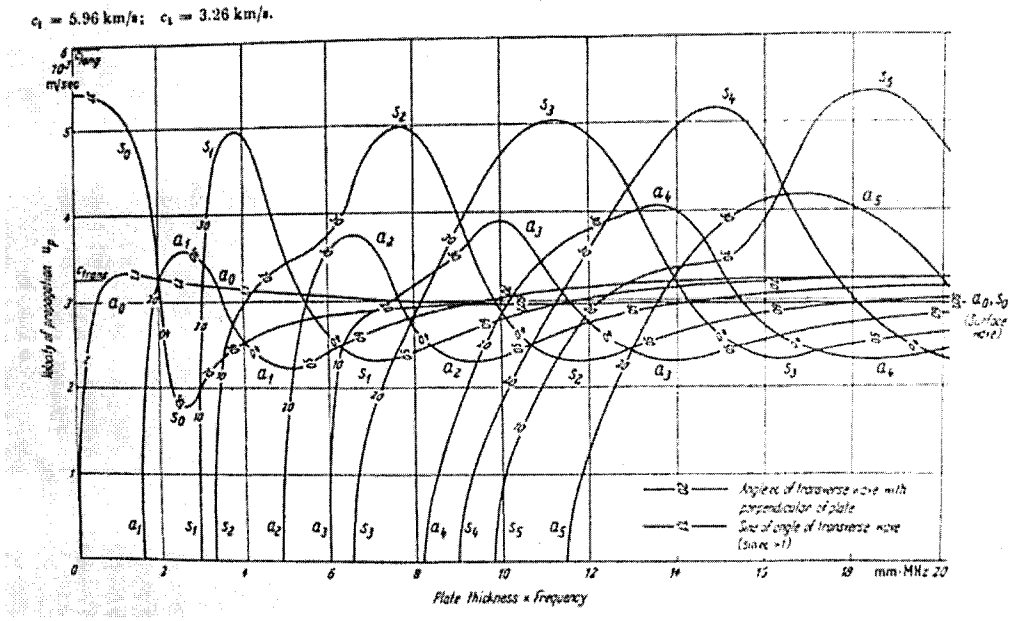

Fig. 2.11 Velocity of propagation of lamb waves in steel to the multiplicity of modes [Ian, 1991]

- Summary

Table 2.2 summarizes the various wave mode presented in the above discussion.

Table 2.2 Summary of wave modes

Wave Types	By name	Particle Vibrations		Solid medium
Longitudinal	Pressure, compressional	Parallel to wave direction		Thickness larger than wave length
Transverse	Shear	Perpendicular to wave direction		Thickness larger than wave length
Surface - Rayleigh		Elliptical orbit - symmetrical mode		On the surface of a solid
Surface - Love		Parallel to plane layer, perpendicular to wave direction		A thin layer of material lying on a substrate
Plate	Lamb	Sym.	At surface: elliptical orbit At center: Similar to longitudinal wave.	Thickness is comparable to the wavelength
		Asym.	At surface: elliptical orbit At center: Similar to transverse wave.	Thickness is comparable to the wavelength

Wave propagation in isotropic solid materials is defined by the wavelength, the frequency, and the velocity. The wavelength is directly proportional to the velocity of the wave and inversely proportional to the frequency of the wave. This relationship is shown by the following equation: Wavelength (λ) = Velocity (v) / Frequency (f)

Table 2.3 Acoustic properties for some common materials [Turner, 1991]

Material	*Young's Modulus* (N/m^2)	*Density* (kg/m^3)	*Wave velocity* (m/s)	*Characteristic impedance* (Ns/m^3)
Nickel	2.2×10^{11}	8800	4970	4.4×10^7
Steel	2.1×10^{11}	7800	5200	4.1×10^7
Aluminium	6.9×10^{10}	2720	5030	1.4×10^7
Glass	6×10^{10}	2400	5000	1.2×10^7
Concrete	3×10^{10}	2400	3500	8.4×10^6
Lead	1.7×10^{10}	11400	1230	1.4×10^7
Hardwood	1×10^{10}	600	4000	2.4×10^6
Nylon	2×10^9	1140	1320	1.5×10^6
Water	2.3×10^9	1000	1500	1.5×10^6
Mineral oil	1.6×10^9	800	1400	1.1×10^6
Air	1.4×10^5	1.2	340	407

The velocities on Table 2.3 are group velocities for longitudinal waves. The relationship between the group velocities and the phase velocities can be simply grasped as phase velocity = $dc_{group}/d\omega$, where c_{group} is group velocity and $\omega = 2\pi x$ frequency [Frederick, 1965]. The velocity with which energy is propagated down the plate (the group velocity) may be calculated from phase velocity [Fitting, 1981]. Longitudinal wave travels at the

highest speed of all modes. The speeds of waves with different modes in concrete and steel are listed in Table 2.4.

Acoustic Impedance, an important parameter, is defined as:

$$Z = \rho c$$

Where Z is acoustic impedance; c is wave velocity and ρ is density of medium

The important relationship is that the pressure and velocity are directly proportional to one each other for any waveform at any instant as following equation [Turner, 1991]:

$$p = \frac{\partial u}{\partial t} \rho c$$

Where p is the pressure.

Acoustic Intensity is defined as $I = p^2/2\rho c$, where p is pressure and ρc is acoustic impedance, or $I = \rho c(\omega\xi)^2/2$, where $\omega$is frequency and $\xi$is the maximum amplitude of particle vibration [Frederick, 1965].

The energy distribution of corrosion AE source at the steel-concrete interface can be derived from the comparison of acoustic intensities of steel and concrete. In the source where AE wave is generated, the amplitude of the AE wave in concrete or in steel at the interface is assumed constant. Thus, the ratio of I_{steel} and $I_{concrete}$ is equal to the ratio of their acoustic impedances, which is approximately 5:1. As a result, steel reinforcement carries approximately 83% energy of an AE wave that generated at the steel-concrete interface from the corrosion source.

Reflection, refraction and mode conversion

- Reflection and refraction

When an AE / ultrasonic wave passes through an interface between two materials at an oblique angle, and the materials have different indices of refraction, it produces both reflected and refracted waves. This also occurs with light. The reflection angle and incident wave angle are always equal. The angle of refraction follows Snell's law:

$$\frac{\sin\theta_1}{V_{L1}} = \frac{\sin\theta_2}{V_{L2}}$$

Where V_{L1} is the longitudinal wave velocity in material 1; V_{L2} is the longitudinal wave velocity in material 2. An important angle is Critical Angle of incidence θcr. Over this angle, all of the wave energy is reflected back.

$$\sin\theta_{cr} = \frac{c_1}{c_2}$$

Table 2.4 shows the critical angles of waves in steel surrounded by concrete. The velocities are given by NDT Resources Center website www.ndt-ed.org (accessed Oct. 20, 2003). The critical angels are calculated from given velocities. Velocity in concrete 3500 m/s is taken from Table 2.3.

Table 2.4 The velocities and critical angles in steel and concrete

Wave	Longitudinal wave	Transverse wave	Surface wave
Velocity in 4340 steel (m/s)	5200 in bar or rod 5850 in bulk	3280	3018
Velocity in concrete (m/s)	3500*	1440	1320
Critical angle (degree)	42.3 in bar	26.0	25.9

Wave energy reflection coefficient R can be written as:

$$R = \left[\frac{Z_2 - Z_1}{Z_2 + Z_1}\right]^2$$

Where Z is the acoustic impedance. This equation applies when the direction of wave propagation is normal to the boundary. The sum of percentages of transmitted energy and reflected energy always equal to one.

- Mode Conversion

When sound travels in a solid material, one form of wave energy can be transformed into another form. For example, when a longitudinal wave hits an interface at an angle, some of the energy can cause particle movement in the transverse direction to start a shear (transverse) wave. Mode conversion occurs when a wave encounters an interface

between materials of different acoustic impedance and the incident angle is not normal to the interface.

When a longitudinal wave is reflected inside the material, the reflected shear wave is reflected at a smaller angle than the reflected longitudinal wave due to the fact that the shear velocity is less than the longitudinal velocity within a given material.

Mode conversion leads to a complex interaction and multiplication of the number and type of waves within materials. This process causes difficulties in wave analysis and signal interpretation [Santamarina, 1994].

Attenuation

Attenuation refers to the decrease in signal amplitude or intensity as it travels through a medium. In idealized materials, signal amplitude is only reduced by the spreading of the wave. However, natural materials all cause energy loss that further weakens the signal [Cherrouf et al, 2000]. The causes of attenuation can be divided into two general categories: geometric attenuation, scattering and absorption attenuation.

- Geometric attenuation.

This category takes into account the size of source and propagation medium, the wavelength, and the presence or absence of the nearby reflecting surface [Frederick, 1965]. Geometric attenuation is not associated with energy losses, but energy redistribution. The reason is that energy in the wave-front remains constant but the front spreads over a large area until reach the surface of reflection. As the energy is converted to larger area,

the amplitude must decrease. P-wave spreads over a spherical volume of space, the geometric attenuation is proportional to 1/radius. Surface wave travels more in a plane, the attenuation is proportional to 1/√radium [Cascante, 1996].

- Scattering and absorption mechanism

Scattering of waves is a result of material inhomogeneity. The waves break-up through reflection at a very uneven surface or small discontinuities. Scatter also results from reflections from one or more point reflectors, e.g., a cluster of inclusions. In this case the energy is lost, not by random reflection but by dispersal over a large, expanding wave front. For material with inhomogeneities that are very small compared to the wavelength, the attenuation from scattering is negligible. However, attenuation increases approximately with the third power of the grain size. Scattering becomes significant as the size of inhomogeneity becomes 1/10 of the signal wavelength. Scattering produces a large number of echoes or false signals; the true signal may be lost. In the anisotropic material, the scattering may be so severe that the testing and data analysis are very difficult [Krautkramer, 1990].

Absorption is the component of ultrasonic wave attenuation resulting from conversion of ultrasonic energy into other forms of energy such as heat energy. This type of attenuation can be visualized as "braking" or resistance of particle oscillations. The concept also can explain why high frequency oscillations lose energy more quickly than slow oscillations [Krautkramer, 1990]. In general, the energy loss increases with increasing frequency, but a few are independent of the frequency [Frederick, 1965].

- Attenuation coefficient

Attenuation coefficient of a decaying plane wave is expressed as [Blitz, 1964]:

$$A = A_0 e^{-\alpha z}$$

In this expression A_0 is the amplitude of the propagating wave at some location. The amplitude A is the reduced amplitude after the wave has traveled a distance Z from that initial location. The quantity α is the attenuation coefficient of the wave traveling in the z-direction. The dimensions of α are nepers/length, where a neper is a dimensionless quantity. The units of the attenuation value in nepers/length can be converted to decibels/length by dividing by 0.1151. Decibel is a more common unit when relating the amplitudes of two signals.

The equation of attenuation coefficient can be written as [http://www.ndt-ed.org, accessed Oct. 20, 2003]:

$$\alpha = \frac{\log(A/A_0)}{Z \times \log(e)} = [2.304 \times \log(A/A_0)]/Z \qquad \text{nepers / m}$$

Transfer to decibel scale by dividing by 0.1151:

$$\alpha = [20 \times \log(A/A_0)]/Z \quad \text{dB / m}$$

Or in power expression:

$$\alpha = [10 \times \log(PSD/PSD_0)]/Z \quad \text{dB / m}$$

Where Z is the distance from source to the point of measurement. PSD (Power Spectral Density) is presented in Section 2.5.2.

2.4.2 The difference in travel between steel and concrete

The different attenuation nature of steel and concrete determines their characteristics as acoustic medium. As presented in previous section, the grain size and homogeneity of materials as well as the frequency are the most important factors that greatly influence the attenuation coefficient.

Attenuation - steel

The attenuation coefficient for steel bar has not been found, but two references for steel pipe leak AE were found. For AE waves in steel bar, one AE signal contains a series waves with a range of frequencies. In time domain, the attenuation coefficient is an average value over the frequency range.

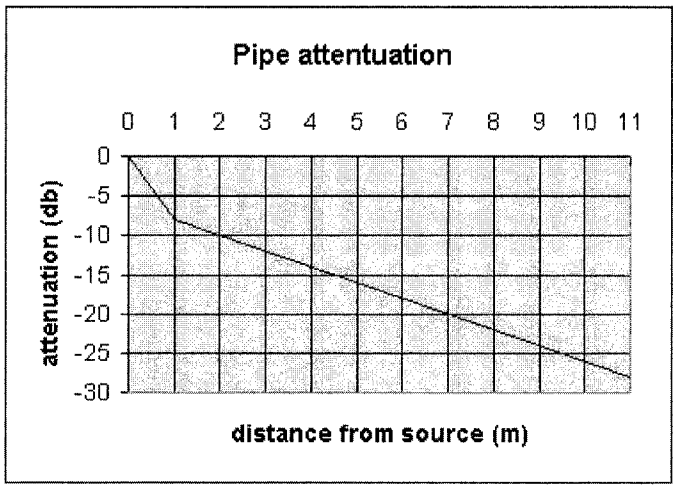

Fig. 2.12 Steel pipe attenuation of leakage AE

Attenuation coefficient of leak AE of steel pipe in Fig. 2.12 was obtained from Acoustic Emission Latin American Group (GLEA) of Comisión Nacional de Energía Atómica (National Commission of Atomic Energy, Argentina). This figure was measured by two

sensors with distance varied from 0 to 11 m [Acoustic Emission Reference Guide, http://www.cnea.gov.ar/cac/endye/glea/mateo/guide.htm, accessed Dec. 12, 2003]. The group velocity for this leakage AE was 3500 m/s. Some useful information can be learnt from this diagram: (i) near field is considered within one meter from source; (ii) attenuation coefficient is 7.5 dB/m at near field and 2 dB/m at far field (beyond 1m); and (iii) the attenuation coefficient in this diagram is an average number over the spectrum of leak AE.

Elias Stepanka found that "the steel attenuation was nearly constant across the frequency range (50-600KHz)". Another data shows steel pipe attenuation 18 decibels attenuation at a 3.658 m specimen with A_0 Lamb wave mode [Park, 1995]. The attenuation in steel pipe is taken as a reference for the study of the attenuation in steel reinforcement.

The following shows the relationship between attenuation and steel grain size and frequency. When the wavelength is much larger than the mean grain diameter, the attenuation coefficient in the Rayleigh region can be written as [Bounda et al, 2003; Pandey et al, 1996]:

$$\alpha(f) = a_1 f + a_2 D^3 f^4$$

Where $a_1$is absorption constant; a_2 is scattering constant; D is mean grain size and f is frequency. If the inhomogeneity of steel is very small compared to the wavelength of ultrasonic / AE wave, the second part of the equation is not significant. The attenuation is proportional to the frequency.

Attenuation - concrete vs. steel

Concrete is a composite heterogeneous material. Its particle and pore size range from nanometer to centimeter (inter-particle spacing between CSH sheets: 1-3 nm; coarse aggregate in size of cm). Reflection in concrete is very complicated phenomenon because of the varying moisture conditions, complex geometry of voids, aggregate, entrapped air and hydration products [Elias, 1998]. Only negligible part of a wave passes through the interface of an air-filled crack and concrete. Same crack filled with water would transfer about 10-25% of the wave energy [Galan, 1990]. Hardened concrete consists of very complex compounds, the various arrangements of hydration products e.g. CH crystals and CSH gel. The porosity of concrete greatly increases the energy loss of a wave. Thus, concrete has high attenuation from scattering and absorption.

In most reinforced concrete structures, concrete is bulk in volume compared with steel reinforcement. Reflections within the surface of steel reinforcement effectively reduce the energy loss of a wave in travel. Conversely the spreading of wave-front in concrete causes energy loss and, therefore, the wave amplitude decreases. So concrete has larger geometric attenuation than steel reinforcement in reinforced concrete structures.

In Elias' research [1998], a relative value MAC (Modified Attenuation Coefficient) was used. It was based on the logarithm of the ratios between reference and output:

$$MAC = -\log(V_{out}/V_{ref})$$

MAC values are defined as positive by multiplying the result from logarithm by the negative one. From Fig. 2.13, the smallest attenuation difference between steel and

concrete is approximately 1.2 MAC unit (Steel and AAR-2 at 50kHz); in linear scale the attenuation of concrete is 15 times higher than that of steel.

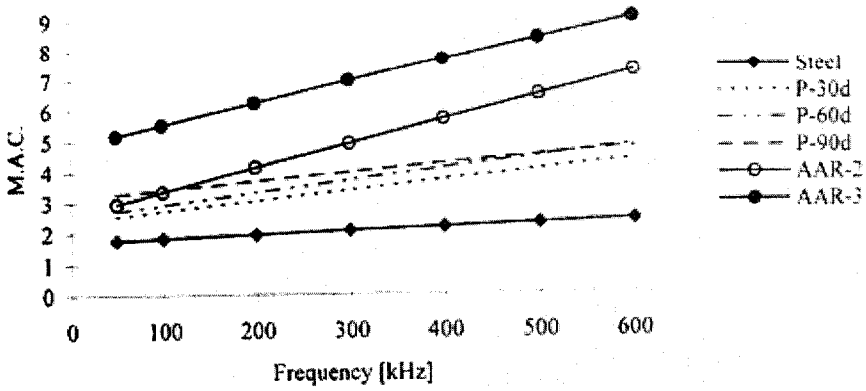

Fig. 2.13 Attenuation vs. Frequency – steel and concrete [Elias, 1998]

2.5 AE Instrumentation

AE systems vary from single-channel and purpose devices to complex multi-channel and multi-processing system. Fig. 2.14 shows a simplified multi-channel system. A typical AE system uses piezoelectric sensors coupled to the test object with a suitable coupling medium e.g. grease. The output of the sensors is amplified and filtered by pre-amplifiers and then sent to the AE processor via shielded coaxial cables. The processor further filters and amplifies the AE signals, processes the data, and displays the results. The results and data are recorded for instance analysis or transferred for post-test analysis via further signal processing [Carlos, 2003; Zdunek, et al, 1995].

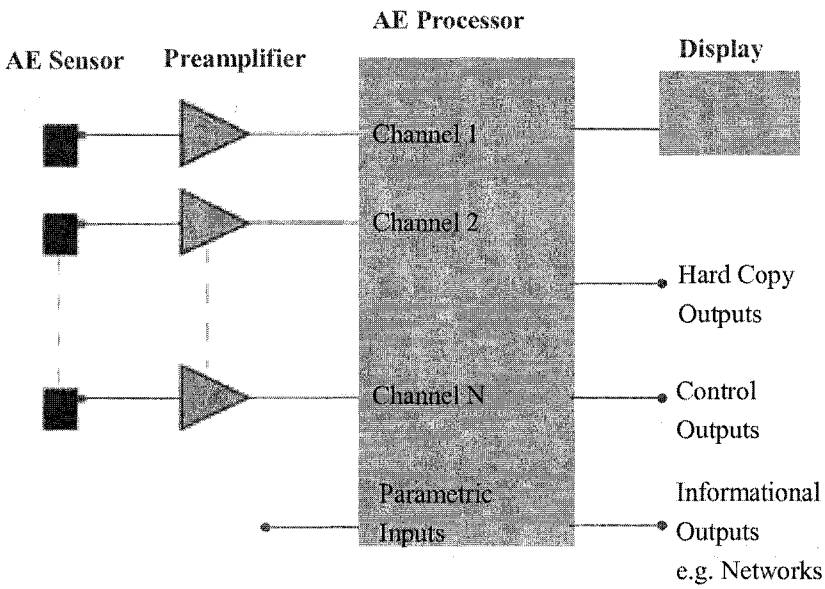

Fig. 2.14 Simplified block diagram of an AE system [Carlos, 2003]

2.5.1 Sensors

The AE sensor is a very important component of an acoustic emission testing system. The first step in taking AE measurement is converting surface displacement into a signal, which can be amplified, digitized and stored. Most AE sensors are of the piezoelectric type due to their very high sensitivities and the ease of coupling [Gautschi, 2002]. Presented here are sensitivity, structure, material, piezoelectric effect, characteristics, and selection of AE sensors, broadband and resonant sensors, calibration, sensors used for corrosion detection, and in addition the fiber optic sensors.

Sensitivity

Their limiting sensitivities of piezoelectric AE sensors are compared with laser interferometer and capacitor microphone on the following Table 2.6. High sensitivity of AE sensors enables the detection of the AE waves in very small magnitudes from corrosion activities.

Table 2.6 The limiting sensitivities of transducers [Ian, 1991; Matthews, 1983]

Type	Limiting Sensitivity (m) [Matthews]	Limiting Sensitivity (m) [Ian]
Broadband Piezoelectric	10^{-12}	10^{-12}
Resonant Piezoelectric	10^{-13}	10^{-13}
Laser Interferometer	10^{-11} ~10^{-12}	10^{-10}
Capacitor Microphone	10^{-12}	10^{-11}

Structure of piezoelectric AE sensors

The design of sensors varies from manufacturers, but the basic components are similar. They are piezoelectric element, wear plate, sometimes matching layer and backing material depending on the purpose (Fig. 2.15). Some sensors also come with a built-in amplifier or mounting bolt.

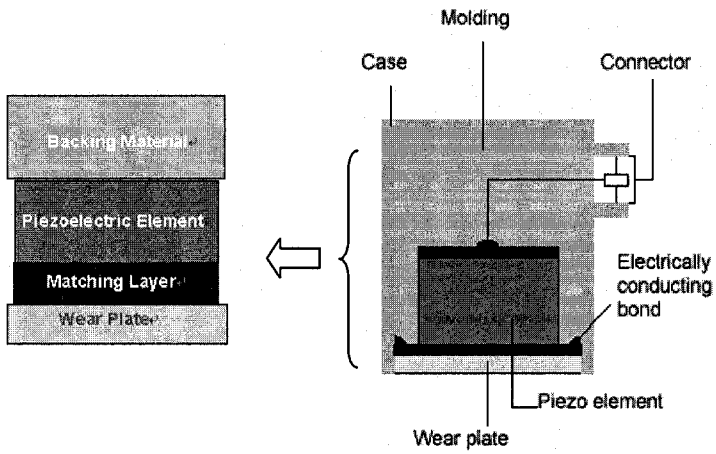

Fig. 2.15 Basic Setup of an AE Sensor [http://www.ndt.net/article/v07n09/05/05.htm, accessed July 14, 2003]

- Piezoelectric Element

The piezoelectric element is usually in shape of disk or cylinder with a thickness of a few mm. Similarly the diameter can be as small as 1mm, but usually is around 5mm. Basically there are three type of piezoelectric element (also called active element due to its electrical self-generation) for AE sensors: Disc element is most common in use and has good broadband characteristics. The thickness of the piezoelectric element is determined by the desired frequency of the transducer. The higher the frequency of the transducer, the thinner the piezoelectric element will be used. Sensor made by planar-concave element are said to have a constant linear sensitivity over an extended frequency range, but they are not in general use. The NBS conical sensor comprises a PZT element in form of

a truncated cone. Conical sensor refers to the small aperture, high fidelity AE sensor.

- Matching layer, wear plate and backing material

To get as much energy out of the transducer as possible, an impedance matching is placed between the active element and the face of the transducer to keep waves that were reflected within the matching layer in phase when they exit the layer. The matching layer is made from a material that has acoustical impedance between the active element and steel. However, some transducers do not have matching layers.

Contact transducers also often incorporate a wear plate to protect the matching layer and active element from scratch and for electrical isolation.

The backing material is often made of epoxy mixed with high-density (e.g. tungsten) particles before curing. The purpose is to let the acoustic waves pass readily into this backing material with as little reflection as possible, and to absorb the wave's energy by scattering the wave on the embedded particles. The backing material supporting the crystal has a great influence on damping characteristics of a sensor. For broadband-type sensors, the backing pad serves to load the piezoelectric element to make it less resonant and to obtain a wider frequency response of the sensor. But resonant transducers do not have backing material, or, in some special application, a backing material with impedance similar to that of the piezoelectric element is used to produce the most effective damping. Such a transducer (Resonant sensor) will have a narrow bandwidth resulting in higher sensitivity. The frequency noted on a sensor is the central or center frequency and

depends primarily on the backing material. Highly damped sensors will respond to frequencies above and below the central frequency [Gautschi, 2002].

Materials of piezoelectric element

The active element of piezoelectric transducers used today is usually a piezoelectric ceramics. Prior to the piezoelectric ceramic, piezoelectric crystals made from quartz crystals and magnetostrictive materials were primarily used. Piezoelectric ceramics became the dominant material for transducers due to their good piezoelectric properties and their ease of manufacture into various shapes and sizes [Gautschi, 2002]. Materials of piezoelectric element are listed as follows:

- Naturally piezoelectric materials:

  Quartz, tourmaline, Rochelle salt, lithium sulfate, lead niobate and artificially grown crystals of ammonium dihydrogen phosphate.

- Piezoelectric materials after special treatment (electrostrictive materials):

  - Barium titanate } Ferroelectric materials (Generally referred as "ceramic")
  - Lead zirconate-titanate (PZT)

  PZT4 & PZT5 are made by adding some amounts of various elements to PZT to improve their properties. Barium titanate and PZT5 are now the most commonly employed ceramic materials for making transducers.

- New materials- piezoelectric polymers:

  PVF &PVF2, PVC, NYLON 11 and Co-polymer of PVDF and TrFE membrane

  Piezoelectric polymers have large piezo constant g. They are supposed respond to the input signal in high fidelity for wide range of frequency with high sensitivity.

Piezoelectric effect

Piezoelectricity is understood as a linear electromechanical interaction between the mechanical and the electrical state in crystals. The direct piezoelectric effect occurs when a force is applied to a piezoelectric material producing an electrostatic charge, which can be amplified. The converse piezoelectric effect means that the piezoelectric material is deformed when an electric voltage is applied [Turner, 1991; Gautschi, 2002].

There are generally three types of piezoelectric effects: the longitudinal effect, the transverse effect and the shear effect. The type of piezoelectric effect is determined by the shape of piezoelectric element and cut orientation from a crystal (Fig. 2.16). The circular, ring-shaped or square plates are usually used for the longitudinal or the shear effect. In all piezoelectric elements cut for the longitudinal effect and in most elements cut for the shear effect, the faces on which the force is applied and the faces on which the output of electric charge appears are the same. In some materials and for special applications, it is also possible to collect the electric charge from faces other than the mechanically loaded ones [Gautschi, 2002].

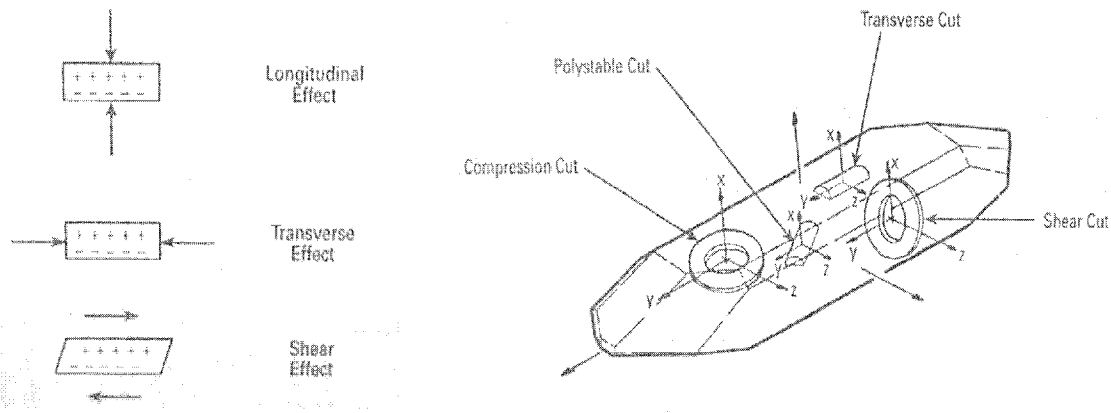

Fig. 2.16 Piezoelectric effects and different cuts of quartz bar [Kistler's catalog]

Characteristics of AE sensors

Sensitivity and bandwidth are two most important characteristics of AE sensors. The sensitivity of piezoelectric sensors can reach values of up to 1000V/μm (60dB, 0dB ref. 1V/μm). A displacement of 0.1 pm generates 100 μVpk then and can be well distinguished from the electrical noise (about 10μVpk). For comparison, atomic radii are in the range of 150 pm. Displacements of 1/1000 of an atomic radius can produce well-distinguished AE signals!

Generally the bandwidths of AE transducers are between several KHz to 2 MHz. The resonant transducer has a narrow bandwidth. The broadband transducers gives more flat response over a wider or much wider frequency range. High fidelity transducer, which usually comes with a small aperture, has very flat response over the frequency range. In different parts of its operating bandwidth, an AE sensor may be sensitive to surface displacement, surface velocity, surface pressure and perhaps surface acceleration.

In some application, size is also important due to the tiny physical geometry of the object on which the transducer is placed.

Signal to noise ratio: AE sensor should be insensitive to low-frequency noise (inherent high-pass characteristic).

Electric and magnetic isolation: The wear plate provides ground isolation. Low-impedance output provides magnetic isolation.

Selection criteria

When selecting a transducer for a particular test one must first of all consider what is desired to measure on and the physical geometry of the object on which the transducer is placed. Generally the criteria are: (i) have a high sensitivity; (ii) have a wide and flat frequency response if the frequency analysis is necessary; (iii) out-of-plane, in-plane or combination for different purpose; (iv) have a good signal to noise ratio, be insensitive to low-frequency noise; (vi) be insensitive to electric and magnetic field; (vii) allow easy mounting, provide good, reproducible and stable coupling to the mounting face; and (viii) suitable size and durable [Dunegan, 2003].

Broadband and resonant sensors

The differences between broadband and resonant sensors are: (i) in sensor design, broadband sensors do not have backing material or the have a backing material with similar acoustic impedance with piezoelectric element; (ii) resonant sensors usually are in larger size than broadband ones; (iii) usually resonant sensor has greater sensitivity at its resonant frequency than broadband sensor, about 15-20 dB, but response at other frequencies is low compared with wideband sensor; and (iv) resonant sensor distorts the waveform in frequency range, so it is not suitable for testing whose primary objective is frequency analysis; (v) AE sensor sensitivity is also a function of sensor diameter. Generally, the larger the diameter of the sensor, the more sensitive it is. Resonant sensor always has larger diameter than broadband sensor; and (vi) for broadband sensor, research has shown that about a 1/4" diameter is the best size for maximizing sensitivity without distortion in the frequency range of interest [DW user's manual, 1997].

Sensor used for corrosion detection

The following Table 2.7 shows AE sensors used for corrosion detection in this project and other researches.

Table 2.7 A list of AE sensors used for corrosion detection

Sensor model	Supplier	Bandwidth kHz	Application	Project or Researcher
R100, B225, B1025	DW	see Chapter 3	Corrosion in R.C.	This project
R15	PAC	100-500	Pitting corrosion in steel	Idrissi et al.
WD	PAC	Broadband	Pitting corrosion in Aluminum alloy	Geng
SE25-P	DECI	Broadband	Stress corrosion	Nieuwenhove et al
B530	PAC	Broadband	Steel corrosion	Landis et al

Calibration

Calibration gives us information of sensor's response and characteristics. Traceability, repeatability and reliability are important features of calibration. Standard and convenient calibrations are presented as following [Esward, 2002; Vahaviolos, 1999; Sachse et al, 1991]. Standard calibration includes the NIST methods and the NSC (Nippon Steel Corporation) method. NIST (formerly NBS) - National Institute of Standard and Technology is the standard calibrations organization for AE sensors.

- Primary Calibration (Absolute Calibration) of NIST standard calibration

Transient Surface Wave Calibration (Step-force sensor calibration) is the method favored by NIST and is outlined in the ASTM guide E1106-86 (Primary calibration of AE sensors). It was first proposed by Breckenridge et al (1991). The testing procedure subjects the sensor to a surface wave similar to an actual AE event. This method uses a standard reference capacitance transducer or laser interferometry with a known step-force AE source on a steel transfer block (0.9m diameter, 0.43m long cylinder). The step-force is generated by the fracture of a glass capillary.

- Secondary Calibration (Face to Face Calibration) of NIST standard calibration

This method is also called White Noise Continuous Sweep (ASTM E976-84, Standard Guide for Determining the Reproducibility of AE Sensor Response). In this method, the sensor to be calibrated and a reference sensor (serving as working standard) are mounted in a symmetric arrangement on the same block and their outputs are compared when AE is induced by breaking a lead mine at a point equidistant of two sensors.

- The NSC (Nippon Steel Corporation) method - standard calibration

This technique is known as a reciprocity calibration. If two sensors, both reciprocal in nature are coupled to a common medium with a known Green's function, the product of the source and the receiver sensitivities can be found from the driving current in the source and the output voltage at the receiver. Hatano et al (1998) took three reciprocal sensors and used them in all the possible pairs of transmitting and receiving sensors.

- Convenient calibrations

The convenient calibration methods include pencil lead fracture, acoustic pressure and dropping elastic ball. Many researchers use pencil lead fracture method (Fig. 2.17).

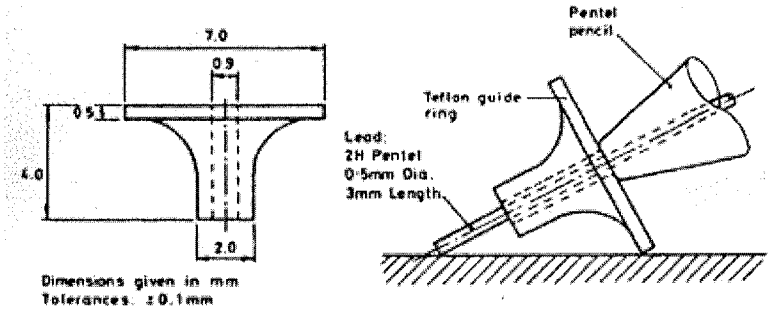

Fig. 2.17 Calibration of pencil lead fracture [Sachse et al, 1991]

- Calibration curves

Generally calibration curves provided by AE sensor manufacturers can be divided to absolute calibration curves and relative calibration curves (Face-to-Face). There are three types of absolute calibration curves: displacement, velocity and pressure. Their units are as follows: Displacement calibration in unit V/μm; Velocity calibration in unit V/(m/s); Pressure calibration in unit V/μbar (1μbar = 0.1 N/m^2).

In a pressure calibration, the sensor responses to continuous excitation, the sensitivity is characterized in term of pressure. The pressure calibration method is easy to reproduce and many standard test certificates are made by this method. These curves are useful for comparing sensor's sensitivity before purchase. Since AE from corrosion source is transient elastic wave, the pressure measurement is not suitable. The displacement calibration is necessary for AE measurement. In addition, only a few manufactures

provide velocity calibration curves. Although the pressure and velocity are directly proportional to one another for any waveform at any instant, the calibration curves of these two methods are different.

Face to face calibration curve is a relative method, which only shows relative sensor response in unit dB. This calibration employs one generator sensor and one receiver sensor. The signal generator sensor can be same as receiver or different. Two choices of testing configuration are available: sensor-to-sensor (no medium) and steel block [Elias, 1998]. This curve is good for spectrum and energy analysis. One should note this method is different from face to face of NIST standard calibration. Digital Wave Corporation employs this calibration method. Calibration curves for sensors used in this project are shown in Appendix A.

Fiber optic sensors (FOS)

As the development of intelligent structures, fiber optic sensors have been used to monitor the strain, deformation, load distribution and temperature or environmental degradation of a structure. It is possible to use FOS for the detection of corrosion activities if it reaches desired sensitivity. FOS has been used to assess the corrosive expansion [Lee, 1998]. FOS measures tangential (in-plane) surface strains at ultrasonic frequencies by sensing the change in wavelength or phase of light traveling through the fiber. The sensitivity for a Fiber Bragg Grating sensor can be 1με[ISIS Canada, 1998]. A research group at the Georgia Tech University declared that they developed FOS with a higher sensitivity $4x10^{-10}$ε[Shi et al, 2002].

2.5.2 Signal processing

The study of signal processing is necessary for post-test analysis of AE signals.

Time domain analysis

Commonly used techniques of time domain analysis are ring-down counts (Fig. 2.18), peak-to-peak amplitude or peak amplitude, total sum (total amplitude), total energy, root mean square of amplitude and amplitude moment and energy moment [Mertins, 1999]

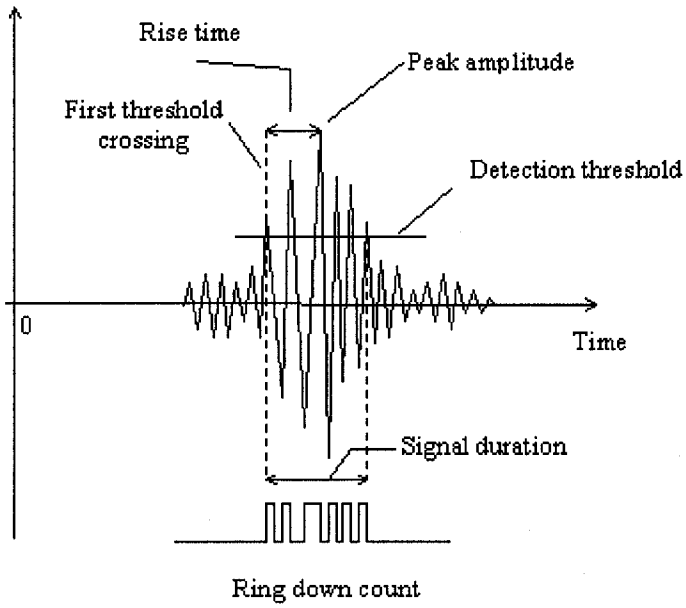

Fig. 2.18 Time domain analysis
[http://www.ndt.net/article/az/ae/ringdowncount.htm, accessed Nov. 22, 2003]

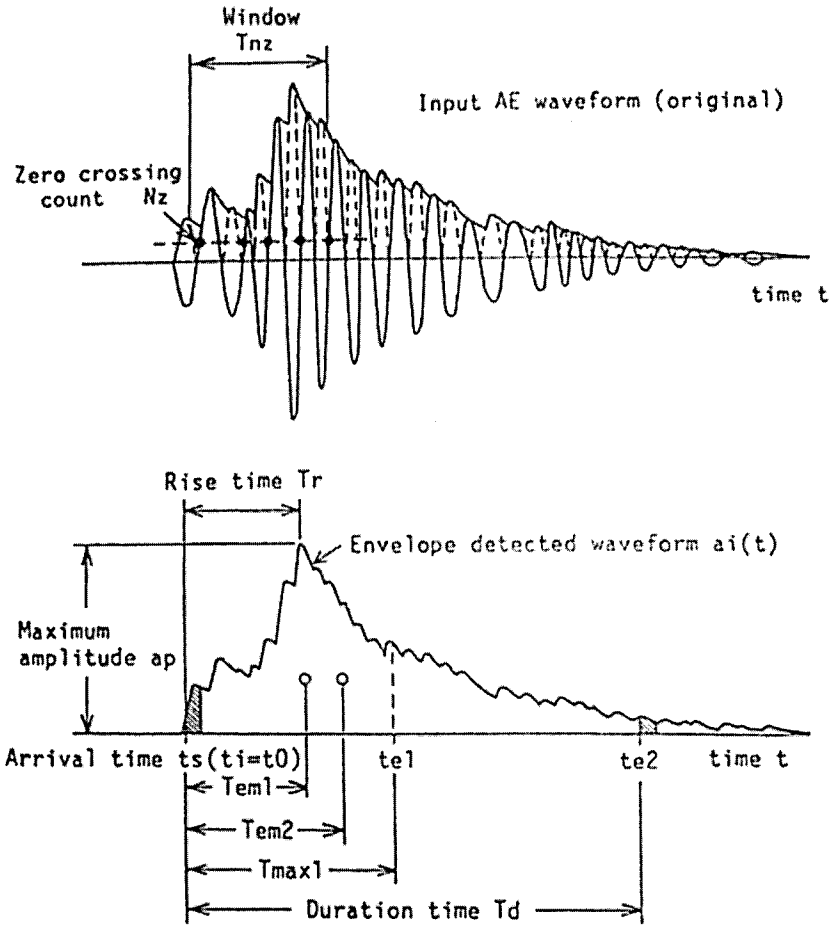

Total amplitude: $$At = \sum_{i=0}^{n} a_i \cdot dt \quad (1)$$

Total energy: $$Et = \sum_{i=0}^{n} a_i^2 \cdot dt \quad (2)$$

1st order amplitude moment: $$Tam = \sum_{i=0}^{n} a_i \cdot ti \cdot dt \,/\, At \quad (3)$$

1st order energy moment: $$Tem = \sum_{i=0}^{n} a_i^2 \cdot ti \cdot dt \,/\, Et \quad (4)$$

2nd order amplitude moment: $$Tam(2nd) = \sum_{i=0}^{n} a_i \cdot ti^2 \cdot dt \,/\, At - (Tam)^2 \quad (5)$$

2nd order energy moment: $$Tem(2nd) = \sum_{i=0}^{n} a_i^2 \cdot ti^2 \cdot dt \,/\, Et - (Tem)^2 \quad (6)$$

where dt is the sampling period of A/D conversion.

Fig. 2.19 Amplitude moment and energy moment analysis [Sachse, 1991]

Total sum is the area under the waveform envelope. Total amplitude is adding the signal amplitude and total energy is adding the square of amplitudes. Usually adding the square of each point in the entire signal did the calculation of total sum. Amplitude moment and energy moment is shown in Fig. 2.19. Ian [1991] defined Root-Mean Square of amplitude as:

$$\text{RMS} = \sqrt{\left\{\frac{1}{T}\int_0^T [f(t)]^2\, dt\right\}}$$

FFT and PSD analysis in frequency domain

It is necessary to analyze signals both in time and frequency domain. The smaller signals masked by the larger in the time domain, but both components of signal appear clearly when it is viewed in the frequency domain, particularly if a logarithmic amplitude scale is used. In general, any function that is "spiky" in one domain will appear spread out in another [Turner, 1991]. Fourier Transform (FT) is a continuous analytic integral. Discrete Fourier Transform (DFT) presents a signal by a set of discrete points. They are both derived from the basic Fourier series.

- FFT

Fast Fourier Transform (FFT) is an efficient algorithm for evaluating the Discrete Fourier Transform (DFT). The algorithm, may in different variants, is the basis of most digital spectrum analysis. Fourier analysis breaks down a signal into constituent sinusoids of different frequencies. Another way to think of Fourier analysis is as a mathematical technique for transforming our view of the signal from time-based to frequency-based [Williams, 1999].

- Expression of FFT

The functions X = fft(x) and x = ifft(X) implement the FFT transform and inverse transform pair. In Matlab Signal Processing Tool, the Fast Fourier Transform is expressed as:

$$X(k) = \sum_{j=1}^{N} x(j)\omega_N^{(j-1)(k-1)}$$

Where

$\omega_N = e^{(-2\pi/N)}$ is an Nth root of unity,

k=mΔf, here m = 1, 2, 3, ... N/2; letΔf = 1 in the frequency plot, thus k = 1, 2, 3, ... N/2.

- Signal processing in Matlab

The Discrete Fourier transform, or DFT, is the primary tool of digital signal processing. The foundation of the Signal Processing Toolbox is the Fast Fourier Transform (FFT), a method for computing the DFT with reduced execution time. Many of the toolbox functions (including z-domain frequency response, spectrum analysis, and some filter design and implementation functions) incorporate the FFT. MATLAB provides the functions fft and ifft to compute the discrete Fourier transform and its inverse, respectively. For the input sequence x and its transformed version X (the discrete-time Fourier transform at equally spaced frequencies around the unit circle), the two functions implement the relationships

- Choice of sampling parameters

A restriction on the use of the FFT is that it can only be used when N is a power of two, that is, when there are 256, 512, 1024, 2048, 4096 and so on data points [DW user's

manual, 1997]. In frequency domain, the FFT is sampled with N/2 real-valued time domain points since it can easily be implemented on a computer [Turner, 1991].

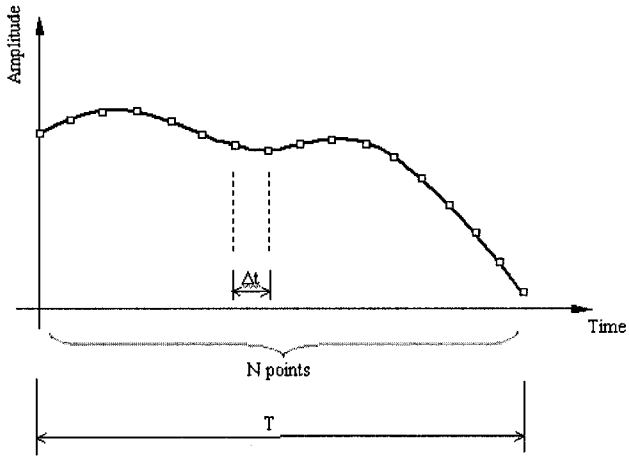

T: length of signal recorded (Memory length);

N: no. of time domain points;

Δt: time interval between points

f_s: sample frequency;

$T = N / f_s$;

$\Delta t = T/N = 1/(2 F_{max}) = 1/ f_s$

Fig. 2.20 Parameters in time domain

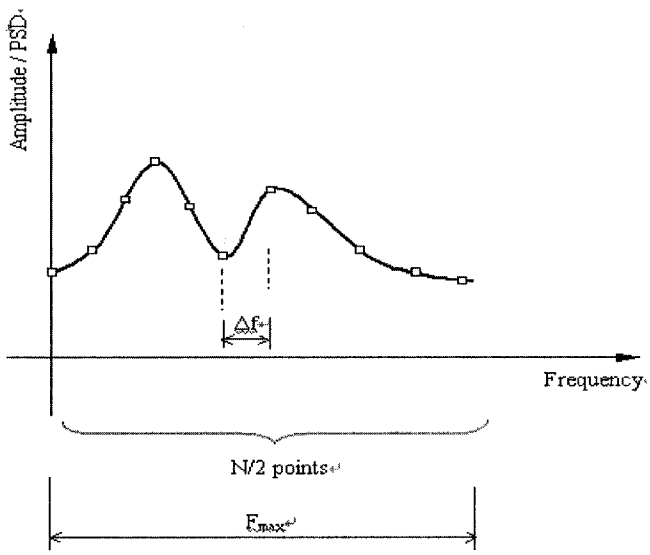

F_{max}: Maximum frequency

N/2: no. of frequency domain points

Δf: frequency interval between points

$\Delta f = 1/T = 1/(N\Delta t)$

$F_{max} = \Delta f \times N/2 = f_s / 2$

Fig. 2.21 Parameters in frequency domain

- PSD

Power Spectral Density (PSD) is one of the common representations in frequency domain. It expresses the energy carried by each frequency component of the signal. PSD is calculated as the vector sum of square of real part and imaginary part. Continuous Fourier Transform $S(f) = \int x(t)e^{-j2\pi ft}df$, due to the kernel of Fourier Transform $e^{-j2\pi ft} = \cos(2\pi ft) - j\sin(2\pi ft)$, can be written in the form $S(f) = a(f) - jb(f)$, where a(f) is the real part (Re) and –b(f) the imaginary part (Im) [Turner, 1991].

$PSD = S^2(f) = a^2(f) + jb^2(f)$ or

$PSD = \mathrm{Re}^2(f) + \mathrm{Im}^2(f)$

For FFT, the unit of PSD is energy per unit of frequency interval in a linear scale. If the PSD compares with a reference PSD_0, the energy can be expressed as decibels scale [Brook, 1991]: $PSD(dB) = 10\log(PSD/PSD_0)$.

2.6 Concluding Remarks on the Literature Review

Corrosion causing deterioration in reinforced concrete has become a multi-billion problem. Existing NDT test methods have their respective limitations. Most methods only detect the latter phenomena of corrosion when significant change in concrete-steel system appears e.g. cracking and spalling. Other disadvantages of these methods, such as time-consuming, depending on concrete condition, expense and immobility of equipment, localized detection, and difficult to perform etc. have also limited the applications of these methods in-situ.

Acoustic emission technique is theoretically expected to be capable of real-time, 24/7, whole-structure, automatically monitoring rather than artificially detecting corrosion from the commencement of corrosion period. Real-time and long-term health monitoring structures is the spirit of the intelligent structures that ISIS has been pursuing.

It is undoubted that AE has great merit for detecting corrosion in reinforced concrete structures. Although high attenuation nature of concrete has been a concern in the past, the placement of sensors on steel should be a solution.

The study of wave transmission and AE instrumentation in the foregoing two sections provides the theoretical foundation for the experimental programs.

CHAPTER 3. EXPERIMENTAL SETUPS

This work uses sonic testing equipment and accelerated corrosion regime to examine the feasibility of detecting acoustic emission (AE) from corrosion sources through steel reinforcement. The specific objectives include:

- Detect AE from plain corrosion (only steel reinforcement)
- Detect AE from corrosion in reinforced concrete
- Prove corrosion causing AE by experimental setup and half-cell potential measurement
- Compare the measurements on steel vs. on concrete
- Estimate maximum detectable distance away from the corrosion source
- Determine the location of corrosion source

In this chapter, the experimental programs are presented for the above objectives. Prior to the experimental setups, the sonic testing equipment and accelerated corrosion regime are introduced.

3.1 Introduction of AE Equipment and DW Setting

The equipment used in this project is Digital Wave (DW) Active Testing System, manufactured by Digital Wave Corporation. This multifunctional equipment was designed primarily for testing of metals, but it is also suitable for fundamental testing of concrete. It has two different but relevant functions: Acoustic Emission (AE) testing and

Ultrasonic Pulse Transmission (UPT) testing. Fracture Wave Detector (FWD) software is used in AE testing and Laminated Plate Wave Analyzer (LPWA) software in UPT testing.

3.1.1 General view of setup of AE testing system for this project

For AE testing, no signal generator is required to create ultrasonic signal. The typical configuration that is illustrated in Fig. 3.1 and Fig. 3.2 consists of piezoelectric sensors, pre-amplifiers, filter trigger module (FTM) and PC.

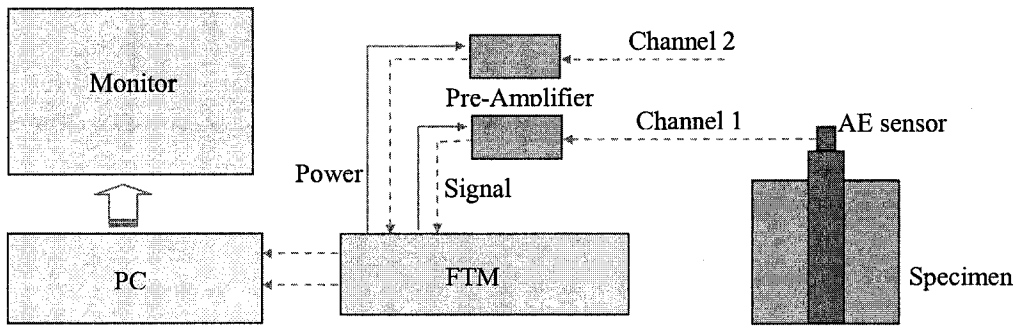

Fig. 3.1 Sketch of DW AE testing system

The hardware components for this two-channel AE testing system consists of:

1. Transducers (please see 2.2 'AE sensor' for detailed information)
    - Broadband transducers B1025 (2 pieces)
    - Broadband transducers B225 (2 pieces)
    - Resonant transducers R100 (2 pieces)
2. PA2040 G/A Broadband preamplifiers (2 pieces)
3. DW- signal filter/amplification unit – Filter Trigger Module (FTM) (1 piece)
4. Sonix STR*825 8-bit A/D board (1 piece)

5. Parametric A/D board (1 piece)
6. DWC-232 Serial Connector (2 pieces)
7. 6m preamplifier signal cable assembly with BNC connector (2 sets)
8. 1.2m preamplifier signal cable assembly with BNC connector (2 pieces)
9. 0.9m Sensor cable assembly with micro dot / BNC connector (2 pieces)
10. Industrial computer: 133 MHz, 16M RAM, 2G HD, keyboard, mouse (1 set)
11. FWD96 Data acquisition and analysis software (1 set)
12. Viewsonic 17" color monitor (1 piece)
13. Electrical connection cable (4 pieces)

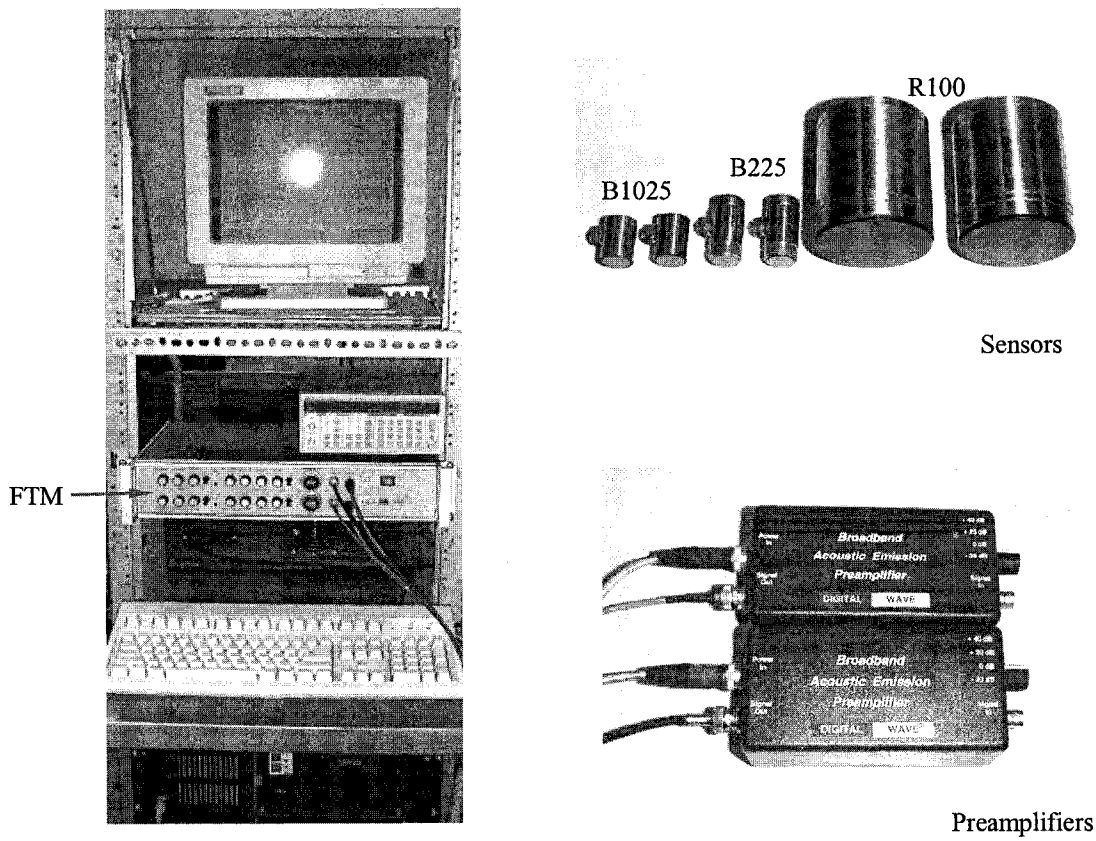

Fig. 3.2 Picture of DW AE system

3.1.2 Introduction of sensors, preamplifiers, FTM and connectors

Piezoelectric sensors used in this study are resonant sensors R100, broadband sensors B225 and B1025 (The manufacturer's calibration curves and lab verification curves are list ed in Appendix A).

Broadband sensors B225

Frequency Bandwidth: 30 KHz - 300 KHz

Peak sensitivity 55 dB (dB ref 1 V/μm)

Central response at 225 KHz

Dimension: 0.375"OD x 1.0"H

The B225 is relatively broadband and has a flat response with high sensitivity. It is suitable for testing that both high sensitivity and frequency analysis are required. The B225 provides additional sensitivity at low frequencies, which is useful when inspecting thick plates, highly attenuate specimens and far sources. The B225 is suitable to inspect concrete with high attenuation coefficient and to detect corrosion causing AE signals through long rebar.

Resonant sensors R100

Frequency bandwidth: 5 KHz -150 KHZ

Major output frequency: 20 and 75 KHZ

Central resonant frequency: 70 KHZ (Lab verification found second peak around 25KHZ)

Dimension: 1.25"OD x 1.5"H

R100 was designed with high sensitivity (Appendix A shows the calibration curves) and was developed for testing in which frequency content usually is not analyzed, since the resonance distorts the output over the frequency range. The sensor has very good repeatability and reliability. R100 is excellent for using on high attenuation materials or long distance measurement. The absolute calibration curve of R100 is not available. The absolute sensitivity at resonance frequency can be calculated by comparison with B225. The peak sensitivity of R100 is 16 dB higher than that of B225. Theoretically speaking, R100 should has peak sensitivity 71 dB (dB ref 1V/μm). However, laboratory verification shows the real sensitivity is lower than this number. R100 and B225 have similar sensitivity. This can be explained by aperture effect.

Broadband sensors B1025

Frequency Bandwidth: 50 KHz –2 MHz

Peak sensitivity: 43 dB (dB ref 1 V/μm)

Dimension: 0.365"OD x 0.5"H

Active Element: 0.25" diameter low Q piezoelectric ceramic.

The output signal from the B1025 is typically between 10μV and 10mv. The B1025 is high fidelity piezoelectric sensor, which are designed specially for acoustic emission measurement. It has lower sensitivity (15-20 dB) than R100 and B225.

Preamplifiers

Each DW PA2040 G/A broadband preamplifier provides amplification –20, 0, 20, 40 dB.

Filter Trigger Module (FTM)

FTM provides signal filter and max.42 dB signal amplification for both channels. The setting for both channels on each FTM as follows:

~ High Pass Filter	20 KHz (min. frequency)
~ Low Pass Filter	4000 KHz (max. frequency)
~ Threshold level	0.1 V

The high and low pass filters were set to keep unwanted signals out of expected frequency range. In this study, high pass was always set at 20KHz and low pass was 4000 KHz.

MicroDot / BNC connectors and connect cables

The sensor cable connects sensor and preamplifier with microdot and BNC connectors. It is usually less than 1.2 m. Co-axial cable connects preamplifier and FTM with BNC connectors. This cable can be up to hundreds meters.

3.1.3 Software FWD

The Fracture Wave Detector (FWD) system is designed for the acquisition and analysis of wideband AE signal waveform. Totally there are four modules in this software, Data acquisition module, Post-test Module, Material Analysis module and Location Module. Here only most important items are introduced; detailed information is shown in User Manual. Data acquisition parameters are configured in Acquisition Setup window, the left half of the screen is for waveform setups, and the right half is for definition of parametric for signals from other measurement devices, so we can omit the setting of right half part.

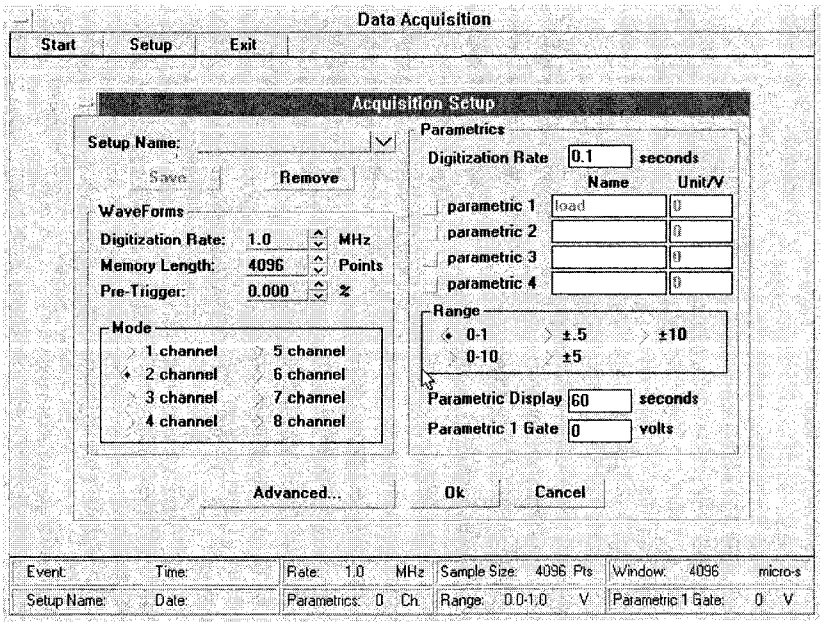

Fig. 3.3 Data acquisition setup

Sampling frequency (Digitization rate)

The suitable sampling frequency is determined by maximum frequency expected in frequency domain, required signal length and resolution both in time and frequency domain. Sampling frequencies f_s in FWD are 0.5, 1,5, 12.5 and 25MHz. Therefore, the maximum frequencies F_{max} will be 0.25, 0.5, 2.5, 6.25 and 12.5MHz (F_{max} =0.5f_s, explanation in Section 2.5.2).

Memory length

It is important that the Sampling Frequency and Memory Length together define the duration of time (Time Duration = Sampling Frequency / Memory Length). For example, in this study, the most often settings of these two parameters are 0.5 MHz and 4096 points (the number of points for FFT is constrained to be a power of two), the time duration of data capture is 8192 μs.

Signal amplitude

The default value of computer output is 0 to 0.5 V and maximum output is 1 V. The signal amplitude was controlled by main amplifier unit (0-42 dB) in FTM and preamplifier (-20 to +40 dB); totally maximum amplification rate is 82 dB.

3.2 Experimental Programs

To examine the feasibility of use acoustic emission to detect the onset of corrosion in reinforced concrete, the following experimental programs were set up:

- Experiment-I: AE from plain corrosion
- Experiment-II: AE from reinforced concrete
- Experiment-III: Sensor on steel vs. on concrete
- Experiment-IV: Effect of distance
- Experiment-V: AE vs. Half-cell potential

Experiment-I and Experiment II examine whether steel corrosion can be "heard" by the AE sensors; Experiment-II and Experiment-V checked the AE signals in reinforced concrete were caused by corrosion or other processes; Experiment-III compared measurements of coupling sensors on the steel and on concrete; Experiment-IV estimated how far we can measure away from the corrosion source.

Accelerated corrosion

Accelerated corrosion regime was utilized at Experiment-I to IV in this project. The corrosion was accelerated by the following methods:

- Imposed voltage to sample and cathode, 6 –12 V
- Sample was immersed to 2% - 3% NaCl solution
- The surface area of cathode was much larger than anode
- Sufficient oxygen supply, wet-dry cycling was used for reinforced concrete specimen

Sensor-Specimen connection (Coupling)

Sensor-Specimen connection was very important to obtain expected signals. The contact surfaces of specimens were well polished. The coupling material was vacuum grease. Contact pressure was provided by sensor's own weight or by clamps.

3.2.1 Experiment-I: AE from plain corrosion

In this experiment, samples were bare steel bars without casting into concrete. Accelerated corrosion was applied. The major targets were to see whether or not AE signal from corrosion can be detected by DW AE equipment, and to determine what kind of sensors are suitable for corrosion causing AE.

The cathode was copper plate with large surface area (totally about 0.5 m^2) and was rolled to three layers. The specimen was supported by concrete block to get small submerging area (about 0.007 m^2). Large difference of surface area caused the fast pitting corrosion. The experimental setups were shown in Fig. 3.4 and Table 3.1.

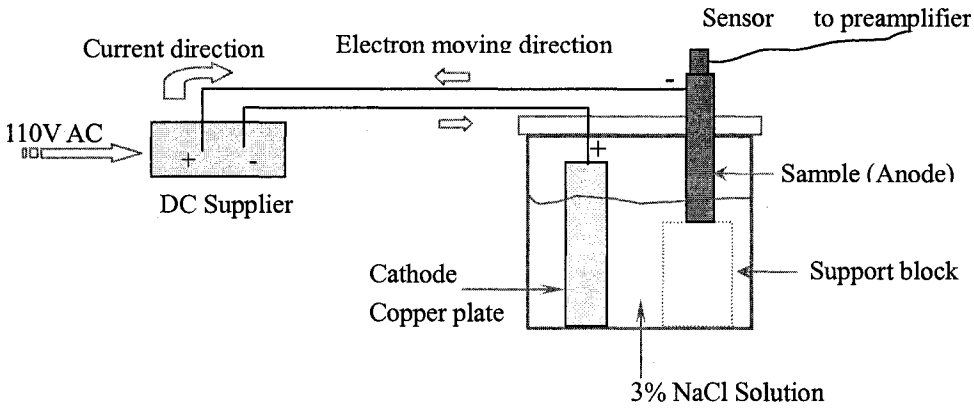

Fig. 3.4 Setup of Experiment-I

The DW settings were as follows: Sampling frequency was set at 0.5 MHz. Number of recorded points was 2048. Amplification setting was adjusted from 61dB to 49 dB, it was found that 49 dB was an optimum setting for R100 sensor.

Table 3.1 Samples and settings in Experiment-I

Sample	Solution	Applied current	Sensor
1.Cold rolled Steel plate 20 x 100 x 300mm	3% NaCl Solution	0.6A 0.7V	R100
2. Coated rebar with 2 notches D55mm x L300mm	3% NaCl Solution	0.6A-1.8V to 0.8A-2.6V	R100 B1025(CH1) B225(CH2)
3. Ordinary rebar D55mm x L300mm	3% NaCl Solution	0.9A 6.4V to 7.9V	R100

3.2.2 Experiment-II: AE from reinforced concrete

This experiment examines whether the AE signals from corrosion in reinforced concrete can also be effectively detected.

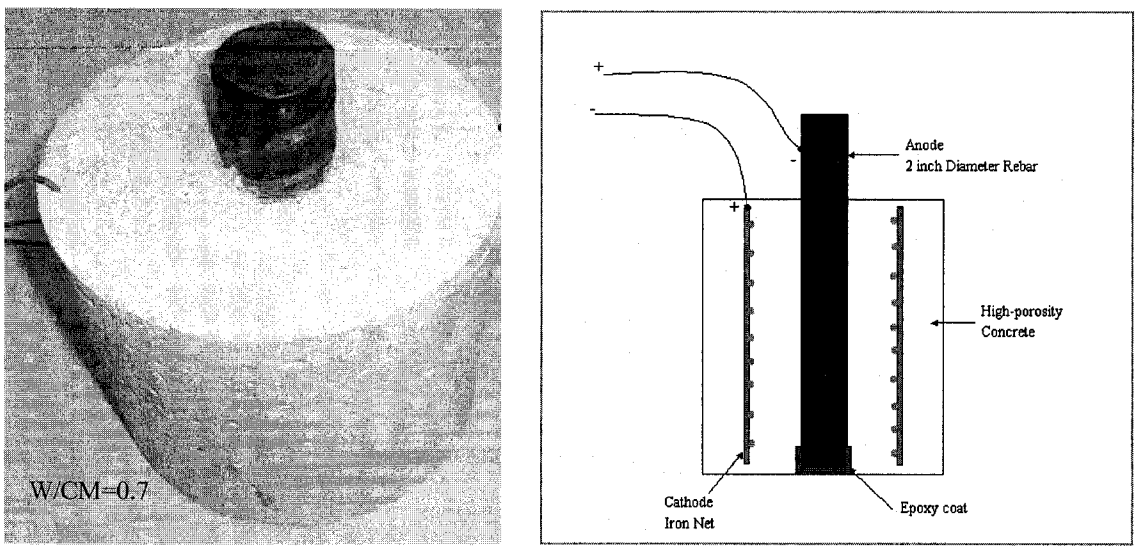

Fig. 3.5 Specimen of Experiment-II

The accelerated corrosion mechanism was the same as Experiment-I. Wet-dry cycling was applied to introduce air into the cathode (Fig. 3.6). The specimen was designed as shown in Fig. 3.5. The cathode was an iron net that was cast into a concrete to let the corrosion occur at dry cycle. The high water to cement ratio of concrete mix design provided sufficient porosity to absorb water and entrap air in a fast rate. The solution was 2% NaCl solution and the applied current was 6V/9V~ 0.07-1.5A.

The DW settings were as follows: Amplification setting was +49 dB. Sampling frequency was 0.5 MHz. Number of recorded points was 4096. Sensor used in this experiment was

R100 from day 1 to the 29th day. From the 30th day to the 32nd day, broadband sensors B225 and B1025 were tried (the 30th & 31st day: R100 +B225; the 32nd day: R100/43 dB + B1025 /70 dB).

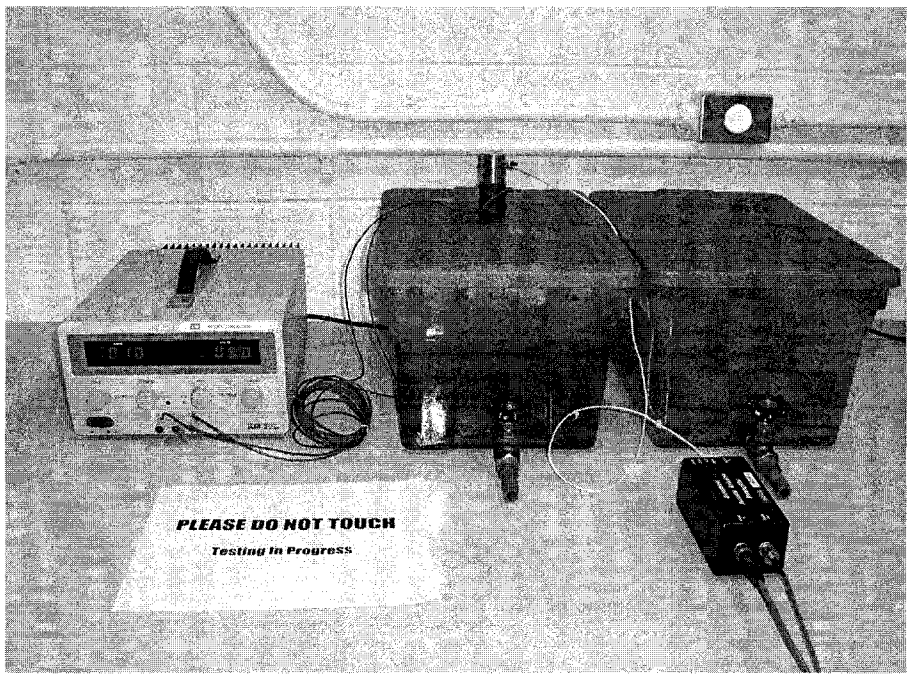

Fig. 3.6 Testing in wet cycle of Experiment-II

During the over one month testing, another specimen from same batch as the one under accelerated corrosion was put in water (only water without salt and applied current) and under same wet-dry cycling. Sensor used for this specimen was R100 as well. Two specimens were under same conditions except one was corroding but the other one was not. The purpose of this setup was to see if the received AE signals were from corrosion sources or other processes.

3.2.3 Experiment-III: Sensor on steel vs. on concrete

The goal of experiment was to see whether detection of corrosion causing AE through steel reinforcement had significant advantage comparing with detection on concrete.

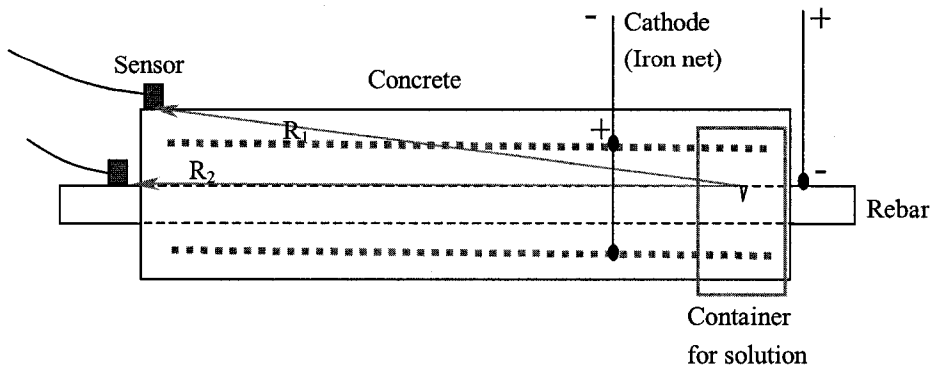

Fig. 3.7 Setup of Experiment-III

The specimen was 150 x 150 x 600 mm concrete with 2 inches diameter steel bar. Two pieces of iron nets were cast into concrete as cathode (Fig. 3.7 & 3.8). Instead of applying wet-dry cycles, the 2% NaCl solution only covered half part of specimen that enabled another half part to entrap air. The applied current was 12~15 V / 0.32 ~ 0.42 A. Two 200 g weights were put on the top of two sensors to provide same contact pressures for both channels as shown in Fig. 3.8.

Channel 1: B225 sensor, on concrete, amplification setting +61 dB

Channel 2: B225 sensor, on steel, amplification setting +49 dB

Sample frequency: 1 MHz; Number of recorded points: 4096

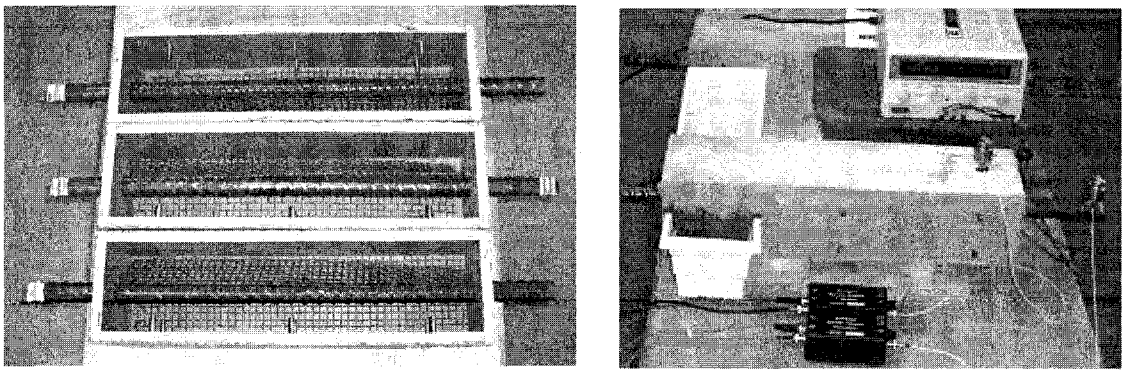

Fig. 3.8 Specimens before cast and testing in progress

3.2.4 Experiment-IV: Effect of distance

The goal of this experiment was to find how far we could measure away from the source and to determine the source location. The maximum distance between corrosion AE source and sensor can be calculated by attenuation coefficient in rebar. This experiment was applied to measure the attenuation coefficient of rebar toward AE waves. The setup was shown in Fig. 3.9 and Fig. 3.10.

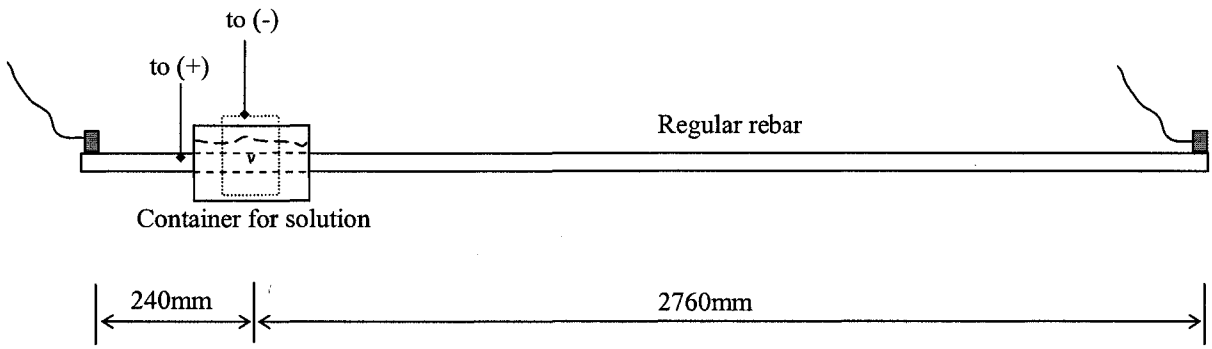

Fig. 3.9 Setup of Experiment-IV

Specimen diameter: 1 inch

Specimen length: 3 m

Solution: 3% Nacl solution

Applied current: 10 V~1.02 A

Transducers: 2 nos. of B225

Amplification setting of Channel 1: +43 dB

Amplification setting of Channel 2: +40 dB

High pass filter: 20 kHz

Low pass filter: 4000 kHz

Sample frequency: 1.0 MHz

Memory length: 4096 points

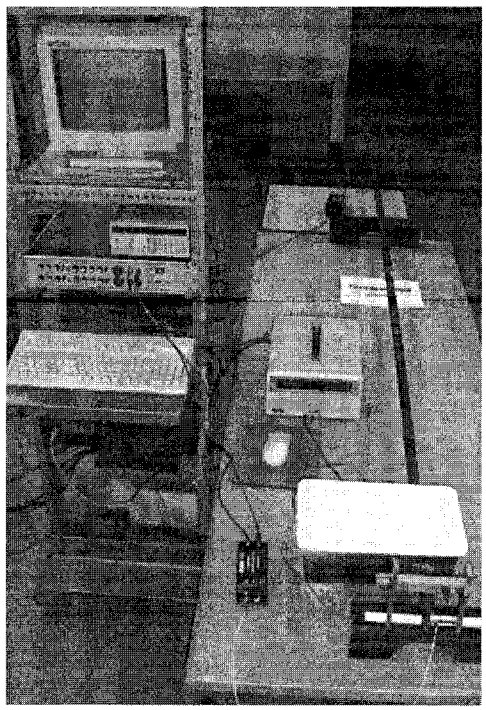

Fig. 3.10 Picture of Experiment-IV

A notch was made at 240 mm from one end where the corrosion occurred. Except the notch, the part of rebar inside container was coated by epoxy material in order to let the corrosion occur at the position wanted. An U-clamp and a quick clamp (Fig. 3.11) were used to apply constant pressures on transducers to obtain maximum sensitivities.

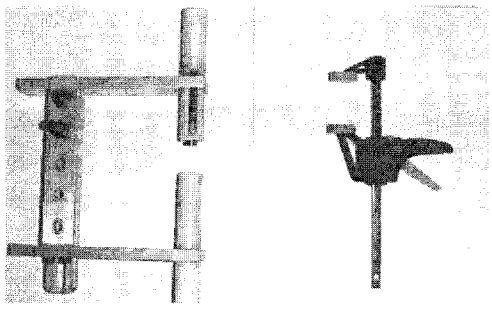

Fig. 3.11 U-clamp and quick-clamp

Calibration of the two channels is very important step to precisely measure attenuation. It is very difficult to adjust exact same pressure on two sensors. Moreover, even if the applied pressures are the same on both channels, the lengths of signal cables, the sensitivities of the two sensors (same model) and amplifiers themselves also influence the signal output. In order to get accurate result of attenuation, the calibration has to be done.

The calibration process was as follows: after the sensors were fixed by U-clamps, the amplification rates were adjusted to relatively equal outputs of the two channels by breaking 0.5mm-2H pencil lead at exact middle point between two sensors. In this experiment, the amplification rate of channel 1 was +43 dB and that of channel 2 was +40 dB. The calibration results are shown in Fig. 3.12. Both time domain and frequency domain show similar peak amplitude and PSD distribution from two channels. +/-3 dB was acceptable.

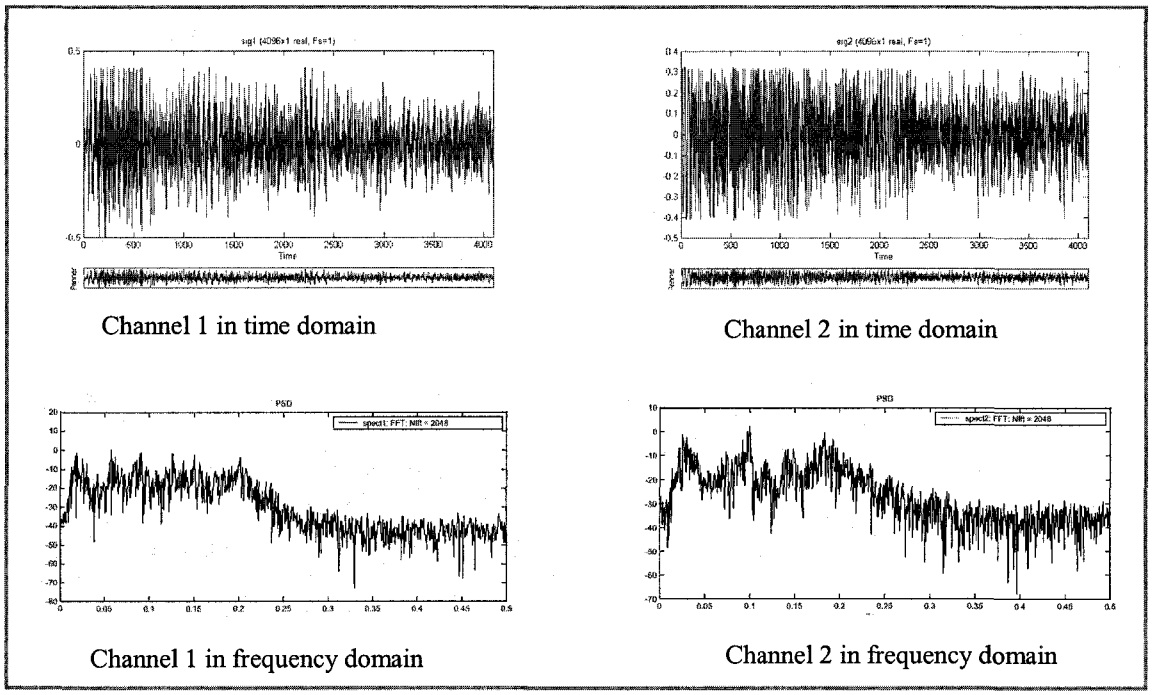

Fig. 3.12 Pencil lead breaking calibration for two channels

The waveforms of pencil lead fracture directly on sensor surface were quite transient. However, since the facture was at the middle of a long rebar, signals received by sensors at both ends of rebar had undergone many times reflections and mode conversions, which caused waveforms in nearly continue type.

3.2.5 Experiment-V: AE vs. Half-cell potential

To bring convenience for reading, the introduction of half-cell potential corrosion measurement equipment and the setups were merged to next chapter experimental results and discussions (Section 4. 5).

CHAPTER 4. RESULTS AND DISCUSSION

This chapter presents the results and discussion of the five experimental programs corresponding to the four key topics. From Section 4.1 to Section 4.5, the results and analysis of the following five experimental programs are presented respectively.

- Experiment-I: AE from plain corrosion
- Experiment-II: AE in reinforced concrete
- Experiment-III: Sensor on steel vs. on concrete
- Experiment-IV: Effect of distance
- Experiment-V: AE vs. Half-cell potential

The Section 4.6 summarizes the discussion of the following four key topics:

- Can steel corrosion be "heard" by the AE sensors?

  Experiment-I & II provide the answer.
- Are the AE signals in reinforced concrete due to corrosion or other processes?

  Experiment-V & II examine it; Experiment-III & IV also can be evidences.
- Is it better to put the sensors on the steel or concrete?

  Experiment-III compares the measurements of coupling on steel and on concrete.
- How far can we measure away from the corrosion source?

  Experiment-IV gives data to estimate the detectable distance away from the source.

4.1 Experiment-I: AE from Plain Corrosion

An accelerated corrosion regime was applied to obtain a corrosion source within a short time (first event arrival within 24 hours). Various currents were imposed to find a suitable voltage for producing AE. Since the major target of this experiment was to examine whether we can receive AE from corrosion activities, resonant sensors were used due to their high sensitivities and ease of coupling (certain contact pressure was provided by sensor's own weight).

4.1.1 Experimental results

Table 4.1 List of AE events in Experiment-I

Sample	Cold rolled steel plate	Epoxy coated rebar with notches		Ordinary rebar
Solution	3% NaCl solution	3% NaCl solution		3% NaCl solution
Applied current	0.6 A 0.7 V	0.6 A - 1.8 V to 0.8 A - 2.6 V		0.9 A 6.4 V to 7.9 V
Duration	21 hrs	34 hrs	49 hrs	47 hrs
Sensor	R100	R100	B1025 (CH1) B225 (CH2)	R100
Events	0	96	0	16
Comment	Uniform corrosion	Pitting corrosion	No event due to contact pressure	Pitting corrosion

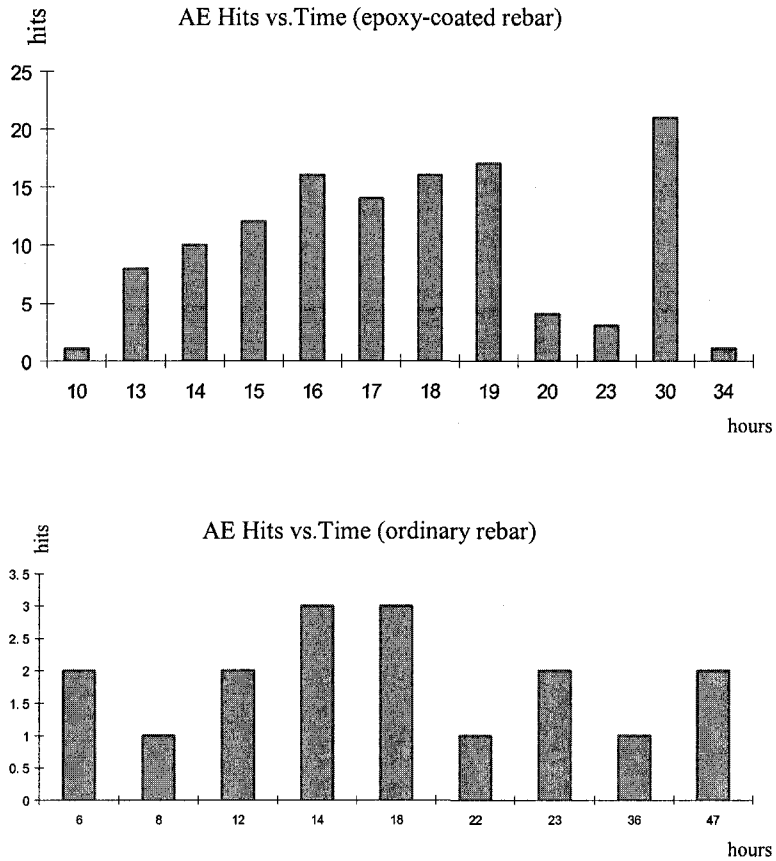

Fig. 4.1-a Hits vs. Time of Exp. I

The experimental data shown in Table 4.1 and Fig. 4.1-a was obtained according to the time record at the bottom of Data Acquisition screen. Fig. 4.1-b shows the example.

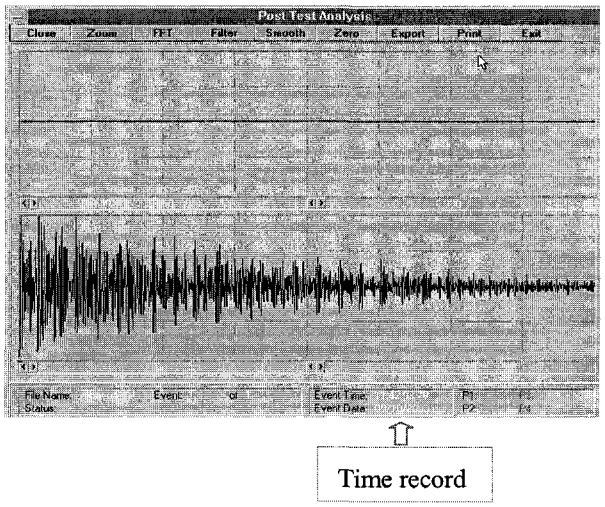

Fig. 4.1-b Data acquisition

Generally the events increased with time from the first event, but it was not linear. The first event came earlier with higher voltage. Certain contact pressure to broadband sensor on testing was important to receive signals. Because the self-weights of broadband sensors were unable to provide enough contact pressure and the co-axial signal cable produced distortion forces that made the sensor lose contact with the specimen, no signal was received by broadband sensor in this experiment. However, from the latter experiments, broadband sensors are found to be suitable for corrosion AE testing. A Study of sensor's sensitivity vs. contact pressure is shown in Appendix C. Prior to rebar, a cold rolled steel plate was used for a trial. Because only uniform corrosion occurred on the specimen, no AE event was received. Current AE equipment is not sensitive enough to detect very weak acoustic emission from uniform corrosion. The acoustic emission signals were successfully detected from specimens of epoxy-coated rebar and ordinary rebar, where pitting corrosion occurred with significant steel loss as shown in Fig. 4.2.

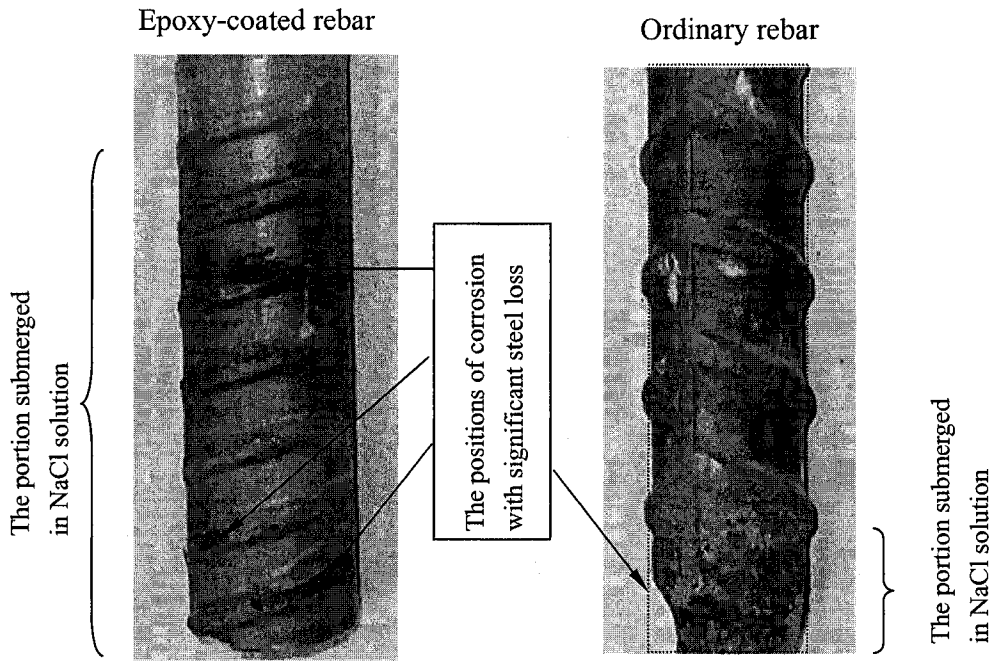

Fig. 4.2 Pictures of corroded specimens

4.1.2 Analysis of the typical corrosion AE signal

Pitting corrosion in both epoxy-coated rebar and ordinary rebar generated lots of AE signals that were recorded. As the wave propagation in epoxy-coated rebar was different from that in ordinary rebar, the following analysis focused on the typical signal from ordinary rebar.

Time domain analysis

In time domain, peak amplitude and signal amplitude distribution are discussed as follows. The ring down counts will be discussed in Section 4.2 by comparing with Experiment-II.

.

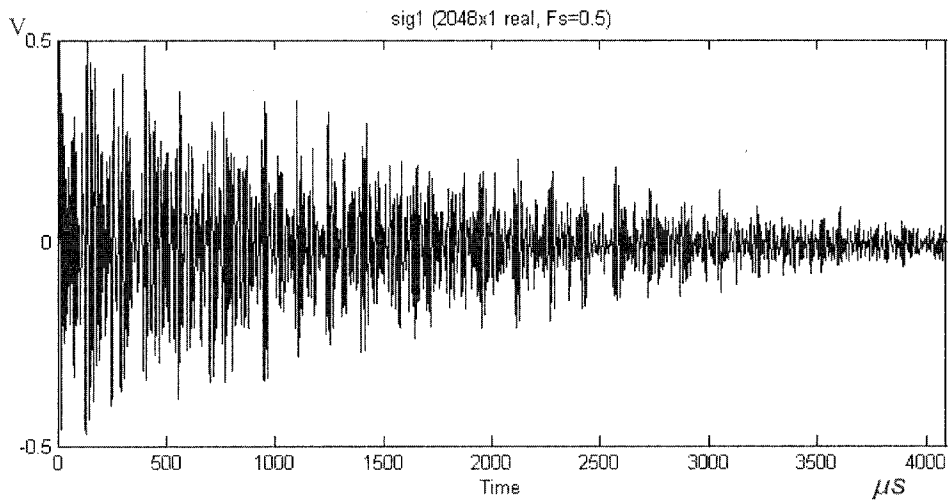

Fig. 4.3 Typical AE signal from regular rebar

[Memory length: 2048 points; Sample frequency: 0.5 MHz; Total amplification: 49 dB]

- The peak amplitude

The peak amplitude is 0.5 V where the amplification rate is 49 dB, so the sensor output is 1.77 mV. Sensor output is only comparable for data obtained by same sensor or same

model of sensor. But it is not comparable with data from other sensors. The surface displacement of particle at the sensor-specimen interface is the parameter that associates with the nature of wave propagation. The detailed calculation process is presented in section 4.4. The sensitivity of R100 sensor is 42 dB (dB ref 1V/micrometer) at 70 kHz (the resonance frequency) by comparing with B225 sensor. Therefore, the surface displacement is 1.4 $x10^{-11}$ m (Equations in Section 4.4.1).

- Amplitude distribution

The waveform in Fig. 4.3 is not very transient. In fact, the corrosion causing AE should be more transient. The reason is the sensor position was 30cm away from the bottom of the specimen, and therefore the sensor received not only the original AE signal but also the repeated waves due to wave reflections and mode conversion during wave propagation. It took approximately 350 microseconds to receive the first repeated signal that reflected from the bottom of specimen according the wave velocity and the length of specimen.

This phenomenon can be explained by comparison of the pencil lead fracture on the sensor surface directly and via steel block. Left figure of Fig. 4.4 shows direct fracture of pencil lead on the sensor's surface. It is of quite transient type. The signal was not interfered with any reflection, which is the original signal of pencil lead fracture.

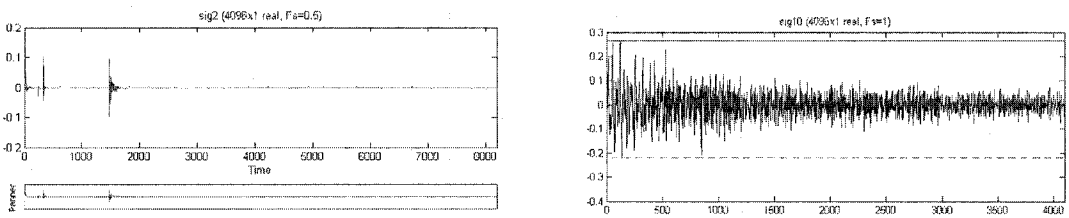

Fig. 4.4 Comparison of pencil lead fracture on steel block and sensor's surface

However, when the original signal from pencil lead fracture travels through a steel block to sensor, the received signal looks like the right figure. As traveling distances of reflected waves are different, the arrival times are also different, which result in the waveform change. This phenomenon makes the received signals much more complex and brings a difficulty to signal processing, because every time the boundary conditions are not same.

Frequency domain analysis

Transferred by Fast Fourier Transform (FFT) at Matlab.

Sample frequency f_s =0.5 MHz

Memory length of recorded signal in time domain (N) is 2048 points.

Thus, the number of frequency domain points (N/2) is 1024

Maximum frequency F_{max} =Δf x N/2 = f_s/2 =0.25 MHz

The frequency interval between points $\Delta f = F_{max} / (N/2) = 1/ f_s$

(Fig. 2.20 & Fig. 2.21 in Section 2.5.2)

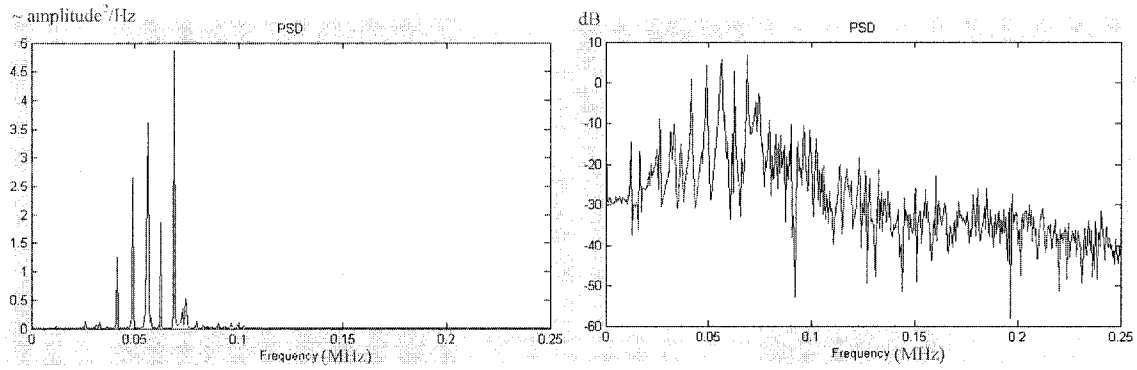

Fig. 4.5 PSD of typical signal in frequency domain (linear & decibel)

The PSD can be expressed in linear scale (Fig. 4.5 left) or in decibels scale (Fig. 4.5 right) in Matlab's Signal Processing Tool (SPTool). From the energy distribution we can find that the major energy is located at 40-70 KHz, and the peak PSD is at 70 KHz, which correctly reflects the characteristics of resonant sensor R100. The peak energy location is useful for calculating the absolute displacement of particle vibration at sensor-specimen interface, which has been done in time domain analysis. Since the resonant sensor distorts the frequency spectrum, more frequency domain analysis is not necessary.

4.1.3 Discussion

AE signals from corrosion sources were successfully received by DW's AE testing system (totally 112 AE events). It is proved that the application of AE technique to corrosion detection is possible (further discussion in Section 4.6). It was observed that pitting corrosion could produce detectable AE, while general corrosion could not, which was in a uniform rate over the specimen surface. The energy released from uniform corrosion was not large enough to trigger the displacement of the sensor's piezoelectric element. In other words, the vibration of particle of AE wave from uniform corrosion was below the sensor's sensitivity limit (currently, 10^{-13} m). The size of the breaking piece determines the energy release. In pitting corrosion, the size was of the unit mm, and in general corrosion it was of the unit 10^{-2} mm ~10^{-3} mm. We assume amplitude of particle vibration of AE wave is proportional to the size of steel breaking piece. The absolute displacement of particle vibration from pitting corrosion is in the order of 10^{-11} m; if divided by 100, it will be 10^{-13} m ~ 10^{-14} m for general corrosion, which is over the sensor's limiting sensitivity at present.

4.2 Experiment-II: AE in Reinforced Concrete

In this experiment, reinforced concrete specimens were under wet-dry cycling; cathode iron nets were cast into samples to make corrosion continue both in dry and wet conditions. Specimens were submerged in 2% NaCl solution but no salt had been sprayed into the specimen. Applied currents were 6-9 V / 0.07-1.5 A. Resonant sensor R100 was employed at the major part of the experiment to get comparable result with plain corrosion. Then, the broadband sensors B225 and B1025 were used for detection. All these sensors received AE signals from corrosion sources.

4.2.1 Experimental results

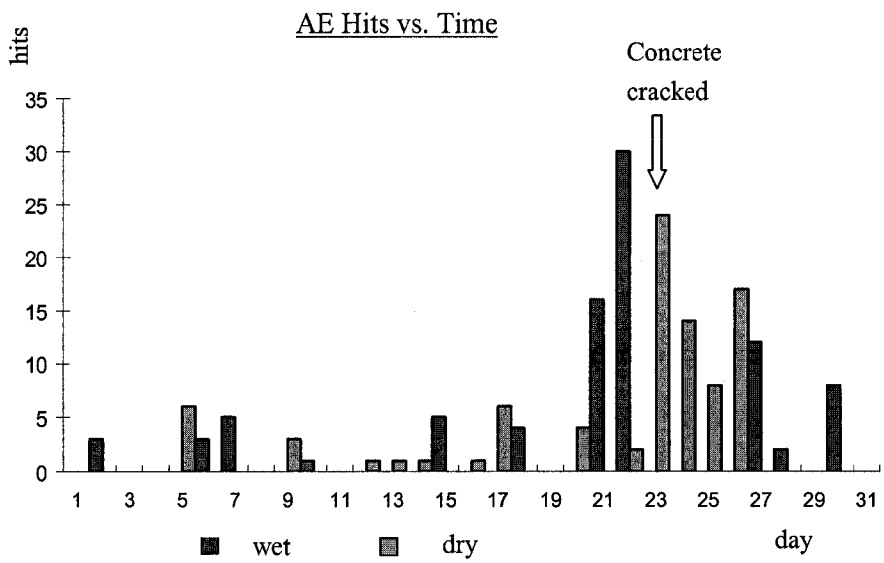

Fig. 4.6 Hits vs. Time of Experiment-II

AE events were recorded during one month testing, as shown in Fig. 4.6. The first event came at the second day. For comparison, the first event in Experiment-I arrived within one

day. Concrete cracked after the emission of large numbers of AE events. The corroded specimen and steel reinforcement are shown in Fig. 4.7. The rust, steel loss and crack of concrete were clearly observed. Both wet and dry cycles produced AE events.

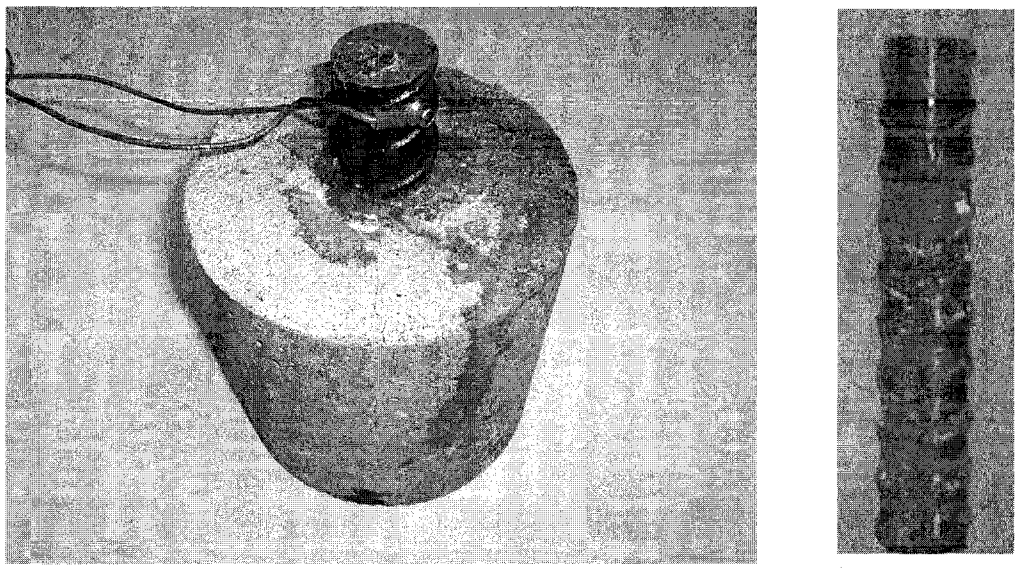

Fig. 4.7 Corroded specimen and steel reinforcement

4.2.2 Analysis of the typical signal

Most AE signals from this experiment are in the waveform shown in Fig. 4.8 (type-1):

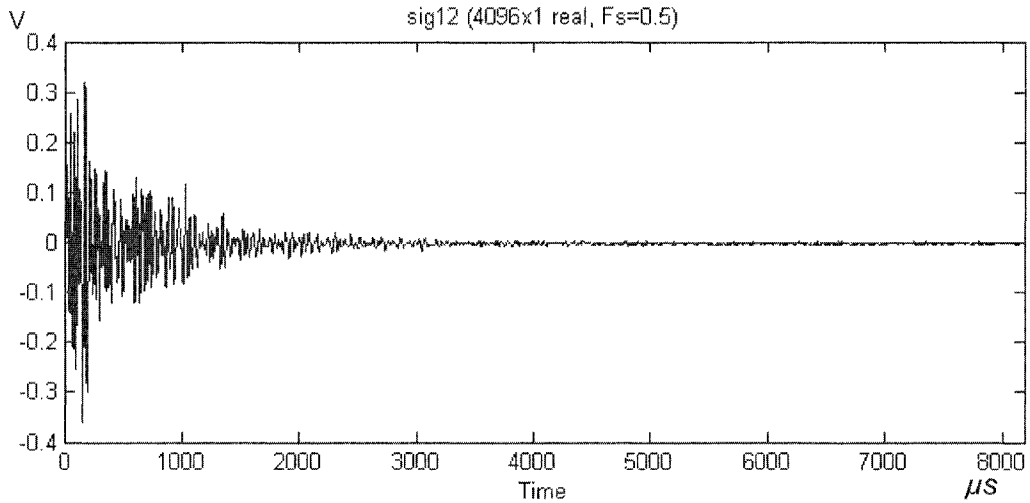

Fig. 4.8 Typical AE signal from Experiment-II (type-1)
[Memory length: 4096 points; Sample frequency: 0.5 MHz; Total amplification: 49 dB]

After FFT transform, the waveform in frequency domain is shown as Fig. 4.9. Sensitivity of R100 at 25 KHz is 31 dB (dB ref 1V/micrometer), which is 2 dB lower than B225. Maximum displacement at sensor-specimen interface can be approximately calculated as: U $=0.35\ V / (10^{(31+49)/20} V/um)=3.5 \times 10^{-11}$ m. The peak amplitude is located at 25 kHz.

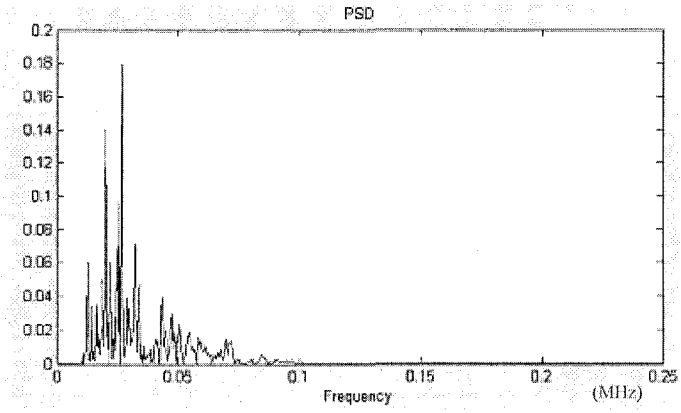

Fig. 4.9 Typical signal in frequency domain

Compare the typical signals from Experiment-I and Experiment-II

At the first glance in time domain, the predominant repetitive waveforms in two experiments (Fig. 4.3 and Fig. 4.8) are different. However, the waveform in Fig. 4.3 actually consists of many repeated signals as explained in Fig. 4.4 by the fractures of pencil leads on the surface of sensor and on the steel block. If the original parts of signal in Fig. 4.3 (the first 350 microsecond) and in Fig. 4.8 (the first 500 microsecond) are taken out, and a detection threshold 0.05 V is set to get rid of DC offset, the ring down counts of both signals are 32. This demonstrates the coherence of the two experiments in some extent. Signals in Experiment-I generally have larger amplitudes than signals in Experiment-II. At the same amplification setting 49 dB, some signals in Experiment-I exceeded the detection limit 0.5 V,

but signals in Experiment-II kept in the limit. However, the peak amplitudes of signals in Experiment-I located at 75KHz, which is the resonance frequency of sensor R100. Resonant sensor has stronger response at resonance frequency. Tracking to the displacement of particle vibration at specimen's surface, the results of two experiments are in same level. In the frequency domain, Exp.-I got peak energy at 75kHz and Exp.-II at 25 kHz. It seems quite confusing, however, the laboratory verification of R100 sensor shows that this type of sensor has a second peak response at 25 kHz.

Other types of signals in Experiment-II

Two other types of signals as shown in Fig. 4.10 occurred when concrete cracked. These signals are related with the concrete crack or debonding between steel and concrete.

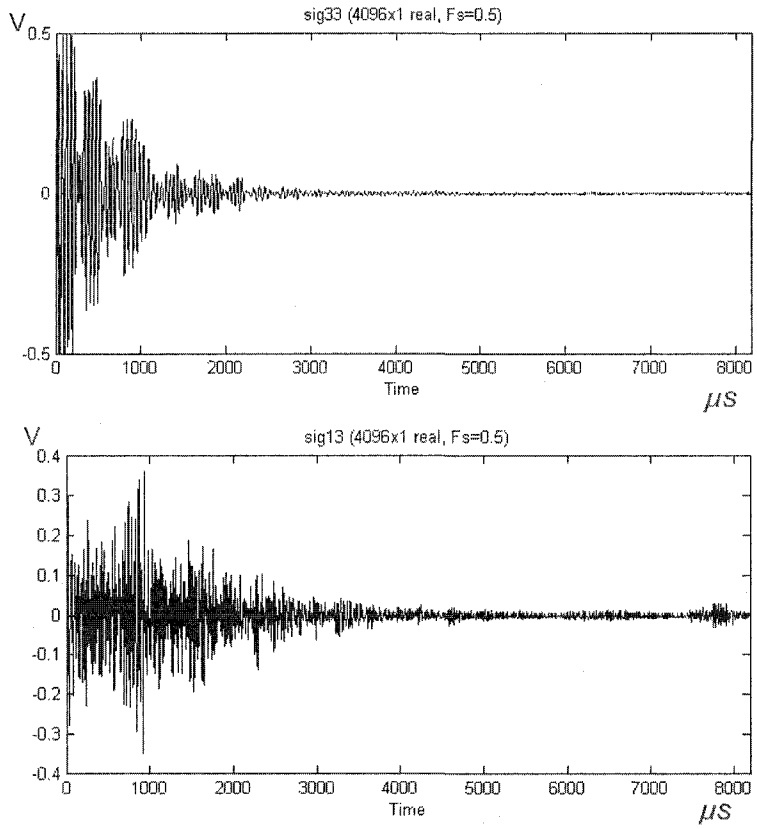

Fig. 4.10 Signals related with concrete crack and debonding

Concrete crack and debonding associate each other; it is difficult to distinguish which one caused the specific type of signal. Concrete cracking AE signals from other researchers are available, but they are not comparable because waveforms vary with different sensors used.

Another type of signals was received during concrete cracking (Fig. 4.11). They were considered as combination of two corrosion signals in the detection duration (8192 microseconds), not related to concrete crack.

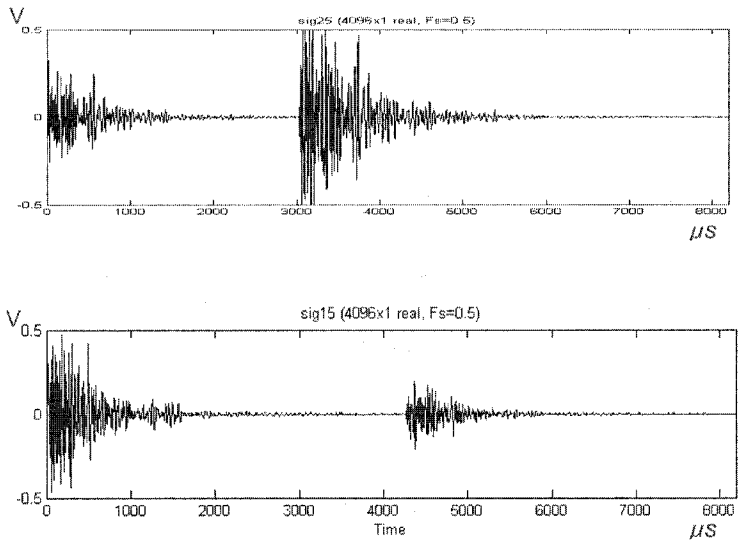

Fig. 4.11 Signal type-3 of Experiment-II

4.2.3 Identification testing at Channel-2

When corrosion-AE testing was in progress (Channel 1), another specimen from same batch (Channel 2) was subject to same conditions: same model of sensors, wet-dry cycles amplification setting, coupling condition and data acquisition setup etc. The solution for Channel 2 was water and no current was applied (Fig. 4.12).

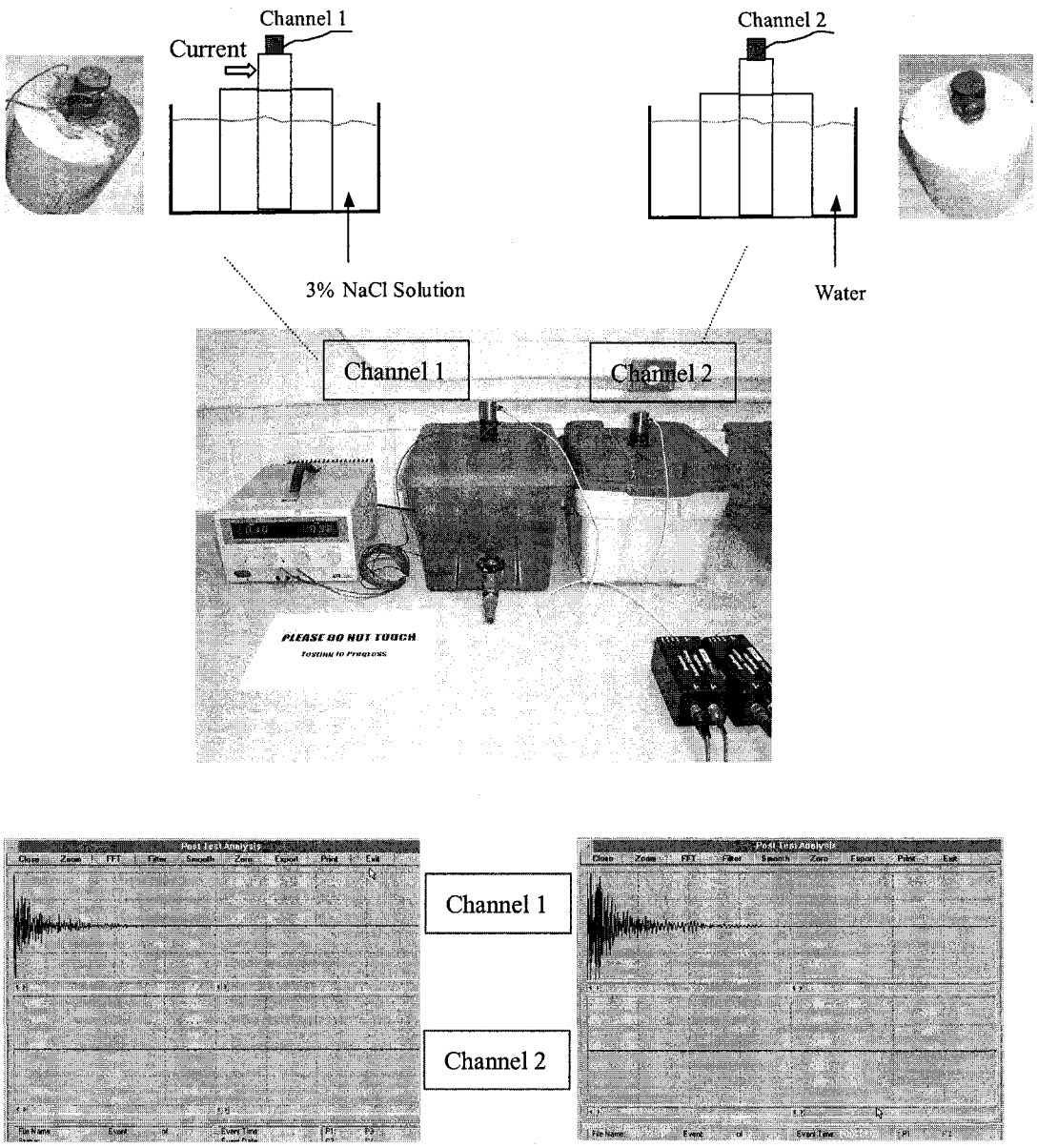

Fig. 4.12 Setup and result of identifying AE signals

The specimen in Channel1 corroded but specimen in Channel 2 not. Correspondingly, only Channel 1 received AE signals, Channel 2 not. Fig. 4.12 shows two example signals. This result can be evidence that AE signals were not from concrete expansion by wet-dry cycles and other interferences. Experiment-V compared the AE measurement to half-cell potential measurement and strongly proved that AE signals connected to corrosion activities tightly.

4.2.4 Discussion

In total, 177 AE events were recorded during one month testing. The first AE event came at the second day. Concrete cracked when large numbers of AE events occurred. Different waveforms were recorded during concrete cracking. AE events occurred at both wetting and drying cycles. The surface displacement of particle at sensor-specimen interface was also in the order of 10^{-11} m (Equations in Section 4.4.1). At the end of experiment, broadband sensors were tried and recorded AE events. It indicated that broadband sensors were also suitable for corrosion detection. Most important contribution of this experiment was that corrosion causing AE signals in reinforced concrete were successfully recorded by AE system. The identifying test can be an evidence to prove the AE signals were emitted from corrosion sources. Experiment-V further proved this fact by comparing AE with half-cell potential measurement.

4.3 Experiment-III: Sensor on Steel vs. on Concrete

Experiment-III examines whether measurement on steel is better than on concrete.

4.3.1 Results and analysis

In the experiment, one B225 sensor was put on concrete (Channel 1), another B225 sensor was put on steel (Channel 2). Sensor of Channel1 was 480 mm away from the center of corrosion source, and it was 650 mm for Channel 2. The amplification setting was +61dB for Channel1, and +49 dB for Channel 2. Fig. 4.13 shows a pair of typical signals. The peak-to-peak amplitude of Channel 1 is 0.25 V, and it is 0.67 V at Channel 2. The difference of peak amplitudes between two channels is (61-49) + 20log(0.67/0.25) = 20 dB (i.e. 10 times).

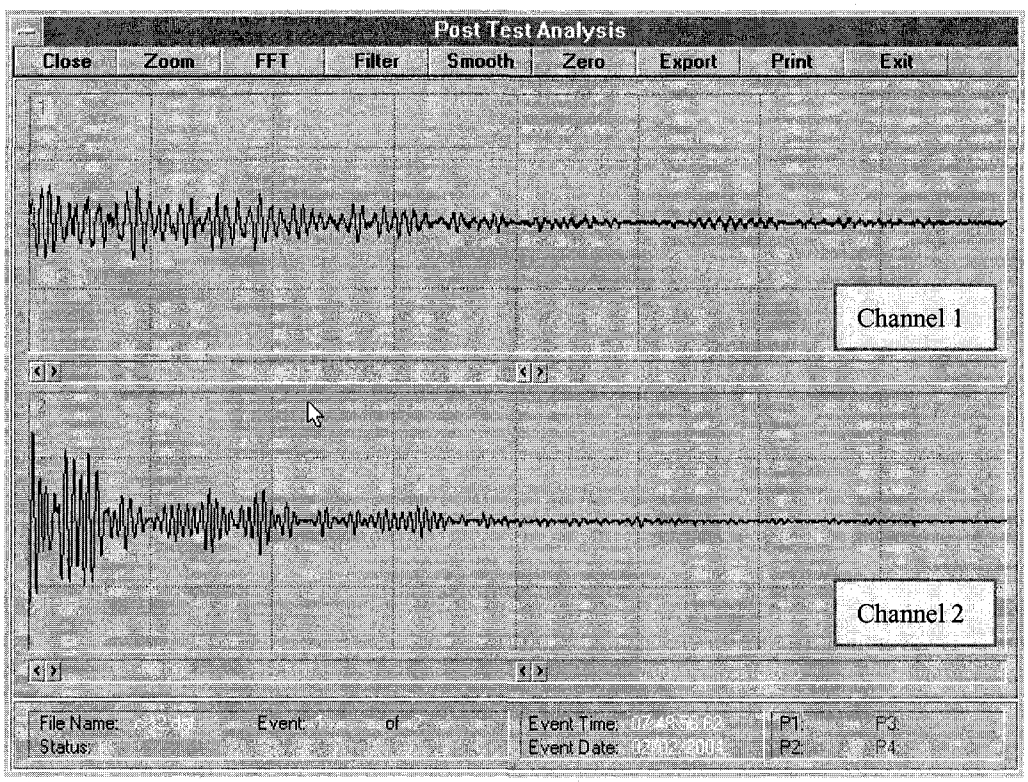

Fig. 4.13 Typical AE event of Experiment-III

Table 4.2 Results of typical events from Experiment-III

Events	1	2	3	4	5	Average
Difference between two channels (dB)	20	19	20	17	18	18.8

More results of typical events are shown in Table 4.2. The average difference between two channels in peak-to-peak amplitude is 18.8 dB. Considering the effect of distance, the difference of amplitudes between two channels is: 18.8 + 20 log(650/480) = 21.4 dB (12 times), which means the amplitude of AE signal detected by sensor on steel is 12 times of that on concrete if the distances to the corrosion source are same. Alternatively, the maximum detectable distance by sensor on steel will be 12 times larger than on concrete.

4.3.2 Discussion

Concrete has much higher attenuation than steel due to its heterogeneous nature. The result of this experiment was an average number over the frequency range of corrosion AE. Elias [1998] compared the attenuation of ultrasonic wave in concrete with that in steel.

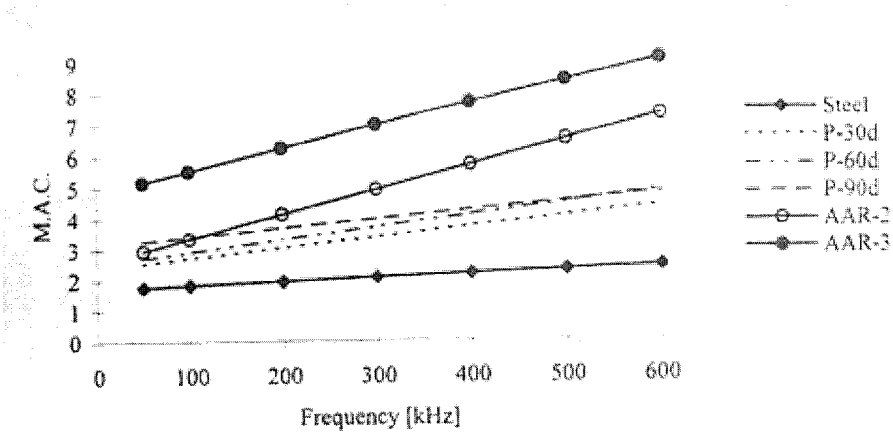

Fig. 4.14 Attenuation vs. Frequency-all materials [Elias, 1998]

She measured the MAC using single frequency ultrasonic wave from 50 KHz to 600 KHz. The MAC (Modified Attenuation Coefficient) was defined as MAC = -log (V_{out} /V_{ref}). Fig. 4.14 shows the differences of MAC between concrete and steel are minimum 1.2 at 50 KHz and max 6.5 at 600 KHz, and the number increases with increasing frequency. Steel has relatively constant attenuation coefficient over the frequency range 50-600 KHz. The Attenuation Coefficient (= 20 x MAC) of concrete is 24 dB (16 times) at 50 KHz or 130 dB (3160 times) at 600 KHz higher than that of steel. 50 KHz is located in the frequency range of corrosion causing AE. At 50 KHz, the attenuation of concrete is 24 decibels higher than steel. Elias' result is coherent to the result of this experiment.

4.4 Experiment-IV: Effect of Distance

This experiment estimates how far we can measure away from the source.

4.4.1 General process of estimating maximum detectable distance

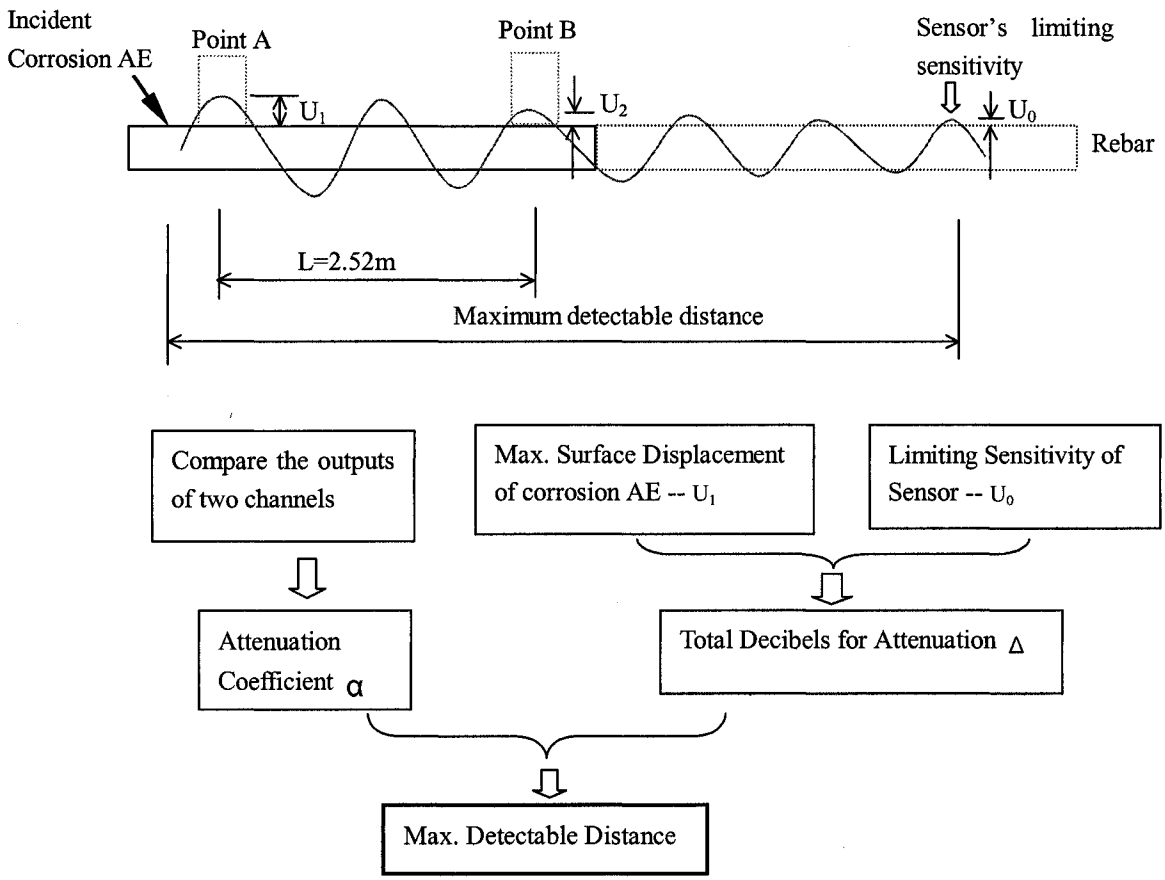

Fig. 4.15 Flowchart of calculation of maximum detectable distance

As depicted in Fig. 4.15, the first step to determine the maximum measurable distance from corrosion source is to find the attenuation coefficient (dB/m) over the frequency range of interest. Secondly, the maximum surface displacement of particle vibration at contact surface has to be found from the corrosion causing AE signals. It is an absolute value,

which reflects the intrinsic characteristics of an AE wave. Then, the maximum surface displacement is compared with limiting sensitivity of sensors to obtain the total decibels for attenuation. Finally, the maximum measurable distance is worked out by divided total decibels by attenuation coefficient.

Equations

- Simplified equations for estimating maximum detectable distance

Attenuation coefficient $\alpha = (20\log(U_1/U_2))/L_c$ dB / m

or in power expression: $\alpha = (10\log(PSD_1/PSD_2))/L_c$ dB / m

Total decibels for attenuation $\Delta = 20\log(U_1/U_0)$ dB

Max. detectable distance $L_{max} = \Delta/\alpha$ m

Where

U_0, U_1 and U_2 are displacements as shown in Fig. 4.15; PSD is Power Spectral Density; L_c is calculation length considering the effect of near field (1 m), L_c equals to 4.61 m in this experiment. Calibration correction for two channels should be considered in calculating the attenuation coefficient.

- Calculation of Surface Displacement $UU = A_{peak} / 10^{(n+R)/20}$ (m or pico-m)

Where A_{peak} is peak amplitude of signal output (V);

n is total amplification rate combining preamplifier and FTM (dB);

s is sensor's sensitivity at absolute displacement calibration (dB, dB ref. 1v/ μm e.g. 40dB = 100V/ μm). The following figure shows the processes.

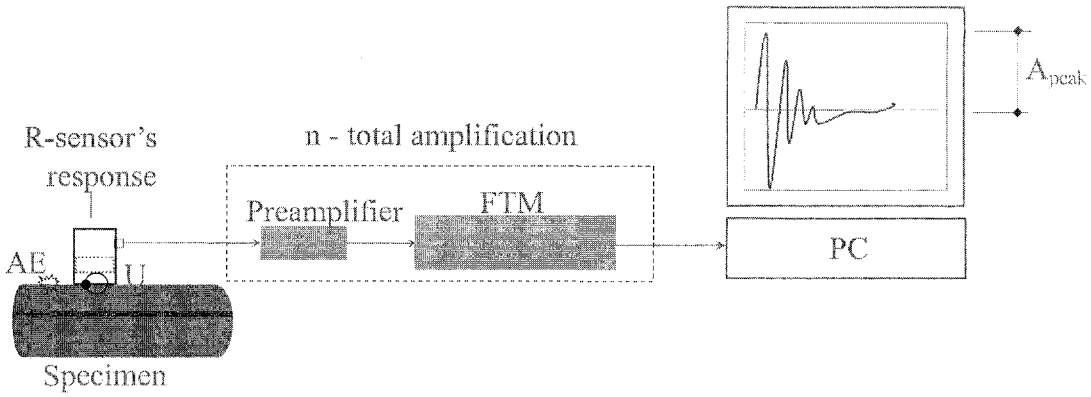

Fig. 4.16 Illustration for the calculation of surface displacement

Near field and far field

Near field is considered within 1 m from AE source. The ratio of attenuation constant in near field to far field is 3.75:1 (GLEA, Leak AE of steel pipe). At near field, the wave energy loss quickly due to severer refraction and mode conversion. Wave propagation is relatively stable at far field (Fig. 4.17).

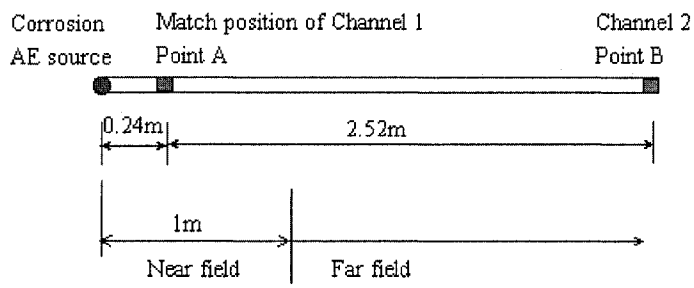

Fig. 4.17 Assumption of near field and far field

Calibration Correction (Cc) for outputs of sensors in both channels

In order to get accurate result of attenuation, the calibration was performed by fracture of pencil lead (0.5mm / 2H / 3mm long) at exact middle position between two sensors after certain pressure had been applied. The amplification settings were +43 dB for Channel 1 and +40 dB for Channel 2. It was very difficult to adjust the outputs of two channels to an exact level, thus the waveform analysis of calibration data was necessary.

From time domain of calibration, the peak-to-peak amplitude of Channel 1 is 0.9 V and that of Channel 2 is 0.7 V. Therefore, the deference in decibels scale of peak-to-peak amplitude between two channels is $20\log(0.9/0.7) = 2$ dB, Channel 1 is 2dB higher than Channel 2. In the following calculation, total attenuation calculated in time domain should reduce 2 dB, the calibration correction. As a result, Cc = -2dB.

4.4.2 Analysis of the typical events

As an example, Fig. 4.18 shows a pair of signals from a typical event.

Calculation of attenuation coefficient in time domain

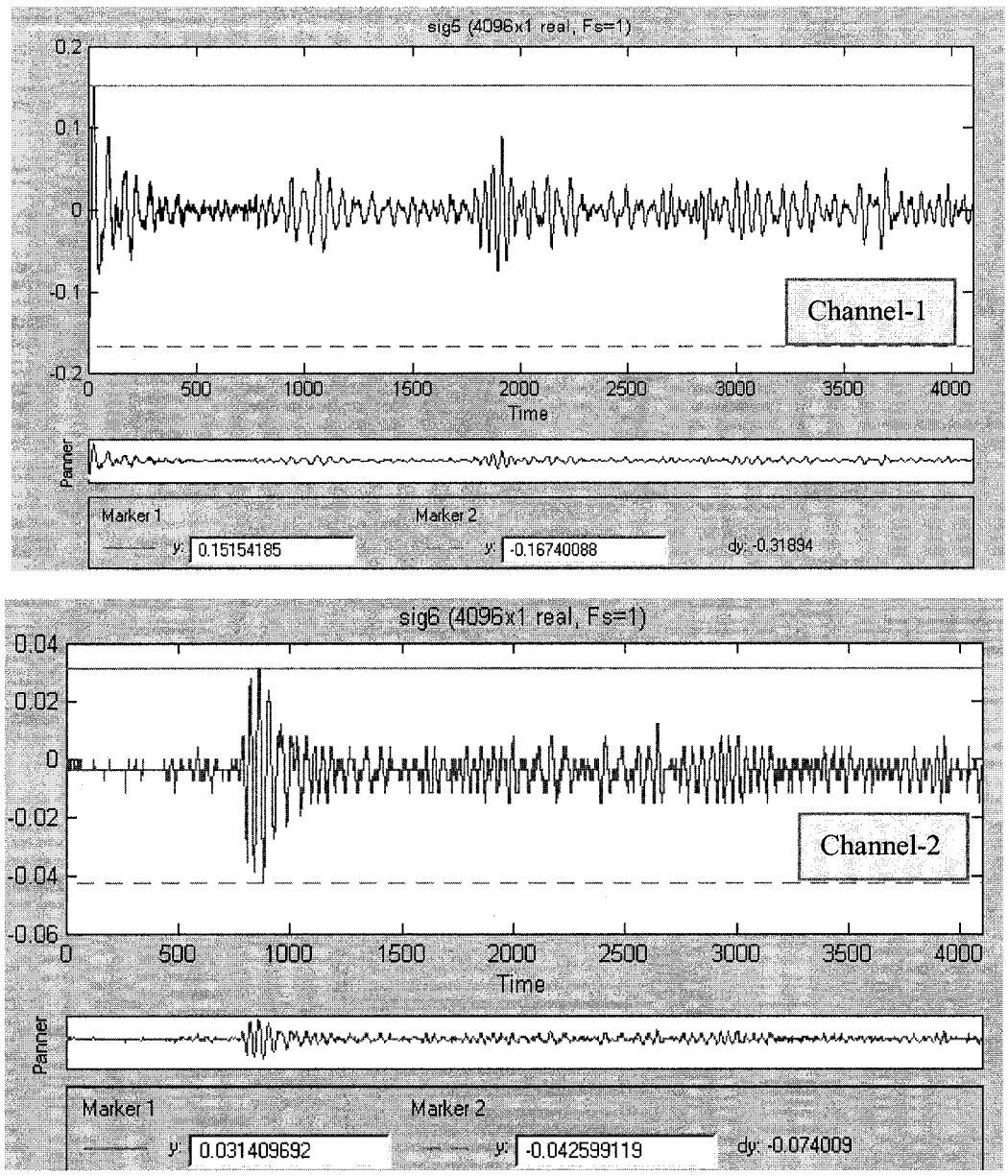

Fig. 4.18 Typical AE event from Experiment-IV

[Sensors:B225; Memory length 4096points; Sample frequency1MHz; Amplification: see Section 4.4.1]

The peak-to-peak amplitude is 0.319 V at Channel1 and 0.074 V at Channel 2. The time duration of data capture is 4096 microseconds (4096 points / 1 MHz) as shown in Fig. 4.18. From equations in Section 4.4.1, the attenuation coefficient is 2.3 dB/m.

Calculation of attenuation coefficient in frequency domain

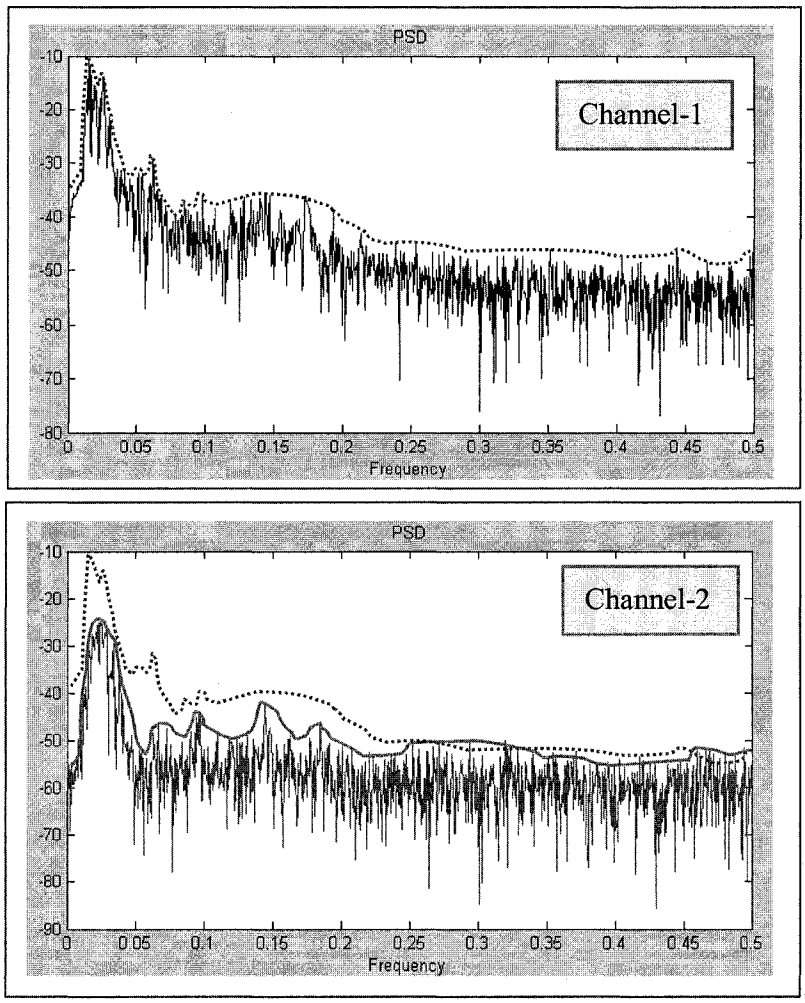

Fig. 4.19 Typical signals of Experiment-IV in frequency domain (decibels scale)

In frequency domain, signal envelopes of two channels in decibels scale were compared as Fig. 4.19, the attenuation of major components of signals (Channel1: 15-32 KHz, 1st peak at 15 KHz, 2nd peak at 25 KHZ; Channel 2: 15-37 KHz, peak 25 KHz) is 11 dB at 25 KHz.

Taking 11 dB for calculation and considering the calibration correction –2 dB, the attenuation coefficient is 1.9 dB/m. More results are shown in Table 4.3.

Table 4.3 Attenuation coefficient of events

Typical Events	1	2	3	4	Average
Attenuation Coefficient-Time	2.3	2.1	3.2	3.6	2.8 dB/m
Attenuation Coefficient-Frequency*	1.9	1.7	2.6	3.1	2.3 dB/m
*Attenuation of major component 15-37 KHz in frequency domain					

Calculation of total decibels for attenuation

The limiting sensitivity of AE commercial sensors U_0 is 1x 10^{-13} m. Form time domain; peak amplitude is 0.168 V, for which the amplification setting was 43 dB. From absolute calibration of the B225 sensor, sensitivity at peak energy frequency (16-17 KHz) is 32 dB, dB ref 1V/micrometer. The absolute displacement at point A (Match position of channel-1) for the typical event is U_1 is 2.99 x 10^{-11} m and the total decibels for attenuation Δin Table 4.4 is calculated according to equations at Section 4.4.1.

Table 4.4 Summary of surface displacements U_1 and total decibels for attenuation Δ

Typical signals from	Experiment-I~III			Experiment-IV typical events				
	I	II	III	1	2	3	4	Average
U_1 (x 10^{-11}m)	1.4	3.5	2.5	2.99	2.99	3.38	5.55	3.73
Δ(dB)	U_1 for reference			U_1 for calculation				51.4

Only data in Experiment-IV was used, because the displacements measured in Experiment-I & II were in longitudinal directions, and the distance between sensor and corrosion sources in Experiment-III was different from Experiment-IV.

Calculation of maximum detectable distance

The maximum detectable distance L_{max} in time domain is 17 m, based on the sensor's limiting sensitivity 10^{-13} m. For the chosen major component in frequency domain, L_{max} equals to 21 m. If the sensor's sensitivity limit can be extent to 10^{-14} m, the total Decibels for Attenuation Δwill be 71.4 dB, then, L_{max} will be 24 m in time domain and 29 m for major component in frequency domain. The results are illustrated in Fig. 4.20. The major component in frequency domain refers to the component carries high energy with relatively low attenuation.

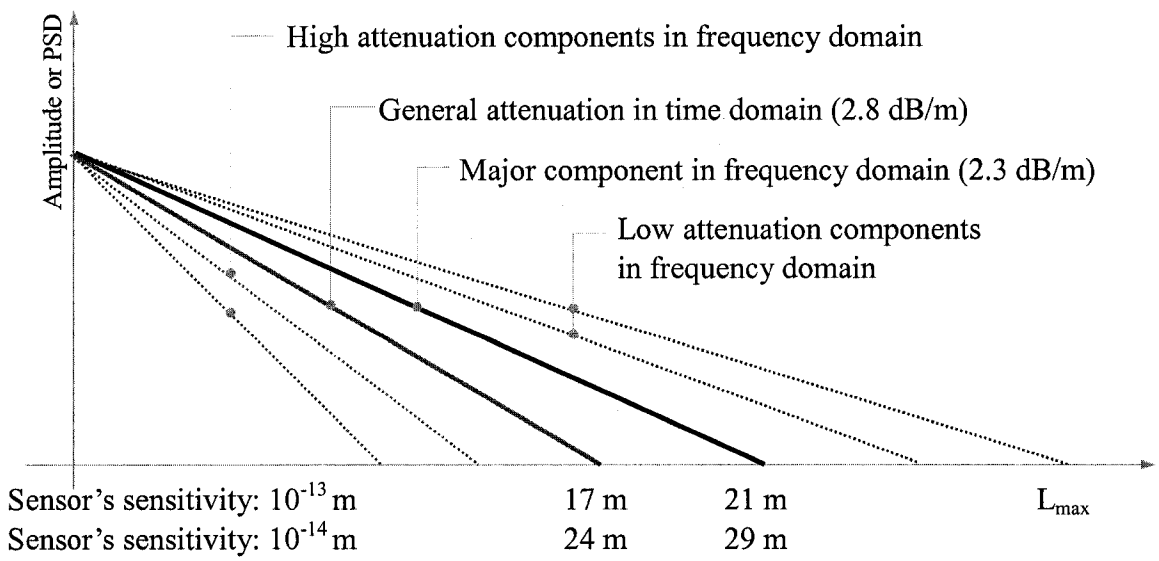

Fig. 4.20 Maximum detectable distance L_{max}

4.4.3 Discussion

The results in Fig. 4.20 are subject to the following conditions: (i) rebar size or other geometrical factors of testing object; (ii) the assumption of near / far field and the ratio of attenuation coefficient; (iii) sensor's limiting sensitivity; and (iv) material component of rebar, grain size and the homogeneity of grains.

For the overall frequency range in Fig. 4.19, the attenuation was not linear, even in some frequencies the PSD increased due to the slight difference of response between two sensors with same model, and the complicated mode conversion during wave propagation, which caused certain frequencies convert to other frequencies. The attenuation in 250-500 KHz was flat, and less significant than 10-250 KHz. This result was coherent with the result of Stepanka Elias, who found that "the steel attenuation was nearly constant across the frequency range (50 KHz to 600 KHz)" regarding the ultrasonic testing (details in Section 4.3.2). The attenuation significantly increases with frequency in concrete and many common materials; steel attenuation is relatively flat, particularly in a short frequency range, although the attenuation mechanism in steel depends on frequency and the ratio of grain or particle size to wavelength.

Generally speaking, current commercial sensors with sensitivity 10^{-13} m can detect AE signals from about 20 m away from corrosion sources. Beyond that distance some AE signals still can be detected, but many vanished.

4.4.4 Location of AE source

The location of corrosion can be one-dimensionally determined by comparing the first peak arrivals of signals from two channels as shown in Fig. 4.21 and Fig. 4.22.

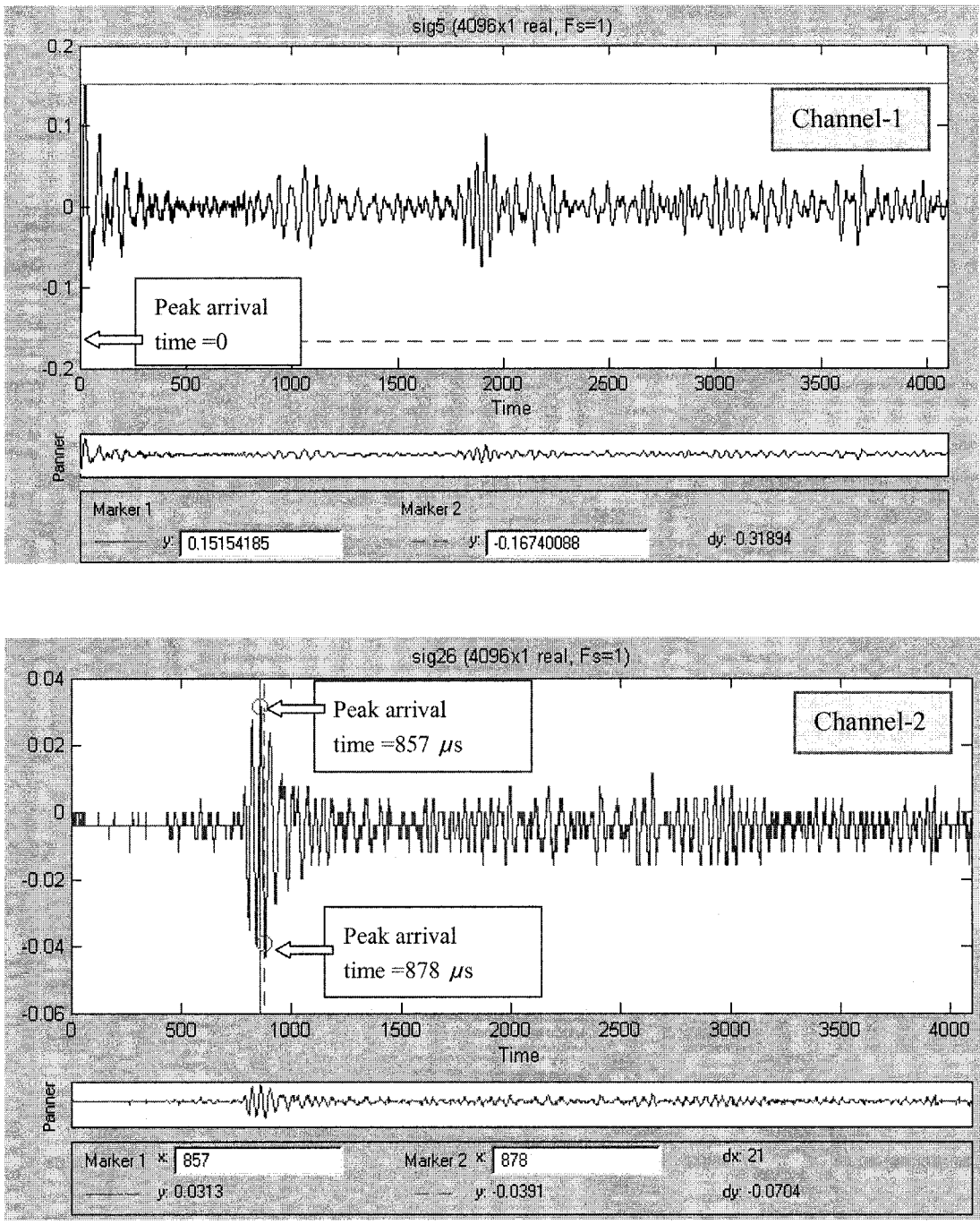

Fig. 4.21 First peak arrivals at two channels

Because two sensors were located at two sides of source (Fig. 4.22), the time interval of wave propagation between two sensors should be 857 μs, not 878 μs. When one sensor met the wave peak, another one met the valley.

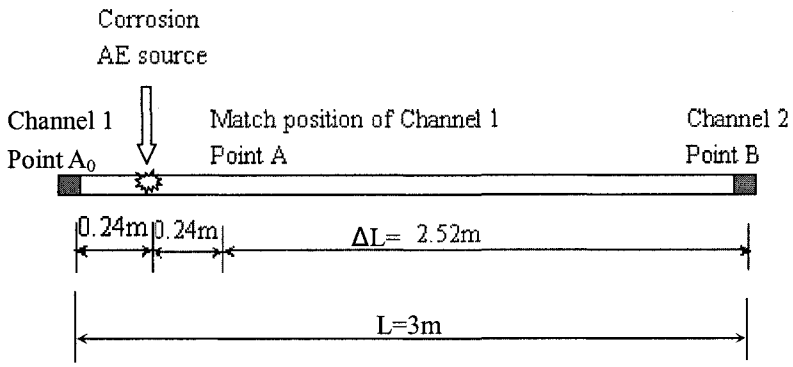

Fig. 4.22 Sketch for determining location

From wave propagation theory, the velocities are various with the materials and wave modes. Table 4.5 lists velocities given by NDT resources center [http://www.ndt-edu.org, accessed Oct. 20, 2003].

Table 4.5 Group velocities in steel and concrete

Wave	Longitudinal wave	Transverse wave	Surface wave
Velocity in steel (m/s)	5900 in bulk 5200 in rod or bar	3280	3018
Velocity in concrete (m/s)	3650 (3500)	1440	1320

The predominant wave mode in rebar is surface wave by comparing the wavelength (Table 4.6) with rebar size. Thus, 3018 m/s is used to calculate the AE source location. The

velocity 3018 m/s is an approximate number that varies with specimen size, chemical components, grain sizes, frequency and wave mode. The distance difference between two sensors to corrosion source: $\Delta L = 3018$ m/s x 857×10^{-6} s $= 2.586$ m, which is generally coherent with the real number is 2.52 m.

Table 4.6 Wavelength vs. Frequency

Wave	Velocity	Wavelength(mm) vs Frequency									
		25KHz	50KHz	100KHz	150KHz	200KHz	250KHz	300KHz	400KHz	500KHz	1000KHz
Longitudinal	5200	208.0	104.0	52.0	34.7	26.0	20.8	17.3	13.0	10.4	5.2
Transverse	3280	131.2	65.6	32.8	21.9	16.4	13.1	10.9	8.2	6.6	3.3
Surface	3018	120.7	60.4	30.2	20.1	15.1	12.1	10.1	7.5	6.0	3.0

The source location is $(L-\Delta L)/2$ from one end or $(L+\Delta L)/2$ from another end. If two sensors are located on same side from source, ΔL equals to L. The location of corrosion source can't be determined, but it can be estimated by attenuation and rearrangement of sensor's positions.

In reverse, calculation of velocity can determine which wave mode is predominant in wave propagation. It can be proved that predominant mode of AE wave propagating in long rebar is Lamb wave. "The distance-attenuation characteristics of these waves, bulk waves tend to couple to Lamb waves and at great distances from source Lamb waves are likely to predominate" [Ian, 1991].

4.5 Experiment-V: AE vs. Half-cell Potential

This special experiment aimed to further identify corrosion causing AE.

4.5.1 Introduction of CANNIN Half-cell equipment

The half-cell potential measurement is an electrochemical technique commonly used to assess the severity of corrosion in reinforced concrete structures. CANNIN is the corrosion-analyzing instrument made by Proceq, Switzerland. Swiss Federal Institute of Technology initiated CANNIN and has provided scientific support. CANNIN accurately measures corrosion potentials ranged from +270 mV to –950 mV. Measuring with rod electrode according to ASTM C876 is suitable for laboratory and field tests. A measuring surface of more than 4000 m^2 can be managed with the large memory and the wheel electrode (Fig. 4.23).

Fig. 4.23 CANNIN half-cell equipment with rod and wheel electrodes

The mechanism of half-cell equipment is shown in Fig. 4.24.

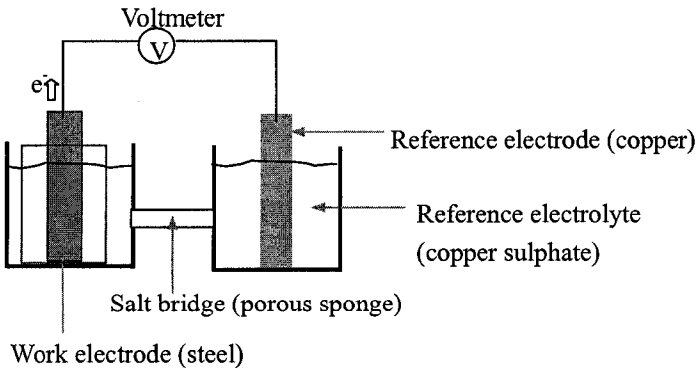

Fig. 4.24 Mechanism of half-cell with a CSE ref. electrode

4.5.2 Examination testing of Half-cell equipment

This testing was used to verify if the half-cell equipment could work properly.

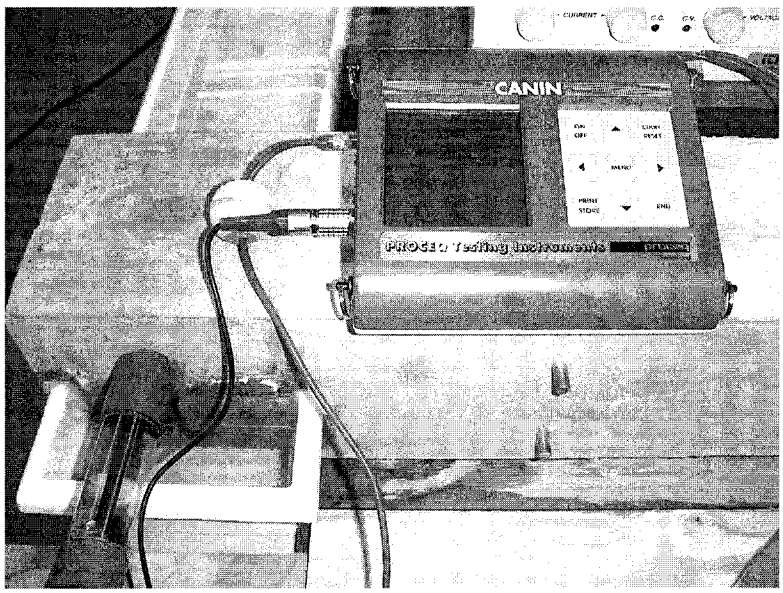

Fig. 4.25 Examination test using corroded specimen of Experiment-III

The specimen for Experiment-III was used to examine the half-cell equipment. It was known that steel corrosion had obviously occurred in this specimen. Ten observing points

were taken on the surface of specimen. Before salt solution was added, potentials at these points were: 75, 160, 110, 72, 270, 270, 270, 252, 136, 53 mV. After applying 12 V DC on the specimen for three hours, no current was applied, but some part of the specimen was immersed in 3% salt solution. After nine more hours, the potentials at 10 points dropped to –386, -56, -7, 2, -30, -142, -195, -274, -364, -349 mV respectively. During this period, 4 AE events were received by AE detection system. The half-cell equipment worked stably and the potentials were generally coherent with AE. It was proved that the equipment worked well. However, it was observed that applied current greatly influenced the half-cell potentials. About two hours after termination of applying current, the potentials returned to normal level. Thus, no current will be applied to specimens in formal test.

4.5.3 Experimental setup

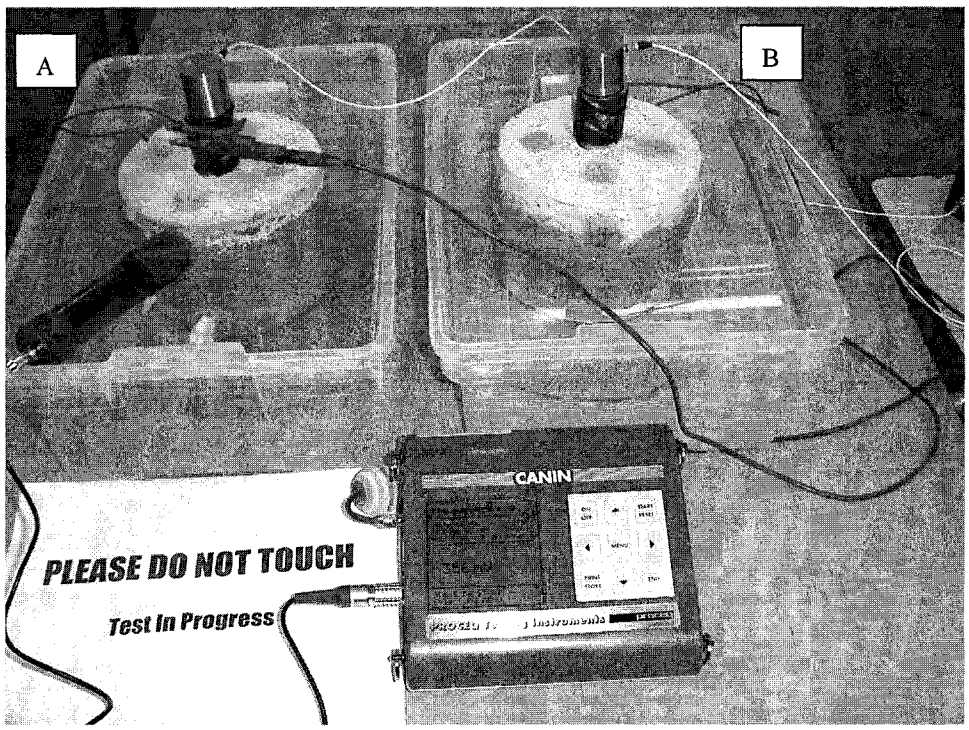

Fig. 4.26 AE vs. Potential testing in progress

Two cylinder specimens were cast with same batch of Experiment-II six months ago (Oct. 2003). Specimen A was put in 3% NaCl solution (Channel 1), specimen B was put in pure water (Channel 2). 3/4 height of specimen was immersed in solution or water.

No current was applied. Two R100 resonant AE sensors were put on the top of two specimens. The total amplification settings were 49 decibels for both channels. Sample frequency was 1 MHz and the memory length was 4096 points. The formal test had lasted for 100 hours. Half-cell potentials were measured every four hours in the daytime and 12 hours at night. Six measuring points were chosen at each specimen and every time measurements were made at same positions.

4.5.4 Results and discussion

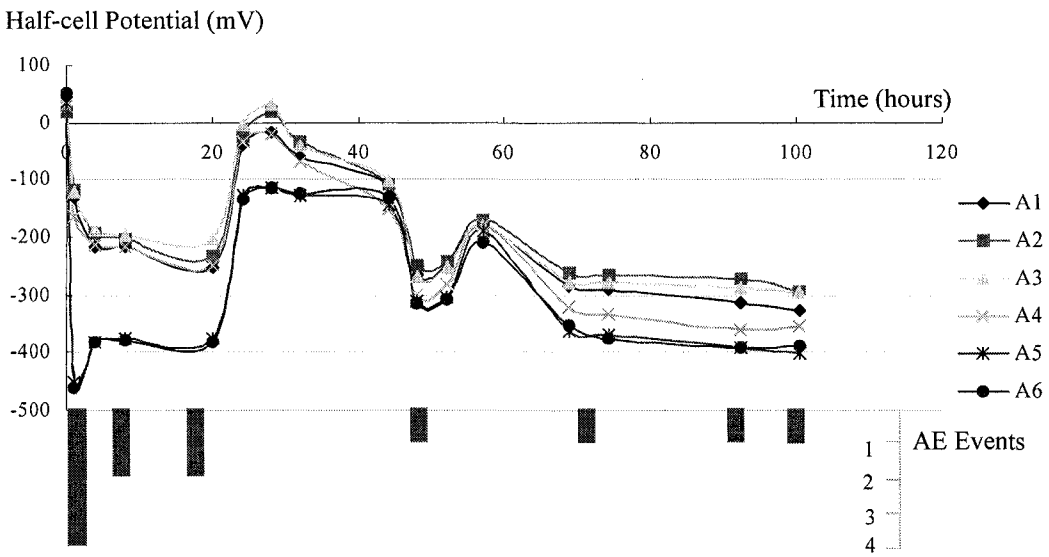

Fig. 4.27 AE Event vs. Potential- Specimen A in 3% salt solution

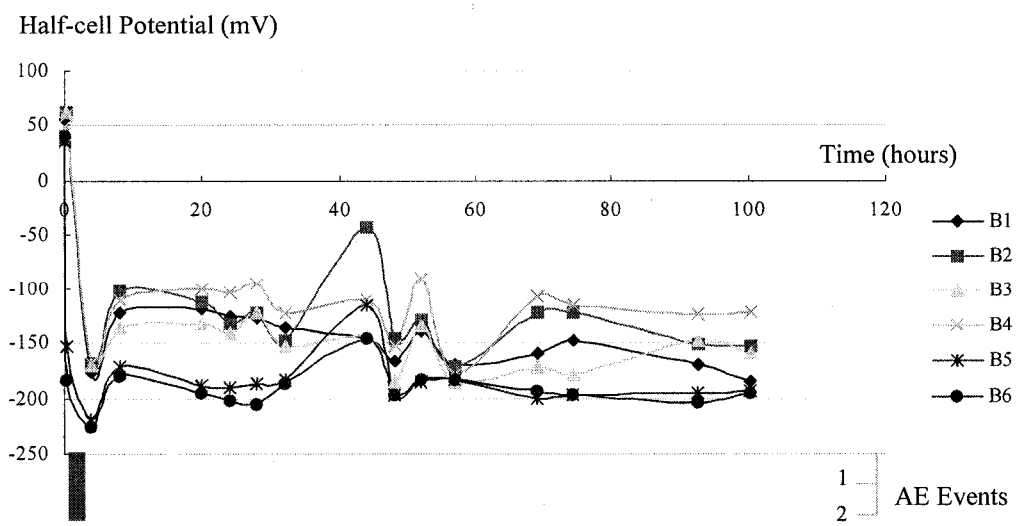

Fig. 4.28 AE Event vs. Potential- Specimen B in water

As soon as the specimens were put in salt solution or water, the half-cell potentials of two specimens dropped to negative level quickly. Specimen A in salt solution was much faster than specimen B in water, but specimen B did drop too. This result demonstrated that corrosion had occurred in both specimens already! The specimens had been placed in lab more than six months. The laboratory environment at basement was a little moist and sometimes a little bit chemical-aggressive, it was normal that corrosion occurred in these specimens. This was good for comparing AE events with half-cell potentials without imposing current.

The testing results shown in Fig. 4.27 and Fig. 4.28 demonstrated general coherence with half-cell potential measurement standard ASTM C876 (CSE) in Table 4.7. Specimen A in salt solution: most AE events emitted when the potentials were below –350 mV.

Table 4.7 ASTM C876 (CSE)

Measured Potential	Risk of Corrosion
<-350mV	90%
-200mV to -350mV	50%
>-200mV	10%

Specimen B in water: only two events were received at beginning when the potential sharply dropped below –200mv. After that, the lowest potentials were around –200 mV, no AE event was received. The result is consistent with standard ASTM C876: above –200 mV the risk of corrosion is 10%. If detecting the corrosion for a very long time, it is possible that some AE signals will be received, but not definitely. The half-cell potentials of Specimen A in salt solution were much lower than Specimen B in water, and Specimen A consistently emitted much more events than Specimen B. Visual inspection also showed corrosion in Specimen A was much severer than Specimen B as Fig. 4.29.

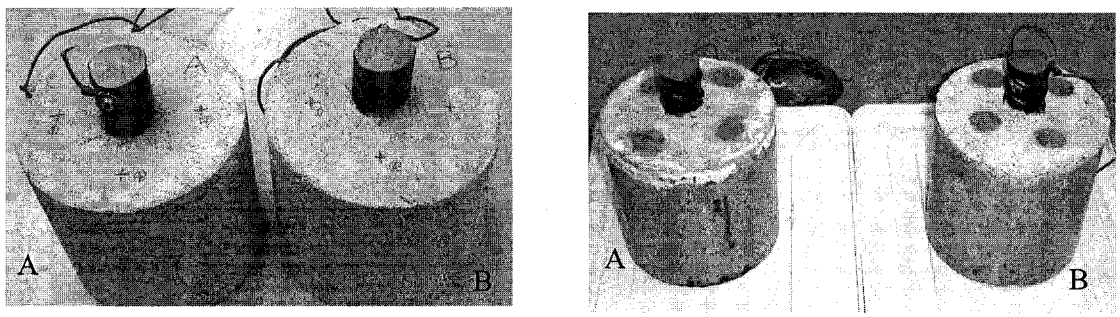

Fig. 4.29 Specimens before testing (left) and after testing (right)

As a result, it is proved that AE technique can effectively indicate the corrosion activities in reinforced concrete.

4.6 Summarized Discussion

1. Can steel corrosion be "heard" by the AE sensors?

The results of Experiment-I in Section 4.1and Experiment-II in Section 4.2 give the exciting answer that steel corrosion can be "heard" by AE sensors both in plain corrosion and in reinforced concrete.

The localized corrosion produced strong AE signals. The displacements of particles at specimen's surface, on which the sensors had been put, were in the order of 10^{-11} m. Both broadband sensors and resonant sensors were capable of detecting corrosion causing AE.

2. Are the AE signals in reinforced concrete due to corrosion or other processes?

The following evidences or reasons proved the received AE signals in corrosion tests were generated by corrosion activities, not noise or interferences e.g. from concrete expansion by wet-dry cycles.

- Experiment-V (Section 4.5)

A special experiment had been performed to compare the AE events with the half-cell potentials of corrosion activities. The coherent result showed that AE events exclusively connected to corrosion activities.

- Identification setting in Experiment-II (Section 4.2.3)

When Channel-1 was in corrosion testing progress, Channel-2 was set to subject to same conditions e.g. same wet-dry cycling, specimen from same batch, sensor with same model and same coupling material, but no accelerated corrosion regime was applied to Channel-2.

The result was that only Channel-1 received signals but Channel-2 did not.

- Results of Experiment-III & IV (Section 4.3 & 4.4)

In these two experiments, the attenuation of AE waves in steel and in concrete was consistent with other researches regarding attenuation of ultrasonic waves in frequency range 50-600KHz. In addition, Experiment-IV correctly located the corrosion position. Those results also strongly supported the fact that the AE signals received were from corrosion sources.

- Laboratory environment and the time of signal arrival

The lab was quiet, especially in the mid-night noise was usually unavailable in lab. But many AE signals arrived at mid-night during testing.

- Filter function of DW AE equipment

Firstly, the sensors were designed un-sensitive to low frequency noises. They only responded to direct-hit elastic vibration. It was tried that direct-hit on specimen by a small steel bar can cause AE signals, but hit on table or on the ground couldn't. Secondly, the filter function of FTM unit of DW system (Minimum high-pass: 20KHz) filtered most noises out. For reference, human audible sound is from 20Hz to 16-20 KHz.

- Numbers and wave from of signals

Large amount of signals were received, totally 112 AE signals in Experiment-I and 177 in Experiment-II. A lot of signals were in similar waveforms. This fact excluded the occasional external interference.

- The visible corrosion and steel loss occurred when large numbers of AE waves emitted

3. Is it better to put the sensors on the steel or concrete?

Yes, it is better to put the sensors on steel than on concrete.

The results of Experiment-III (Section 4.3) indicated the amplitude of an AE signal received from sensor on steel was 21.4 dB (12 times) in average more than that from sensor on concrete. In other words, if the maximum detectable distance is 12 m for putting sensors on steel reinforcement, it will be 1 m for concrete. It is an approximate number, which depends on the concrete mix design, rebar size, and coupling of sensor etc. However, the number is persuasive.

4. How far can we measure away from the corrosion source?

From the analysis of Experiment-IV in Section 4.4, the maximum detectable distance away from the corrosion source is 17 m ~ 21 m for 10^{-13} m sensor's limiting sensitivity and 24 m ~ 29 m if the sensor's sensitivity extends to 10^{-14} m. The results were obtained both in time domain and in frequency domain. They are subject to the geometric conditions of specimen and the assumption of near field effect.

In addition, while the high-pass filter (20 KHz) of the DW's AE equipment blocked off noises, it razed out part of an AE signal. The experimental results showed that spectra of corrosion AE were from 10 KHz (or lower) to 100 KHz. If equipment with lower high-pass filter is used, the detectable distance L_{max} might greatly increase. In return, de-noising process should be required for post-test analysis.

CHAPTER 5. CONLUSIONS AND RECOMMEDATIONS

5.1 Conclusions for the Four Key Questions

1. Can steel corrosion be "heard" by the AE sensors?

   Yes, it can.

2. Are the AE signals in reinforced concrete due to corrosion or other processes?

   The identification of AE signals was presented in Section 4.2, 4.5 and 4.6. The AE and half-cell potential measurements got coherent results for detecting corrosion in reinforced concrete specimens.

3. Is it better to put the sensors on the steel or concrete?

   Yes, it is much better to put the sensor on steel.

4. How far can we measure away from the corrosion source?

   The maximum detectable distance is expected to be 17 m - 21 m by using commercial piezoelectric sensors with limiting sensitivity 10^{-13} m. These numbers are subject to conditions described in Section 4.4.3 and Section 4.6.

5.2 Other Conclusions

1. In this study, the surface displacement at the very near field of specimen (within 30 cm from corrosion source) was measured in the order of 10^{-11} m for AE from localized corrosion of steel reinforcement.

2. The major part of energy (PSD) distribution of corrosion AE is less than100 kHz, particularly in the range of 15 - 40 kHz. No data was obtained below 10 kHz due to the high-pass filter function (20 kHz) of DW's AE equipment.

3. The average attenuation coefficient of corrosion AE in one-inch diameter steel reinforcement is 2.3 - 2.8 dB/m at far field based on the assumption of near / far field. It was found that the predominant AE wave propagating in steel reinforcement was Lamb wave, which correctly located the corrosion source.

4. Both resonant and broadband sensors (out-of-plane) can be employed to detect corrosion AE for different purposes. Minimum contact pressure 29 kPa was observed to reach maximum output of broadband sensor B225. It was found that B225 and R100 had similar sensitivities due to the aperture effect. The optimum setting of total amplification was 40-49 dB for detecting corrosion AE by sensor B225 and R100.

5. Diffused general corrosion was not significant enough to trigger the response of sensors used in this work.

5.3 Recommendations for Future Research

1. Distinguish corrosion AE from load-induced concrete crack AE and field noises by threshold of hearing, amplitude distribution, spectral range (energy distribution) and other waveform analysis tools.

2. Further study AE wave propagation and source characterization e.g. near field effect, "steel micro-cracks" and concrete micro-cracks caused by corrosion activities.

3. Find or develop optimum transducers with high sensitivity and flat response over the range of several kHz to 100 kHz, and AE equipment with lower high-pass limit and more advanced signal analysis software.

4. Conduct an in situ experiment to detect corrosion AE in a reinforced concrete structure.

5.4 A Look of Real-time Monitoring Corrosion in RC Structures

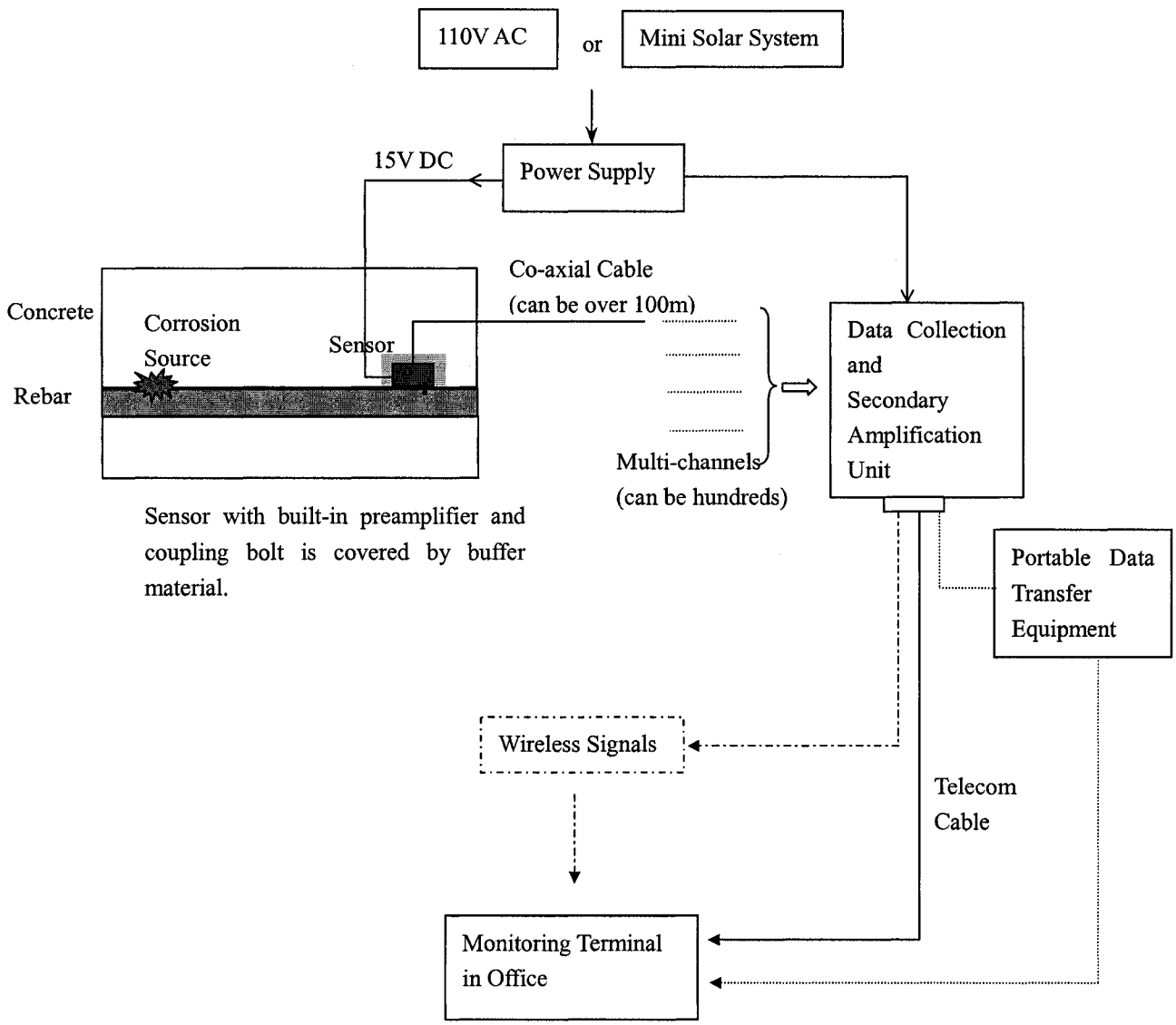

REFERENCES

ACI Committee 222, ACI 222R-85, *Corrosion of Metals in Concrete*, American Concrete Institute, pp. 222R-1 to 222R-2, 1985

ACI Committee 224, ACI 224.1R-93, *Causes, Evaluation and Repair of Cracks in Concrete Structures*, American Concrete Institute, pp. 224.1R-2 to 224.1R-10, 1993

Baboian R., *Corrosion Tests and Standards,* ASTM, pp. 45-60, 1995

Bedford A., Drumheller D. S., *Introduction to Elastic Wave Propagation*, John Wiley & Sons Ltd, pp. 21-54, 1994

Blitz J., *Elements of Acoustics,* Butterworths, pp. 23-132, 1964

Brasunas A. et al, *Corrosion Basics- An Introduction,* NACE, pp. 23-103, 1984

Brunner A., *Acoustic Emission standards and guidelines 2002: a comparative assessment and perspectives,* The e-Journal of Nondestructive Testing, Vol.7 No.09, Sept. 2002

Brook D., Wynne R. J., *Introduction to Signal Processing,* Wiley & Sons, pp. 21-35, 1991

Bounda A. B. et al, *Ultrasonic NDE of Materials Grain Size and Hardness*, Elsevier, pp. 733- 736, 2003

Carlos M. F., *Acoustic emission: heeding and warning sounds from materials,* ASTM, pp. 1-5, 2003

Cherrouf Z. et al, *The Steel Grain Magnification Influence on the Ultrasound Wave Attenuation,* 15th WCNDT, pp. 1-5, 2000

Cottis R. A.., and A. Llewellyn, *Electrochemistry for corrosion,* UMIST, pp. 1-11, 1996

Cullington D. W., *Evaluation of continuous acoustic monitoring as a means of detecting failures in post-tensioned and suspension bridge,* London, pp. 1-15, 1998

Dervisoglu O., *Use of attenuation to monitor load-induced damage in plain & fiber reinforced mortars*, Thesis, University of Windsor, pp. 23-39, 2002

Digital Wave User Manual - Ultrasonic/ AE System, 1997

Dual J., *Vibrations, Wave Propagation, Non-destructive Evaluation,* pp.1-7, 2003

Duke J. C., *Health monitoring of post tension tendons,* Virginia Transportation Research Council, pp. 1-16, 2002

Dunegan H. L., *Considerations of Selection of Advanced AE Transducers,* DECI report, pp. 1-2, 2003

Dunegan H. L., *Transducer Performance Terminology*, the DECI report, pp. 1-2, 1996

Elias S., *The Use of Elastic Pulse Attenuation for Damage Assessment of Concrete*, Thesis, University of Toronto, pp. 4-140, 1998

Esward T. J, et al, *An Investigation Into the Establishment and Assessment of a Test Facility for the Calibration of Acoustic Emission Sensors*, NPL Report CMAM 82, pp. 5-59, 2002

Fitzpatrick R., *Green's Functions*, Utexas lectures, pp. 1-4, 2002

Frederick J. R., *Ultrasonic Engineering*, John Wiley & Sons, pp. 12-209, 1965

Galan A., *Combined Ultrasound Methods of Concrete Testing*, Developments in Civil Engineering, Elsevier, pp. 33- 34, 1990

Gautshchi G., *Piezoelectric Sensorics*, Springer, pp. 199-244, 2002

Geng R. S., *Corrosion-related Acoustic Emission and Its Identification*, Beijing ATRC, 10th APCNDT, pp. 1-6, 2001.

Goujon L., and Baboux J. C., *Behavior of acoustic emission sensors using broadband calibration techniques*, Meas. Sci. Technol. 14 (2003) pp. 903-908, 2003

Gu P., and Beaudoin J. J., *Obtaining effective half-cell potential measurements in reinforced concrete structures*, Institute for Research in Construction, pp. 1-4, 1998

Haynes G. S., Baboian R., *Laboratory Corrosion Tests and Standards*, ASTM, pp. 275-296, 522-561, 1983

Hansson C. M., *A critical Assessment of Methods of Measuring the Rate of Corrosion of Steel in Reinforced Concrete, Ministry of Transportation*, Ontario, pp. 1-29, 1986

Hearn N., *On the Corrosion of Steel Reinforcement in Concrete*, 1st Structural Specialty Conference, CSCE-SCGC, pp. 763-774, 1996

Holland R., *Design of Resonant Piezoelectric Devices*, Ryerson Polytechniqic University, pp. 3-11, 1969

Holroyd T., *Acoustic Emission & Ultrasonic Monitoring Handbook*, Coxmoor Publishing, Abstract, 2000

http://www.cnea.gov.ar/cac/endye/glea/mateo/guide.htm, *Acoustic Emission Reference Guide*, Acoustic Emission Latin American Group (GLEA) of National Commission of Atomic Energy, Argentina, pp. 1-6, accessed Dec. 12, 2003

http://www.ndt-ed.org, *NDT Resources Center,* accessed Oct. 20, 2003

http://www.ndt.net/article/v07n09/05/05.htm, *AE Testing Fundamentals, Equipment, Application,* accessed July 14, 2003

http://www.ndt.net/article/az/ae/ringdowncount.htm, *Time domain analysis*, accessed Nov. 22, 2003

Ian G. S., *Basic acoustic emission*, Gordon and Breach Science Publishers, pp. 6-179, 1991

Idrissi H., and Liman A., *Study and characterization by AE and electrochemical measurements of concrete deterioration caused by reinforcement steel corrosion*, NDT&E International 36 (2003), Elsevier, pp. 563-569, 2003

ISIS Canada, *Proceeding of the Third Annual ISIS Canada Conference*, Theme 2-3, 1998

Kinsler L. E., et al, *Fundamentals of Acoustics*, John Wiley & Sons, 1982

Kishi T., Ohtsu M. et al., *Acoustic Emission – Beyond the Millennium*, Elsevier, pp. 1-213, 2000

Kosmatka S. H., et al, *Design and Control of Concrete Mixtures*, CAC, pp. 14-18, 2002

Krautkramer J., *Ultrasonic Testing of Materials*, Springer-Verlag, 4th edition, 1990

Landis E., et al, *Developments in NDE of Concrete*, Northwestern University, pp. 1-6, 1994

Landis E., Shah S., *Frequency-Dependent Stress Wave Attenuation in Cement-Based Materials*, Journal of Engineering Mechanics June 1995, pp. 737-743, 1995

Lee C., *Accelerated Corrosion and Repair of Reinforced Concrete Columns Using CFRP Sheets*, Thesis, University of Toronto, pp. 5-100, 1998

Malhotra V. M., Carino N. J., *Handbook on Nondestructive Testing of Concrete*, CRC Press, pp. 169-333, 1991

Manning D.G., *Reflections on Steel Corrosion in Concrete*, Ministry of Transportation Ontario, pp. 1-11, 1991

Matthews J. R., *Acoustic emission,* Gordon and Breach Science Publishers, pp. 5-129, 1983

Mertins A., *Signal Analysis*, John Wiley & Sons, pp. 15-226, 1999

Mirakowski A., *Application of Acoustic Emission in Evaluation of Pitting Corrosion in Steel, Dept.of Anticorrosion Technology*, Technical University of Gdansk, pp. 1-6, 2001

Nieuwenhove R. V. et al, *Acoustic Emission Detection during Stress Corrosion Cracking at Elevated Pressure and Temperature*, Reactor Material Research, Belgium, pp. 293-298, 1999

Pain H. J., *The Physics of Vibrations and Waves*, John Wiley & Sons, pp. 116-173, 1999

Pandey J. C. et al, *Ultrasonic Attenuation Techniques and Quality of Steel Products*, Proceeding of the 14th World Conference on NDT, New Delhi, pp. 2247-2252, 1996

Park M. H. et al, *Ultrasonic inspection of long steel pipe using Lamb waves*, NDT division, Korea Atomic Energy Research Institute, NDT & E International, Vol. 29, No.1, pp. 13-20, 1995

Rosenberg A., et al, *Mechanisms of Corrosion of Steel in Concrete,* The Danish Corrosion Center, Materials Science of Concrete, pp. 285-309, 2000

Rosh, *Integrity testing of other bridge substructure elements*, US Department of Transportation, pp. 1-11, 2003

Sachse W., et al, *Acoustic emission: current practice and future direction*, ASTM, pp. 11-24, 1991

Sandberg P., *Critical evaluation of factors affecting chloride initiated reinforcement corrosion in concrete*, Sweden, pp. 3-35, 1995

Santamarina J. C., Polak M. A., *Notes on Fundamental Aspects of: Wave Propagation, Signal Processing, Wave Concrete Interactions*, University of Waterloo, Report #1, 1994

Schiessl P., *Corrosion of steel in concrete*, Chapman and Hall, pp. 3-97, 1988

Schubert F., *Numerical Modeling of Acoustic Emission Sources and Wave Propagation in Concrete*, Switzerland, pp. 1-8, 2002

Shi Z. et al, *Sensing Acoustic Emission and Transmission*, Goergia Tech., pp. 1-6, 2002

Tonini D. E. and Gaidis J. M., *Corrosion of reinforcing steel in concrete*, ASTM, pp. 102-131, 1980

Tullmin M. A., et al, *Electrochemical techniques for measuring reinforcing steel*, Queen's University, pp. 1-11, 2003

Turner J. D., and Pretlove A.J., *Acoustic for Engineer*, Macmillan, pp. 4-123, 1991

Vahaviolos S. J., *Acoustic Emission: Standards and Technology Update*, ASTM, pp. 25-176, 1999

Vallen D. H., *AE Testing Fundamentals, Equipment, Applications*, The e-Journal of Nondestructive Testing, Sept. 2002, vol.7 No.09, pp. 1-30, 2002

Vogel T., *Possibilities and limitations of acoustic emission analysis for reinforced concrete*, International symposium NDT-CE, pp. 1-9, 2003

Williams E. G., *Fourier Acoutics*, Academic Press, pp. 21-27, 1999

Williams R. V., *Acoustic Emission*, Adam Hilger Ltd, pp. 1-33, 1980

Zdunek A. D., Li Z. et al, *Early detection on steel rebar corrosion by acoustic emission monitoring*, NACE International, pp. 1-5, 1995

Appendix A

Calibration Curves of Sensors R100, B225 and B1025

Manufacturer's Calibration Curves

R100:

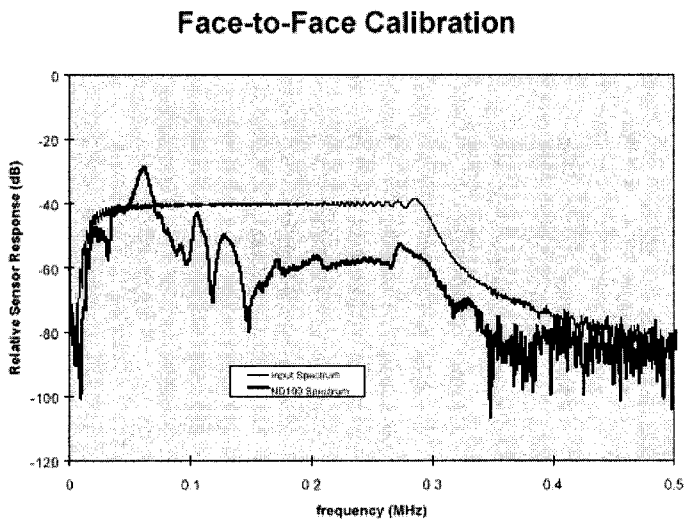

Generator: ND100
Receiver: ND100

(ND100 = R100)

B225:

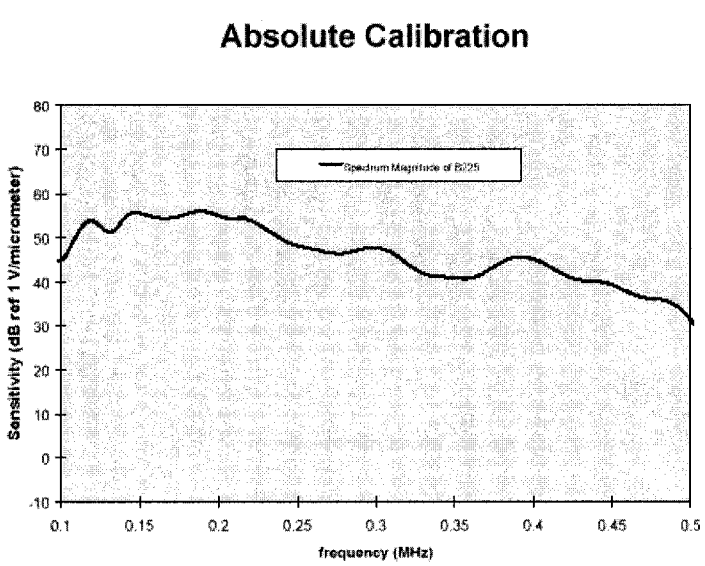

B225(continued):

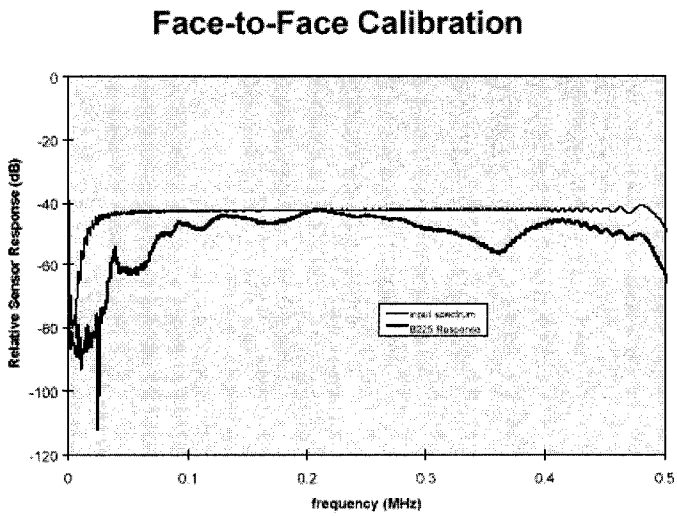

Generator: B1025
Receiver: B225

B1025:

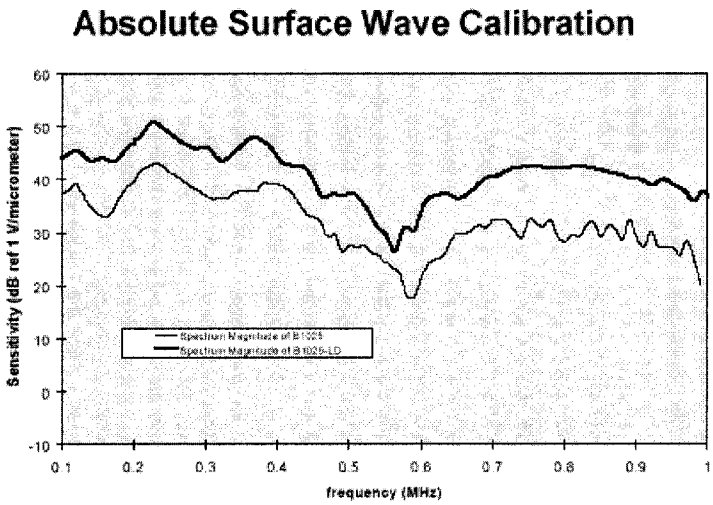

B1025(continued):

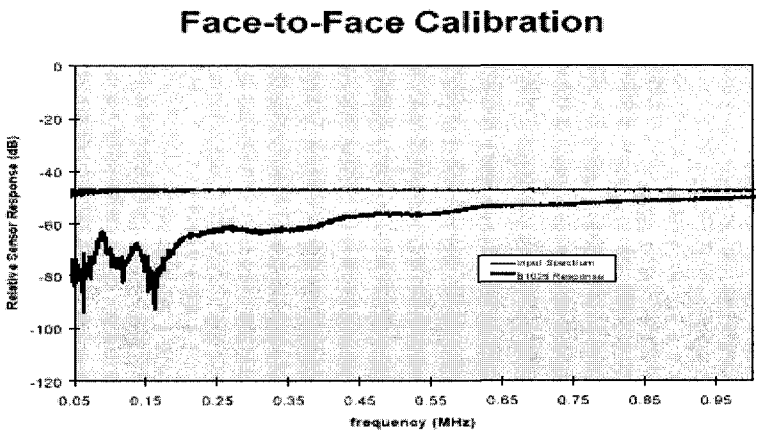

Laboratory Verification of R100 and B225

Verified by fracture of 0.5 mm 2H pencil lead

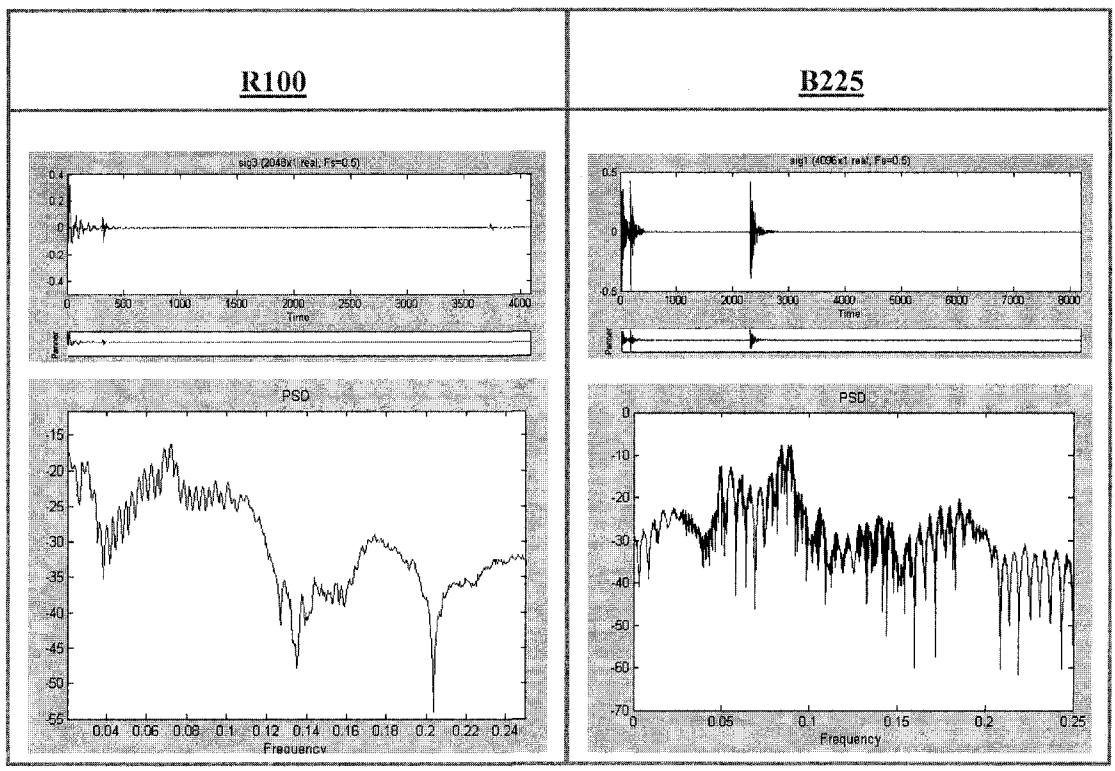

Appendix B

Laboratory Comparison of Sensor B225 and R100

Setup

R100: Own weight 179.7 g; diameter 1.25"; contact surface area: 791 mm^2

B225: Own weight 8.7 g; diameter 0.375"; contact surface area: 71 mm^2

Channel 1-R100: applied load: own weight +500 g; contact pressure = 8.6 kPa

Amplified rate 20db; sample frequency 1 MHz.

Channel 2-B225: applied load: own weight +50 g; contact pressure = 8.3 kPa

Amplified rate 20 dB; sample frequency 1 MHz.

Two channels were regarded as having same contact pressure. As shown in the following picture, two sensors were arranged at the positions with same distances to the center where the pencil lead was broken.

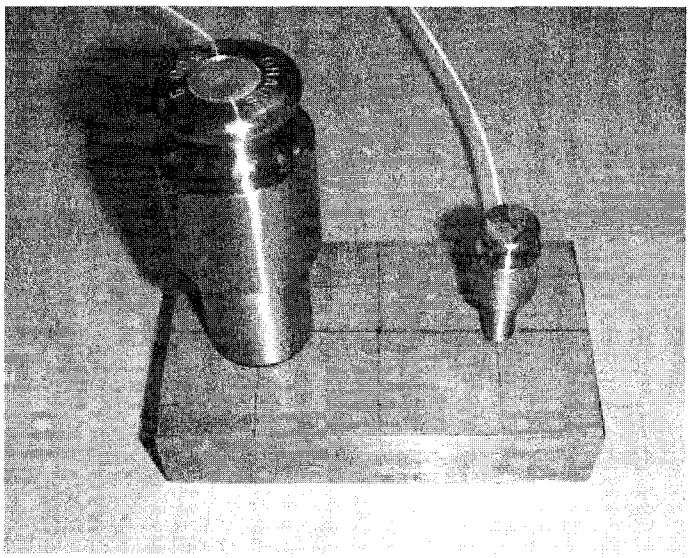

Results

Time domain

Channel 1-R100

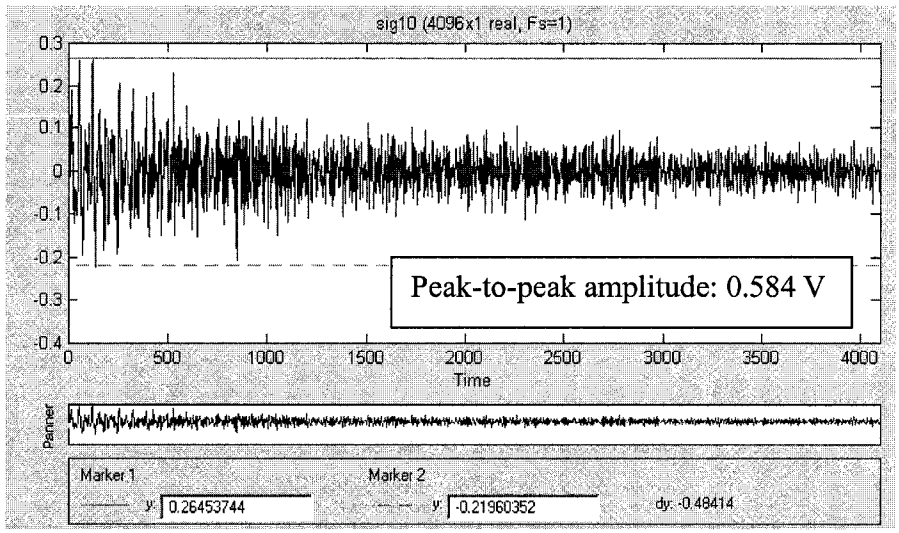

Channel 2 – B225

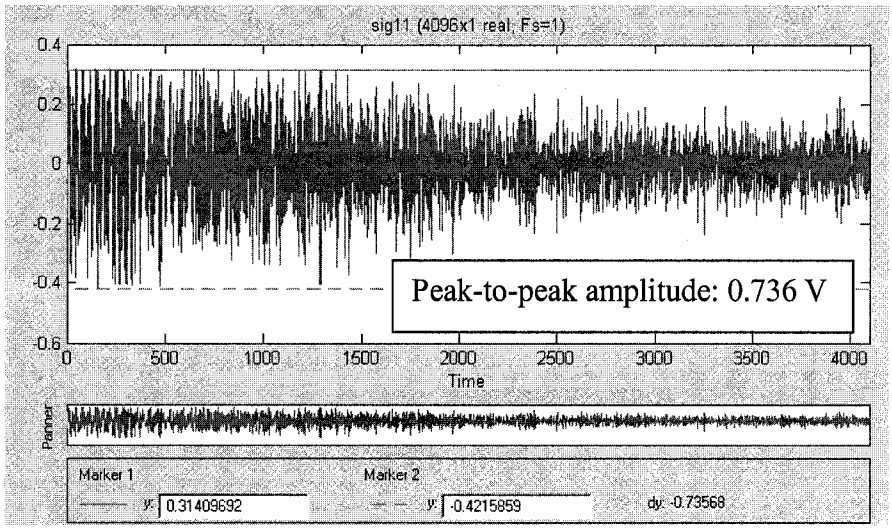

The sensitivity gap between R100 and B225 = 20log(0.584/0.736) = -2 dB

B225 has slightly higher sensitivity than R100.

Frequency domain (decibels scale)

Channel 1-R100

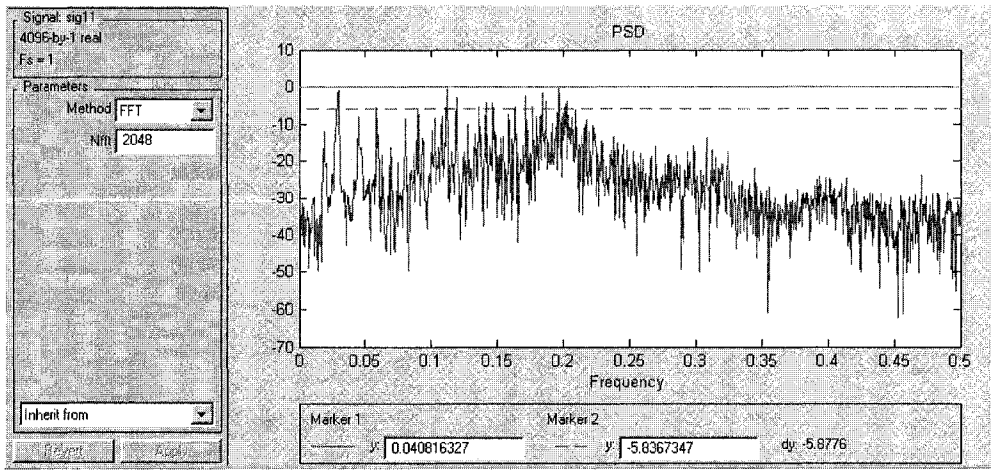

Channel 2 – B225

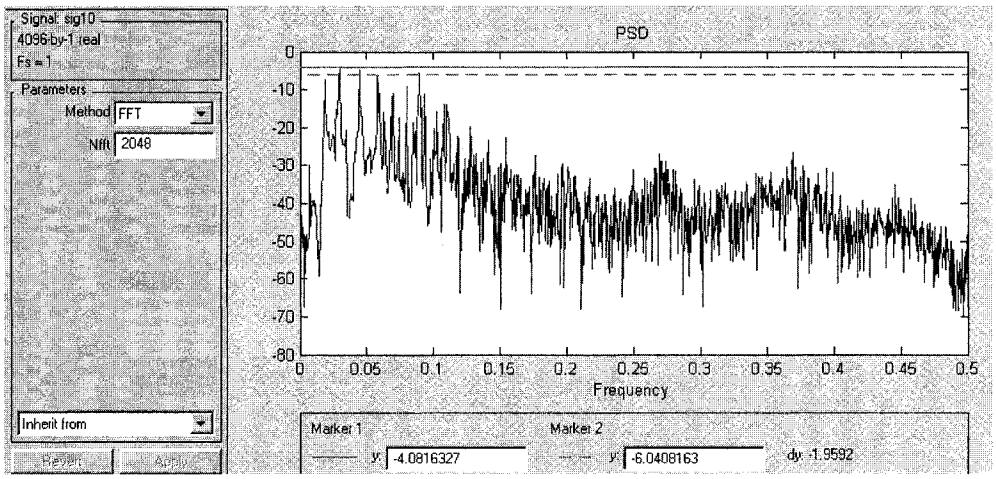

B225 has 4 dB higher Peak PSD than R100. At 70 KHz, B225 and R100 are regarded as the same (R100: -5.8dB; B225: -6.0 dB). Generally, sensor R100 and B225 have close sensitivities over the frequency range 20 to 500 KHz.

Appendix C

A Study of Sensor's Sensitivity vs. Contact Pressure

The study of effect of contact pressure was done by pencil lead (0.5 mm, 2H) fracture at the exact middle position between two B225 sensors, which have very close sensitivities.

The contact pressure was provided by standard weights 0 g, 50 g, 100 g, 200 g, 500 g and 1 kg. B225 has own weight 8.7 g, the diameter 0.375", and contact surface area 71 mm^2. Amplification rates of both channels are 20 dB.

The result shows the maximum output of sensor starts at the contact pressure 29 kPa (+200 g) as the following figure:

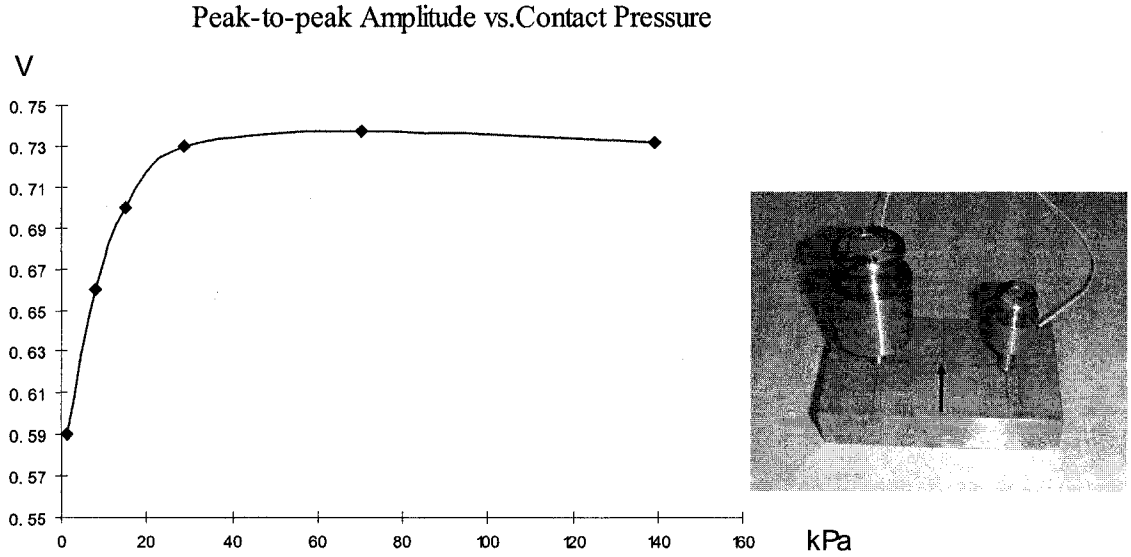

VITA AUCTORIS

Weiben Chen was born in 1972 in Fujian, China. He graduated from Gutian No.1 High School in 1989. From there he went on to the Nanjing University of Technology where he obtained a B.Eng in Civil Engineering in 1993. He is currently a candidate for the Master's degree in Civil Engineering at the University of Windsor and hopes to graduate in Spring 2005.